UNIVERSIDAD NACIONAL DE COLOMBIA

An alternative trajectory planning for a differential wheeled robot, aimed to unknown environment mapping with minimum energy consumption, based on a simplified dynamic model

Mauricio Fernando Jaramillo Morales

Universidad Nacional de Colombia
Faculty of Engineering and Architecture
Departament of Electrical, Electronic and Computer Engineering
Manizales, Colombia
2020

An alternative of a trajectory planning for a differential wheeled robot , oriented to the mapping of unknown environments with minimum energy consumption, based on a simplify dynamic model

Mauricio Fernando Jaramillo Morales

A Thesis presented for the degree of :
Ph.D in Engineering - Automatic

Adviser:
Ph.D. Juan Bernardo Gómez Mendoza

Research Area:
Mobile robotic Research group:
Smooth and Hard Applied Computing (SHAC)

Faculty of Engineering and Architecture
Departament of Electrical, Electronic and Computer Engineering
Manizales, Colombia
2020

"To my parents, sister, and girlfriend, for your unconditional support and love. You are the light of my life."

Acknowledgment

I want to thank my Professor Juan Bernardo Gómez Mendoza, for your constant support during the undergraduate, Magister, and Doctoral studies. To Professor Lino Marques for allow me to work in his research group (the Field and Service Robotics . Portugal) and especial thanks to the researcher Sedat Dogru for everything I could learn about robotic during the internship. Also, this work was financially supported by Colciencias Colombia, National Scholarship - 567, and partially supported by ISR - University of Coimbra, project UID/EEA/00048/2013 funded by FCT - Fundação para a Ciência e a tecnologia.

Abstract

An energy estimation model for a mobile robot can approximate the energy consumption of the robot for any application. In this study, an energy estimation model that takes into account the dynamic parameters of the motor and the robot, is proposed. The proposed model allows us to predict the energy values for different accelerations and different payloads, unlike most previous work. The validation of the proposed model was carried out for straight and rotational trajectories. For straight trajectories, the mathematical estimation model can be simplified by giving a linear estimation of the cost function. For rotational trajectories, the terms related to inertia forces appear again in the model. The Nomad Super Scout mobile robot is used for experimental tests. The experiments showed that the proposed model is able to estimate the energy consumption of the robot accurately, reaching a success rate of 96.67 % along a straight paths and 81.25 % along a curved paths.

The power estimation model is used to build the Hamiltonian function, that under a necessary optimization condition, can provide the optimal velocity of the robot that minimizes the energy consumption for a given straight path. In this study, a closed-form solution of the optimal velocity that takes into account high energy consumption and payload is presented as well. Finally, the optimal velocity of the robot is evaluated in a typical robotic application such as the solution of the SLAM problem.

Key Words: Differential drive mobile robot, power estimation model, energy optimization, SLAM problem .

Planificador de trayectorias alternativo, enfocado al mapeo de entornos desconocidos con gasto mínimo energético, basado en un modelo dinámico simplificado

Mauricio Fernando Jaramillo Morales

Universidad Nacional de Colombia
Facultad de Ingeniería y Arquitectura
Departamento de Eléctrica, Electrónica y Computación
Manizales, Colombia
2020

Resumen

Un modelo de estimación de energía para un robot móvil puede realizar una aproximación del consumo energético del robot para cualquier aplicación. En este estudio, se presenta un modelo de estimación de energía que tiene en cuenta los parámetros dinámicos del robot y de los motores. El modelo propuesto permite predecir los valores de energía del robot para diferentes aceleraciones y pesos de carga, a diferencia de trabajos previos relacionados. La validación del modelo fue realizado para trayectorias lineales y rotacionales. Para las trayectorias lineales, la estimación matemática del modelo puede ser simplificada, entregando una función de costo a optimizar. Para trayectorias rotacionales, los términos relacionados con fuerzas inerciales aparecen de nuevo en el modelo. El robot móvil Nomad Super Scout es usado para las pruebas experimentales. Los experimentos muestran que el modelo propuesto puede estimar la energía consumida por el robot con precisión, alcanzando un porcentaje de éxito de 96.67 % para trayectorias lineales, y de un 81.25 % para las trayectorias curvas.

El modelo de estimación de potencia es usado para construir la función Hamiltoniana, la cual bajo ciertas condiciones de optimización puede entregar la velocidad óptima del robot que minimiza la energía consumida por una trayectoria lineal. En este estudio, una solución matemática de forma cerrada de la velocidad óptima del robot es evaluada en una aplicación típica de robótica como es la localización simultánea y mapeo (Simulaneous Location and Mapping- SLAM).

Palabras claves: Robot de guiado diferencial, modelo de estimación de potencia, optimización de energía, SLAM. .

Contents

1. Introduction

In several robotic applications, the autonomy of the mobile robot movements can be required. For example, in environments where the wireless communication control is deficient, or is repetitive and coverage tasks, like surveillance, cleanness or assembly, where the responsibility of a supervisor can be replaced.

To achieve the mobile robot autonomy is vital developed a trajectory planning, that provides the path and the angular velocity of the wheels desired, for a particular robot task. For mobile robots exist typical applications such as traveling from the start point to the goal point, avoiding an obstacle, coverage task, or mapping of the unknown environments (SLAM problem). At the same time, the trajectory planning can minimize different kinds of variables as time travel, the distance of the path, control effort, or energy consumption.
In the following sections, it is presented a revision of the most relevant researches, related to the mobile robot and motor dynamic models, the power estimation model, the optimization of the robot energy consumption, and the SLAM (Simultaneous Location and Maping) problem.

1.1. Classic Path Planning (State of art)

In recent decades, the study of trajectory planning has been a topic of great interest for researchers in mobile robots. To identify the trajectory planners, the type of path and velocities, and the amount of a priori information observed of the environment is taking into account. Intuitively it is said that smooth paths allow saving robot energy consumption, compared with the non-trajectories. According to those conditions, the trajectory planners can be classified into non-smooth global planners, smooth global planners, non-smooth local planners, smooth local planners, and mixed planners.
The following briefly describes the main characteristics of relevant studies in each classification.

1.1.1. Global non-smooth trajectory planners

Non-smooth global planners refer to planners who have information a priori of the characteristics of the environment and generate discontinuous paths in the direction and speed. A previous stage of the planner is the representation of the environment; this stage presents a high inference in the type of trajectories generated by the planner. In the mid-'80s, the interpretation of

the environment was simplified, representing the elements of the scene in the geometric forms. This methodology is incorporated into the roadmap algorithm [37]. In this case, rhombuses represent the obstacles.
Other planners based on the roadmap are the Visibility Graph and the Voronoi Diagram (Voronoi Diagram) [57]. The difference between them is the location of the path control points. The Visibility Graph Locate the points at the corners of the rhombuses. This control point location may represent a collision risk for the mobile robot if the robot is commanded to move at high speed. The Voronoi Diagram, locates the control points in equidistant positions, at least at three corners of the obstacles. Although this algorithm avoids risks of collision with the obstacles, comparatively with the Visibility graph, more execution time in the initialization process, is needed. A typical application of the Voronoi diagram planner is the distribution of zones for multiple robots [62], and in algorithms that resemble ant colonies to find minimum travel distances for the mobiles robots [85]. Figure **1-1** shows the comparison between the roadmap and the Visibility Graph.
Alongside the Roadmap, a space representation technique is introduced at the beginning of the nineties, in which you get more information about the environment, by classifying the environment in occupied and unoccupied regions. This algorithm uses a cell decomposition [93], which consists of dividing the environment into cells and label them into free and occupied. An example of this representation is given in Figure **1-1**. The limitations of the algorithm they occurred in old processors, where the storage of cell information, exceeded the capacity of the computer.

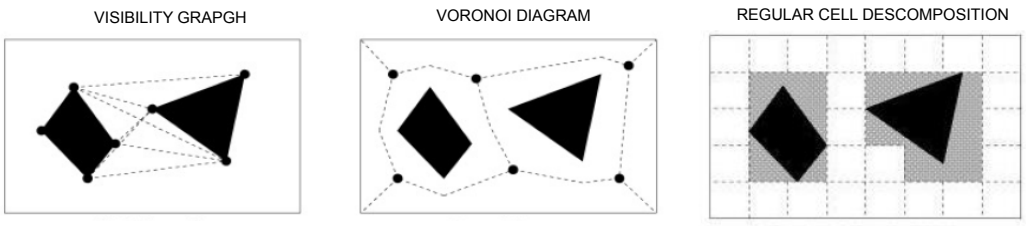

Figure 1-1.: Space classification techniques. Figure take it from [57]

Based on this spatial representation methodology, trajectory planners are introduced, that using different algorithms, unite the free cells to arrive at the objective point. These algorithms employ cost functions, that dependent on attributes given by the surrounding cells, seeking to minimize travel costs. Between these planners are the hierarchical planner [94], the D * lite algorithm [77, 45, 65, 32] and the Dijkstra algorithm [79].
Until that moment, the adaptability that these methods could have for dynamic environments or repetitive tasks was questioned. In these cases, the solution was envisioned in the arrival of methods with intelligence and learning capacity, which is introduced since 2000 with numerous artificial intelligence techniques, applied to the decomposition of cells, among them techniques

neural networks, genetic algorithms [2, 1, 50], probable methods, and fuzzy logic, was used. In these algorithms, the cost function is based on distance path and collision risk. The desired path is obtained through probabilistic methods, focused on finding local minimums of the function cost.
As is evident, computational spending is higher in algorithms that use methods of Artificial intelligence comparatively with the D * Lite algorithm. Because in adaptive algorithms, it is necessary to find all possible paths to the target point, to choose the optimal trajectory feasibly. The use of any of these algorithms depends on the robustness of the required solution, in a given application. Despite reaching good adaptability to specific environments, this type of trajectories non-smooth is not optimal for the hardware of the mobile robot. Because of the higher mechanical and energy effort of inducing the robot to stops to orientate and subsequent moves.

1.1.2. Global smooth planners

In this type of classification, there is a priori information on the environment to be explored, with the advantage of generating trajectories with continuing orientation and displacement, which allows the mobile present less mechanical wear and energy.
The representation of space is a crucial task for these planners .because the behavior of the previous classification influences the nature of the trajectories in the environment.
Along with the discretization of space by cells, another method of spatial representation is introduced, which uses mathematical functions to generate force fields. In this representation, the obstacles and the desired point are classified. The objective point is associated with attractive fields towards the objective point and repulsive fields to the obstacle. The total function that the environment represents will be the sum of the force fields attractive and repulsive. The smooth trajectory will be generated by the path of a particle influenced by the fields. In the literature this planner has taken names such as potential field (force fields) [3, 36, 4] or potential function (power functions) [69, 25].
The first to talk about power functions as a path planner for a mobile robot was Khatib [40] in 1980, in his doctoral thesis. Later in 1990 [13] is introduced a spatial representation with force fields based on Laplace equations. Two years later, a mathematical function is raised to generate force fields, which involves normalized distances between the obstacles, the target point, and the mobile robot [69]. This function is shown below 1-1.

$$\varphi_k = \frac{\|q - q_d\|^2}{[\|q - q_d\|^k + \beta(q)]^{1/k}} \tag{1-1}$$

Where: φ_k is the magnitude of force at the point q of the environment , q_d is the desired point, q is the environment point , $\beta(q)$ is the representation of the obstacles , and k is the smoothing variable of the repulsion field in the obstacles.
The obstacles $\beta(q)$ are represented spherically and are defined as:

$$\beta(q) = \prod_{i=M}^{j=0} \beta_j(q)$$
$$\beta_o(q) = -\|q - q_j\| + \rho_o^2$$
$$\beta(q) = \|q - q_j\|^2 - \rho_j^2$$
for j = 1...M

Where: q_j are the coordinates of the center of the circumference of the obstacles, being j the quantity of obstacles with a maximum of M. ρ_j is the radius of the obstacle j. Figure **1-2** shows the discontinuities in the magnitudes of the force field that allow isolation of the obstacle in the trajectory of the particle. Also, it can be observed that the local minimum force field (field in blue) focuses on the desired objective. It can be analyzed as well that the repulsive field of the obstacle in this planner represents an area in a circular form, as is formulated in the equation 1-1. Finally the trajectory that describes a particle in the force field is determined, having as initial position the external limits of the environment.

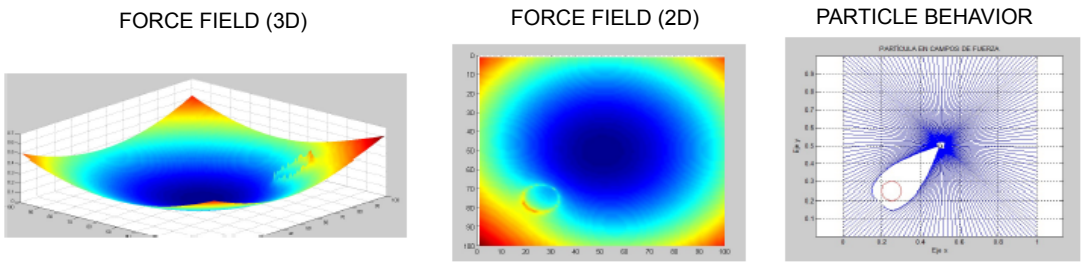

Figure 1-2.: Behavior of the force field, and trajectory of the particle.

There is a prevalent problem in this type of planners, which in the literature is known as goals non-reachable with obstacles nearby(GNRON). In many implementations in real environments, it is necessary to locate an objective point close to an obstacle. In the functions presented above, there is a difficulty when adding repulsive and attractive fields to represent the environment. The proximity of both fields, produces a displacement of the original target point, that in some cases is an impossible point for the mobile robot to reach. Chen in 2014 [76], shows functions with modifications in the force fields near the target point, taking into account the robot kinematic model, and in this way, a solution to the problem GNRON is founded.

1.1.3. Non-smooth local planner

Local planners are characterized by not having a priori information about the environment. It is, for this reason, that to the mobile robots, must have sensors to acquire environment information. This type of planning is useful in unfamiliar, dynamic environments, or changing due to extreme conditions. At the beginning of the nineties, the graph constructor is introduced [18]. In this planner, an unknown environment is explored, which response to a graph-shaped model. The mobile robot moves by the vertices of that graph and labeling them with markers. In this algorithm, there is no type of metric information during the scan, generating in the robot, more intuitive movements than measured.
A family of algorithms, with a greater metric formalism, comparatively with the constructor graphs, are introduced in1986 with a validity that continues today. They are known as algorithms Bug [6, 52], and are widely used in environments similar to offices. As the name implies, this algorithm mimics the movements of bugs, which surround the elements of a scene to reach an objective point. Figure **1-3** shows the most representative Bug algorithms, whose methodological difference in the way of address and abandon the elements of the scene.

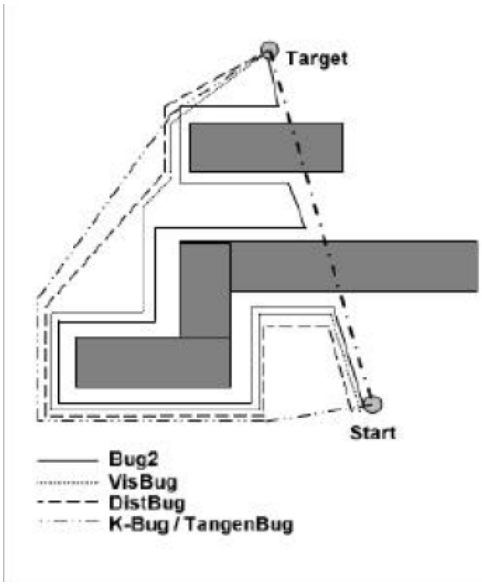

Figure 1-3.: Bug algorithm planners. Figure take it from [6]

At present, taking advantage of the heyday of vision devices, there are planners that with extra information on the scan images, can guide the robot through the scene. This type of processing is used in [43], where lines of images that have zero slopes (horizontal lines) are calculated through

transformation Hough. Those lines represent that the robot is aligning to the normal of a wall. In Figure **1-4** shows the search and subsequent detection of a line with zero slopes (Blue line).

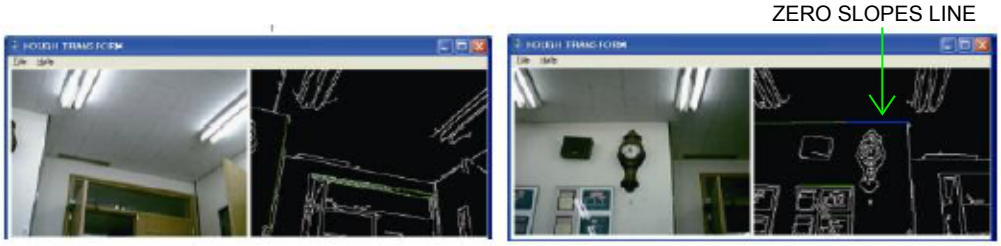

Figure 1-4.: Detection of zero slopes line. Hough transformation. Figure take it from [43]

1.1.4. Smooth local trajectory planner

The algorithms that generate the smooth paths, comparatively with the non-smooth paths, are more involved in the design of controllers and the mathematical formulation of trajectories. In the literature, the most implemented methodology to generate smooth trajectories focuses on joining control points, using non-linear equations that guarantee a low gradient in all sections of the path. One of the issues of the smooth trajectories is the calculation of curves to surround obstacles or to orient the robot. The curve paths can be classified into two categories: Curves generated by functions with expressions in closed form, or parametric curves. A challenge in the parametric curve is the joining of the partial paths. This issue produces discontinuities in the trajectories. Researchers have developed strategies to resolve this problem in different ways. Liscano in [49], uses spiral geometric clothoid functions, to join the arc and straight segments, this methodology is widely used in construction on roads in civil engineering. Kanayama [39], from a set of cubic spirals whose main feature is to have a zero curvature at the ends of the segment, which facilitates the joining with straight sections. Finally, a better softness is shown comparatively with the clothoid functions, when determining a lower deflexion of the normal curvature of the cubic spiral function.
Years later, the methodology is changed to splines. Such geometric functions have the advantage of adaptability. Forming geometric shapes with all kinds of curves can even form easily clotoids [[15], [66]]. Finally, at present, the methodology of generating smooth trajectories, based on Bezier curves, which retain the adaptability of splines, but incorporating computational facilities in their numerical implementation, is introduced [[9], [28], [58]]. Another methodology to generate the curve segments in the smooth paths is through closed mathematical functions. The big difference with the parameter curves is that they don't cause joining discontinuities, although an increase in its level of difficulty is evident, generally using high-grade polynomials equations [34],[61].

1.1.5. Hybrid planners

There are planning methodologies that use hybrid planners, in this case, with complete or partial environment information, a global planning solution is designed. Then, in the exploration, the information given by the sensors is used locally, to adapt changes to the original planning. This type of planning is widely used in dynamic environments, combining a large number of methodologies previously seen it in the global and local classification. In 1990 the first researchers in introducing hybrid planners were Payton and Rosenblatt (P-R) [70]. This methodology is built from two levels of control; the first is called edge tracking of the road (Track Road Edges) (Global Planning). The second level is called Turn by Obstacle (Turn for Obstacle) is related to a set of control decisions to evade the obstacles of the scene, based on sensory information.
Five years later, Yen in [91] continues with the P-R planning methodology but adapts it to a fuzzy logic technique. The benefits that this adaptation of the P-R method to diffuse logic can have are: Simplicity, high adaptability of inputs, and efficient understanding. Simplicity to have a basic controller through a few diffuse control laws to accomplish the task. Efficient interaction between sensors gives adaptability through a suitable logical inference scheme. Artificial intelligence methods such as diffuse logic seem to adapt very well to dynamic environments, and therefore are conducive to the construction of hybrid planners. Xiao [83] in 1997, applies methods of genetic algorithms to implement a hybrid planner or also called in the literature, off-line or on-line planners, to refer to global and local planners, respectively. In this algorithm, both planners are built with evolutionary algorithms and structures in the form of chromosomes. The advantage of using artificial intelligence methods in planning global planners, respect to the methods of P-R, and diffuse logic, is the highest efficiency in finding optimal paths. Nevertheless, it requires expense important computational consumption, when considering all possible paths, from an initial point to the point objective. This type of planning is very frequently used in unmanned aerial vehicles (UAV,) due to the dynamic scenario, with more variables even than the terrestrial scenarios. In 2002[27], a planning and control solution is shown, for various cooperative UAVs, in a given scene, with known objective points and dynamic threats. In recent years, the methodological tendency of hybrid planners has focused on using the Voronoi diagram in global planning, and the planning method by force field functions, for local planning [23, 22], having a better response to uncertainties obstacles in the scene.

1.2. Kinematic and dynamic model of the differential drive mobile robot

There is a great variety of mobile robot architectures, on which its mathematical modeling depends. The robot of study in this proposal, it is the differential drive mobile robot, whose configuration is shown in Figure **1-5**.
Where:

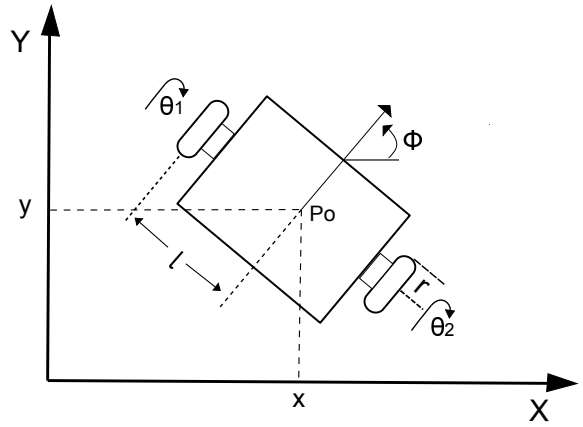

Figure 1-5.: Differential drive mobile robot configuration

v (t) is the linear speed of the midpoint of the vehicle.
w (t) is the angular velocity of the midpoint of the vehicle.
$\dot{\theta_1}$ (t) is the angular velocity of the right wheel.
$\dot{\theta_2}$ is the angular velocity of the left wheel.
r is the radius of the wheel.
l is the separation distance between the middle axis of the vehicle and the drive wheel.

The angular velocity of the wheels achieves the movement of the vehicle. The position and orientation of the robot can be described by the coordinates (x, y), which denote the position of the midpoint of the axis that joins the two wheels, with respect to the system of reference XY, and the angle between the axis of symmetry of the vehicle and the X axis [28]. The cinematic model associates the coordinate position (x, y), with the angular velocities of the wheels. The differential equations that govern this robot model are shown:

$$\begin{aligned} \dot{x} &= \frac{r}{2}\cos\varphi(\dot{\theta_1} + \dot{\theta_2}) \\ \dot{y} &= \frac{r}{2}\sin\varphi(\dot{\theta_1} + \dot{\theta_2}) \\ \dot{\varphi} &= \frac{r}{2l}(\dot{\theta_1} - \dot{\theta_2}) \end{aligned} \tag{1-2}$$

Studies of energy consumption based on the robot kinematic model, generally, they are linked with formulations of mechanics and kinetic energy [51, 50], [44]. The more general mathematical formulation of mechanical energy is $E = u_k m g v_k t_k$.
Where
u_k is the friction of the wheels against the floor.
m is the robot mass.
g is the gravity.
v_k is the robot velocity.

t_k the time during travel.
All the variables evaluated in a section of the path k.
The kinetic energy can be expressed as $E_c = \frac{1}{2}mv(t)2 + \frac{1}{2}Iw(t)^2$, where I is the moment of inertia of the robot.
This methodology can estimate energy consumption, but no take into account dynamic variables. For example, traction forces,or aerodynamic resistances. In this way, associate the kinetic energy consumption of exploration, based on the dynamic model of the robot, allows a more robust analysis, and in consequence a closer energy consumption values. The dynamic model of the movement of a robot can be framed in different conventional methods; among them, we have Newton's second law and Lagrange formulations (N-L) [8]. The mathematical equation that governs Newton's second law is presented below [24].

$$m\frac{d_v}{d_t} = F_t - mg\sin\alpha - \frac{1}{2}\rho ACv^2 - mgf_r\cos\phi \tag{1-3}$$

$\frac{d_v}{d_t}$ is the linear acceleration of the vehicle.
m is the mass of the vehicle.
F_r is the force due to the rolling resistance of the wheels, given by: $mgf_r\cos\phi$.
F_a is the force by aerodynamic resistance, given by: $\frac{1}{2}ACv^2$.
F_g is the strength of resistance on slopes, given by $mg\sin\alpha$.
F_t is the Total tensile force. g is the force of gravity.
f_r is the coefficient of bearing resistance.
ϕ is the angle of the terrain inclination.
ρ is the air density.
A is the frontal area of the vehicle.
C is the coefficient of aerodynamic resistance.
v is the vehicle speed.
α is the inclination of the surface.

On the other hand, Lagrange's formulation for the dynamic model of a mobile vehicle is given by [90]:

$$M(q)\ddot{q} + C(q,\dot{q})\dot{q} + G(q) = B(q)\tau + A^T(q)\lambda \tag{1-4}$$

Where:
$M(q)$ is the matrix of inertia, symmetric, and define positive.
$C(q,\dot{q})$ is the matrix of coriolis forces and centrifuge.
$G(q)$ is the vector of gravitational pairs.
$B(q)$ is the transfer matrix of the inputs.
τ is the dimensional vector of generalized forces.

A^T Jacobian matrix of movement restrictions.
λ is the force restriction vector.

1.3. Power Estimation Model and energy optimization

During typical applications, mobile robots may face large accelerations leading to high currents [68], or their payloads may vary throughout the mission leading to variable energy consumption [68, 5]. Many examples follow this behavior, such as cooperative payload transport using mobile robot groups [71, 53], mobile robots equipped with a lifting mechanism that can be rigidly attached to a desired payload [64, 14], pesticide spraying using agricultural robots [73], payload transport using quadrotor Unmanned Aerial Vehicles (UAV) [81, 67, 89], inspection using autonomous mobile robots [54, 29, 59], navigation and exploration in disaster areas [16, 7, 30], or heavy payload transfer using military mobile robots such as the Dog-Horse [74]. In these scenarios, an energy estimation model can approximate energy consumption values during long term robotic activities. Such a model also estimates battery time autonomy, especially for mobile robots that carry their energy sources, such as batteries [72, 33, 63]. In energy estimation models for mobile robots, motor resistances, load torques, and load friction torques affect the estimated energy considerably. The load torque is due to the motion of the robot, and it is related to the acceleration and payload, i.e., the inertia, of the robot, and it can be calculated using the dynamic model of the robot. The friction torques are due to the friction between the wheels and surface, friction losses inside the motors, and frictional losses in the gears connecting the motors to the wheels. These friction torques can be estimated using the dynamic model of the motor and a calibration procedure. Different surfaces may cause different friction values, changing the energy consumption considerably [60, 78].
It is well known that DC motors driving the wheels of a robot consume a significant amount of energy [60, 78, 42, 41, 87]. Therefore, researchers use the dynamic model of a DC motor to estimate or optimize energy consumption for mobile robots [41, 78]. Kim and Kim [42, 41] calculate the velocity profiles that minimize energy consumption for a differential drive mobile robot along straight and curved paths. They used the dynamic model of the motor as the cost function, but they do not take into account the torque. For that reason, this model gives energy estimates far from the real energy consumption. Kim and Kim describe the minimum energy turning trajectory path using a sequence of two straight lines for translational motions and an arc for rotational movement in between.
Tokekar and Isler [78] proposed a calibration procedure to estimate the parameters of the dynamic model of the motor, including the internal friction torque. They also discussed the influence of friction between the robot wheels and different kinds of surfaces on energy consumption. Their estimation model uses an energy road-map scenario to obtain any path, connecting the sequence of poses with circular arcs or straight line segments. In the results, the energy values of the proposed curve paths and Dubin paths are compared. For the optimization of the

robot energy consumption used a Hamiltonian function based on the dynamic motor model. Sheta et al.[75] focus on the minimization of resistive and frictional power dissipation in a separately excited DC motor. The dynamic parameters, such as the moment of inertia and the coefficient of friction, which depend on the load torque, were obtained using a system identification method. Wahab [80] introduces kinetic energy and friction to the energy model based on the motor model. Wang [82] presents an energy estimation model for an omnidirectional mobile robot based on robot dynamics combining the mechanical and electrical systems. However neither [78, 75, 80] nor [82] take the payload into account.

The dynamic robot model, based on the Lagrange formulation, has also been used to calculate the energy consumption of mobile robots. Kozlowski [46] studied extending the kinematic control law of 4-wheel skid-steered mobile robots at the dynamic and motor levels using Lyapunov analysis. In the process, the model is decomposed into kinematic, dynamic, and drive levels. Bensekane et al. [5] analyzed the power consumption related to the degree of steerability, the degree of actuator redundancy, and curvature of the trajectory for an over-actuated unmanned vehicle.This work also presents experimental results with different load weights.

A power consumption model can be estimated entirely with a calibration procedure. Mei et al. [86] estimate consumed power using a sixth-degree polynomial function. For this, they experiment with a commercial mobile robot called Palm Pilot Robot Kit (PPRK), computing the energy efficiency for different spiral paths. Mei et al. [56] later use a cost function to represent the power estimation model for a differential drive mobile robot taking into account the robot mass and payload and the friction between the wheels and floor. The experiment is performed with a Pioneer 3D-X mobile robot for straight paths and circles. However, the power model is not able to predict the power with varying payload or accelerations. Ramviyas and Prithvi [68] estimate consumed energy, taking into account passive and active components of the mobile robot, such as sensors, communication devices, motors, and payloads. They use a calibration procedure to estimate the dynamic parameters of the model. Ramviyas and Prithvi [68] experimentally validate their model using a Khepera III mobile robot moved over a square path. Conceição et al. [11] use different estimation methods based on the least square methods to obtain dynamic parameters of the robot model such as moments of inertia and friction coefficients. However, due to calibration, the power consumption models cannot predict consumption outside the calibration workspace. Chuy et al. [10] present a power consumption model for skid-steered wheeled platforms in terms of linear velocity and turning radius of the robot. Nevertherless, the load weight is not a variable of analysis.

Finally, a robot energy estimation model can be based on a friction model. Morales et al. [60] analyze a power model based on a friction estimation of skid-steered tracked mobile robots on rigid terrain on two different types of surfaces, marble and asphalt. The power estimation model is evaluated on straight and spiral-like paths. Gupta et al.[31] present a dynamic power model that can be used to predict the energy consumption along a given trajectory for skid-steered autonomous ground vehicles (AGVs) with variation of payloads and terrains. The simulated and experimental results consider an AGV moving at a constant forward velocity on both wood and

asphalt surfaces under various payloads. Hou et al. [35] presented a predictive energy model, considering three major factors: the sensor system, control system, and motion system. The model is tested with a 4-wheel Mecanum mobile robot.Xie et al. [84] uses the same robot configuration to proposed an energy model based on kinetic energy and friction. Similarly, Dogru and Marques [17] propose a friction-based power model for skid steered wheeled platforms, taking into account the influence of varying payload as well. The robot was driven in straight lines, rotated in place and driven along paths of a varying radius of curvature. However, since these works concentrate on skid-steered platforms, the proposed models do not apply to two-wheel differential drive robots.

1.4. Simultaneous localization and mapping (SLAM)

The SLAM problem is an essential issue in robotic and receives significant attention in the robotic researchers. Even so, there is no established methodology in the literature to accomplish this task, but we can identify some common steps that are briefly described:
Acquisition of information and classification of the environment
The exploration of unknown environments supposes not having a priori information of the environment. In this way, the robot must acquire data from the scene in a sensory way.
This information should represent the scene to classify the seen, unseen, and the occupied areas (obstacles) [38]. Figure **1-6** shows an example of the classification of the environment through the decomposition of cells.

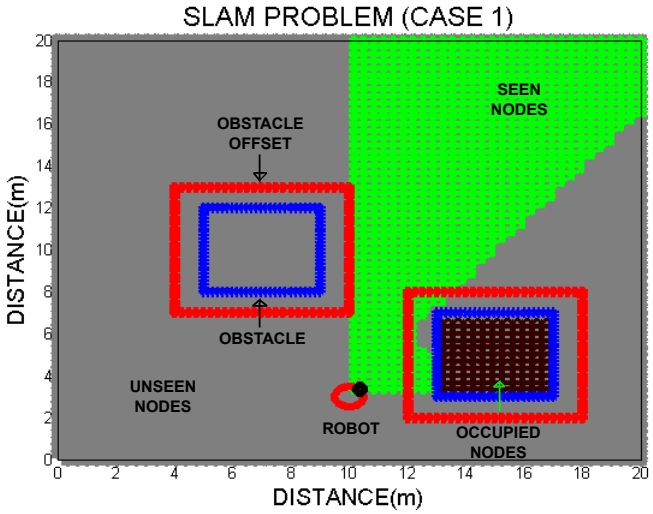

Figure 1-6.: SLAM space classification

1.4.1. The Next Best View (NBV)

The NBV determines the point and orientation where the robot should move, to acquire the maximum of unknown information. Exist many criteria to find the NBV, including minimum distances [77, 45, 65, 32], maximize information on the environment [47, 95]], energy expenditure [48], among others.
The NBV, in the literature, can be obtained naturally or artificially. The natural one refers to sensory acquire the objective points (landmarks) autonomously, and the artificial refers to intentionally planting marks in the environment. In [20] to obtain the maximum information about the environment, the landmarks (NBV) more beneficial is analyzed, to later locate them manually in the environment, so that the robot makes minimal scrolls of exploration. This methodology of determining landmarks in the scene, it would not be convenient in the exploration of hostile environments. As the sensors improved over the years, the methodology of natural landmarks was gained popularity. In 2006 Mei[55] mentions that moving with the criteria of maximizing the information of the environment, can induce crossings of trajectories in the environment, which It would not be efficient. One way to resolve this difficulty is to guide the robot to the NBV sequentially clockwise. This approach is shown to be a more intuitive way than analytic. A year later, Wang refutes that methodology [47], seeking to maximize the information of the environment, minimizing the number of views used by the robot in exploration and travel. The support of this methodology is purely Geometric and does not relate to the kinematic or dynamic modeling of the robot. Finally in 2014 [21], through global planning, focuses maximum visibility on the landmarks, for a differential drive mobile robot, but the paths generated are not smooth.

1.4.2. Mapping and location

The information of the scene elements acquired by the sensors is used to make a representation of the environment. The mapping can be done in several ways, among them, with geometric shapes[6], with graphs [57], or with the decomposition of cells [93], these are the methods in 2D. For the 3D case, the most common mapping used point clouds, which represent the scene in a discretized manner. In this case, the voxelization is used to improve the level of representation. This method consists of discretizing the space through voxels (cubes), showing only voxels occupied by cloud points. Figure **1-7** shows an example of mapping by different types of voxelization.

The mapping of the environment is dependent on the current location of the mobile. This problem is known as SLAM. There are varied methods of solution, the estimation methods being, the most used in the literature [5, 6, 7].

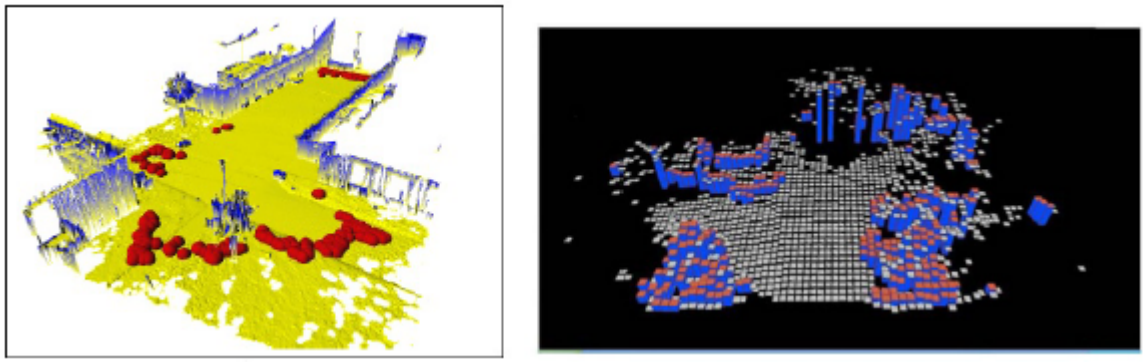

Figure 1-7.: Environment 3D reconstruction.

1.5. Contributions

After the constant reviewing of the literature can be noticed that works related to the study of the differential mobile robot and payload are few or are not reported yet. The only research with these characteristics is [55]. But the mathematical methodology used for the power estimation is based on calibration procedure, the disadvantage of this approach is to change the calibration of the model every time that any variable of the experiment changes as well. Wich implies a lack of adaptability. Taking this into account, the contributions of this work is as follows:

Power estimation model:

A novel power estimation model based on the robot and motor dynamic models is presented. The power model can predictive accurately the energy consumption of any acceleration or payload for a differential guide mobile robot configuration. In the process, it is only needed one initial calibration procedure. A hardware validation is achieved using the Nomad Super Scout Robot, obtaining a MAPE (Mean Absolute Percentage Error) of power estimation of 5.53%.
On the other hand, there is not evidenced so far, in the state of art, regarding energy optimization models related to the differential guide mobile robot configuration and payload. In this case, the other contribution is:

Energy optimization model

A mathematical closed-form energy optimization model is presented. The proposed model based on the hamiltonian function, used as a function cost the power estimation model and takes into account the payload of the robot. The numerical test shows a significant saving of energy, compared with high energy consumption velocities. Also, the energy optimization model is used in the solution of the SLAM problem, showing the same energy-saving behavior.
This study is organized as follows: Chapter 2 develops a mathematical model for energy con-

sumption estimation. Chapter 3 presents the results of experimental validations with the Nomad Super Scout mobile robot. In Chapter 4, the optimal velocity profile that minimizes the robot energy consumption is shown. Finally, conclusions are drawn in Chapter 5.

2. Novel Energy Estimation Model Based on Motor and Robot Dynamic Models

Energy consumption is an important issue for mobile robots that carry a limited energy source like batteries, for a long period of time. A power consumption model can relate the kinematic movements of the robot with the energy consumption values, giving an approximation of the energy needed for the robot to fulfill a specific task. In this section, an energy model that is based on the dynamic parameters of the mobile robot and its motors is proposed. The model can predict the dissipated energy accurately, even when the robot carries different payloads and performs different accelerations. The experimental validation is obtained using the Nomad Super Scout mobile robot, shows both the accuracy of the proposed model and the influence of acceleration and the weight of the payload to the energy consumption of the robot.

2.1. Mathematical Model

In the first section, the dynamic model of a two-wheel differential drive robot, and then the dynamic model of a DC motor, are presented. Later, the two models are combined by matching the load torque values. Finally, a state space realization is used to obtain the power model formulation.

2.1.1. Simbols of the Mathematical Model

In this section, all the symbols used in this work are presented for easy reference.

x and y are the coordinates of the center of the robot (P_o in Figure **2-1**) in a fixed reference coordinated frame X - Y,
ϕ is the heading angle of the mobile robot measured from the X-axis,
w is the angular velocity of the robot,
v is the linear velocity of the robot,
θ is the angular position vector of the wheels,
$\dot{\theta}$ is the angular velocity vector of the wheels,
$\ddot{\theta}$ is the angular acceleration vector of the wheels,
K is the total kinetic energy of the robot,

q_i is the generalized coordinate corresponding to robot pose,
λ_i are the components of the vector of the Lagrange's multipliers,
τ_i are the components of the vector of the load torques applied to the wheels,
a_{ij} are the elements of the constraint matrix,
l is the displacement from each of the driving wheels to the axis of symmetry,
d is the displacement from point P_o to the center of mass of the mobile robot, which is assumed to be on the axis of symmetry,
r is the radius of the driving wheels,
c is a constant that is equal to $\frac{r}{2l}$,
m_c is the mass of the mobile robot without the driving wheels and the rotors of the motors,
m_w is the mass of each driving wheel plus the rotor of its motor,
m_p is the mass of the payload,
m is the total mass, $m_c + 2m_w + m_p$,
I_c is the moment of inertia of the mobile robot and payload without driving wheels and rotors of the motors about a vertical axis passing through the intersection of the axis of symmetry with the driving wheel axis,
I_w is the moment of inertia of each driving wheel and the motor rotor about the wheel axis,
I_m is the moment of inertia of each driving wheel and the motor rotor about wheel diameter,
V and i are the armature voltage and current of a motor,
$V = [V_1\ V_2]^T$ are the armatures voltages of the motors of the robot,
$i = [i_1\ i_2]^T$ are the currents of the motors of the robot,
$P = [P_1\ P_2]^T$ are the power consumed of the motors of the robot,
P and E are the power and energy consumed by the robot,
R and L are the armature resistance and inductance,
ν is the viscous friction coefficient,
τ is the load torque applied to the motor,
T_m is the internal friction torque in the motor,
K_t is the motor torque constant,
k_w is the motor voltage constant,
I_s is the equivalent motor moment of inertia,
n is the gear ratio of the motor.

2.1.2. Constraint Equations

In this section, the motion and constraint equations for a differential mobile robot whose schematic is shown in Figure **2-1** are developed. The mobile robot is driven by two actuated independent wheels with the same dimensions.

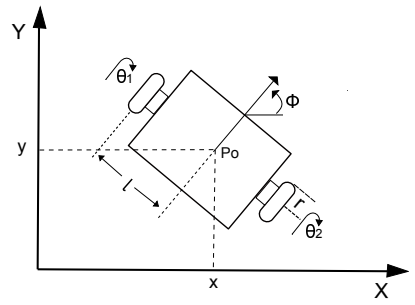

Figure 2-1.: Schematic of the differential drives mobile robot

The mobile robot configuration has two motion constraints:

Constraint 1: The mobile robot cannot move in the lateral direction, hence:

$$\dot{x}\sin\phi - \dot{y}\cos\phi = 0 \tag{2-1}$$

Constraint 2: The wheels of the mobile robot roll but do not slip, hence:

$$\dot{x}\cos\phi + \dot{y}\sin\phi + l\dot{\phi} = r\dot{\theta}_1 \tag{2-2}$$

$$\dot{x}\cos\phi + \dot{y}\sin\phi - l\dot{\phi} = r\dot{\theta}_2 \tag{2-3}$$

The holonomic constraint can be obtained by subtracting equation 2-2 from equation 2-3, giving

$$2l\dot{\phi} = r(\dot{\theta}_1 - \dot{\theta}_2) \tag{2-4}$$

Replacing the constant $c = r/2l$ in equation 2-4 leads to:

$$\dot{\phi} = c(\dot{\theta}_1 - \dot{\theta}_2) \tag{2-5}$$

Adding equations 2-2 and 2-3 yields:

$$\dot{x}\cos\phi + \dot{y}\sin\phi = \frac{r}{2}(\dot{\theta}_1 + \dot{\theta}_2) \tag{2-6}$$

The non-holonomic constraint equations formed by 2-1 and 2-6 can be written in matrix form as:

$$\begin{bmatrix} a_{11} & a_{12} & a_{13} & a_{14} \\ a_{21} & a_{22} & a_{23} & a_{24} \end{bmatrix} \begin{bmatrix} \dot{x} \\ \dot{y} \\ \dot{\theta}_1 \\ \dot{\theta}_2 \end{bmatrix} = 0 \tag{2-7}$$

Where the elements of the constraint matrix are

$$\begin{bmatrix} a_{11} & a_{12} & a_{13} & a_{14} \\ a_{21} & a_{22} & a_{23} & a_{24} \end{bmatrix} = \begin{bmatrix} -\sin\phi & \cos\phi & 0 & 0 \\ -\cos\phi & -\sin\phi & \frac{r}{2} & \frac{r}{2} \end{bmatrix} \tag{2-8}$$

Equation 2-7 can be expressed as

$$A(q)\dot{q} = 0 \tag{2-9}$$

Where q is the generalized coordinate given by

$$q = \begin{bmatrix} q_1 \\ q_2 \\ q_3 \\ q_4 \end{bmatrix} = \begin{bmatrix} x \\ y \\ \theta_1 \\ \theta_2 \end{bmatrix} \tag{2-10}$$

2.1.3. Dynamic Model of the Robot

The system of nonlinear differential equations that represent the dynamic model of the mobile robot can be found by using the Lagrange formulation [92, 88, 26]:

$$\frac{\partial}{\partial}\left(\frac{\partial K}{\partial \dot{q}_i}\right) - \left(\frac{\partial K}{\partial q_i}\right) = \tau_i - \lambda_1 a_{1i} - \lambda_2 a_{2i} \tag{2-11}$$

with i= 1, ...4,
The total kinetic energy of the mobile robot is given by

$$K = \frac{1}{2}m(\dot{x}^2 + \dot{y}^2) + m_c cd(\dot{\theta}_1 - \dot{\theta}_2)(\dot{y}\cos\phi - \dot{x}\sin\phi) + \frac{1}{2}I_w(\dot{\theta_1}^2 + \dot{\theta_2}^2) + \frac{1}{2}Ic^2(\dot{\theta}_1 - \dot{\theta}_2)^2 \tag{2-12}$$

Where $I = I_c + 2m_w l^2 + 2I_m$

Now, the derivatives of the Lagrange Formulation (2-11) can be calculated, in order to obtain the dynamic model of the robot.
for i = 1, the differential equation calculated is:

$$\frac{\partial}{\partial t}\left(\frac{\partial K}{\partial \dot{q}_1}\right) - \frac{\partial K}{\partial q_1} = \tau_1 - \lambda_1 a_{11} - \lambda_2 a_{21} \tag{2-13}$$

The load torques τ_1 and τ_2 are related with the angular velocities of the wheels. In that case this variables are evaluated when i = 3 and 4. Now, Replacing the first state variable q_1 by x, along with elements of the constraint matrix, and using the equation $\phi = c(\theta_1 - \theta_2)$.

$$\frac{\partial}{\partial t}\left(\frac{\partial K}{\partial \dot{x}}\right) - \frac{\partial K}{\partial x} = \lambda_1 \sin\phi + \lambda_2 \cos\phi \tag{2-14}$$

By solving the derivatives of equation 2-14, it is obtained:

$$\frac{\partial K}{\partial \dot{x}} = m\dot{x} - m_c c d(\dot{\theta_1} - \dot{\theta_2}) \sin\phi$$

$$\frac{\partial}{\partial t}\left(\frac{\partial K}{\partial \dot{x}}\right) = m\ddot{x} - m_c d\ddot{\phi} \sin\phi - m_c d\dot{\phi}^2 \cos\phi \tag{2-15}$$

$$\frac{\partial K}{\partial x} = 0$$

Then, replacing the results in the equation 2-14, the first equation of the mobile dynamic model is obtained:

$$m\ddot{x} - m_c d(\ddot{\phi} \sin\phi + \dot{\phi}^2 \cos\phi) = \lambda_1 sin\phi + \lambda_2 \cos\phi \tag{2-16}$$

for i = 2, the differential equation calculated is:

$$\frac{\partial}{\partial t}\left(\frac{\partial K}{\partial \dot{q_2}}\right) - \frac{\partial K}{\partial q_2} = \tau_2 - \lambda_1 a_{12} - \lambda_2 a_{22} \tag{2-17}$$

Replacing the second state variable q_2 by y, along with the elements of the constraint matrix, and using the equation $\phi = c(\theta_1 - \theta_2)$.

$$\frac{\partial}{\partial t}\left(\frac{\partial K}{\partial \dot{y}}\right) - \frac{\partial K}{\partial y} = -\lambda_1 \cos\phi + \lambda_2 \sin\phi \tag{2-18}$$

Solving the derivatives of equation 2-18. It is obtained:

$$\frac{\partial K}{\partial \dot{y}} = m\dot{y} + m_c d\dot{\phi} \cos\phi$$

$$\frac{\partial}{\partial t}\left(\frac{\partial K}{\partial \dot{y}}\right) = m\ddot{y} + m_c d\ddot{\phi} \cos\phi - m_c d\dot{\phi}^2 \sin\phi \tag{2-19}$$

$$\frac{\partial K}{\partial y} = 0$$

Then, replacing the results in equation 2-18, the second equation of the mobile dynamic model is obtained:

$$m\ddot{y} + m_c d(\ddot{\phi} \cos\phi - \dot{\phi}^2 \sin\phi) = -\lambda_1 \cos\phi + \lambda_2 \sin\phi \tag{2-20}$$

for i = 3, the differential equation calculated is:

$$\frac{\partial}{\partial t}\left(\frac{\partial K}{\partial \dot{q_3}}\right) - \frac{\partial K}{\partial q_3} = \tau_1 - \lambda_1 a_{13} - \lambda_2 a_{23} \tag{2-21}$$

Replacing the third state variable q_3 by θ_1, along with the elements of the constraint matrix, and using the equation $\phi = c(\theta_1 - \theta_2)$:

$$\frac{\partial}{\partial t}\left(\frac{\partial K}{\partial \dot{\theta_1}}\right) - \frac{\partial K}{\partial \theta_1} = \tau_1 - \lambda_2 cl \tag{2-22}$$

Now, solving the derivatives of the equation 2-22. It is obtained

$$\frac{\partial K}{\partial \dot{\theta_1}} = m_c cd(\dot{y}\cos\phi - \dot{x}\sin\phi) + I_w\dot{\theta_1} + Ic^2(\dot{\theta_1} - \dot{\theta_2})$$

$$\frac{\partial}{\partial t}\left(\frac{\partial K}{\partial \dot{\theta_1}}\right) = m_c cd(\ddot{y}\cos\phi - \dot{x}\sin\phi\dot{\phi} - \ddot{x}\sin\phi - \dot{x}\cos\phi\dot{\phi}) + I_w\dot{\ddot{\theta}_1} + Ic^2(\ddot{\theta_1} - \ddot{\theta_2}) \tag{2-23}$$

$$\frac{\partial K}{\partial \theta_1} = m_c cd(\dot{\theta_1} - \dot{\theta_2})(-\dot{y}\sin\phi - \dot{x}\cos\phi)$$

Then, replacing the results in equation 2-22. It is obtained:

$$m_c cd(\ddot{y}\cos\phi - \ddot{x}\sin\phi) - m_c cd\dot{y}\sin\phi\dot{\phi} - m_c cd\dot{x}\cos\phi\dot{\phi} + m_c cd\dot{y}\sin\phi\dot{\phi} + m_c cd\dot{x}\cos\phi\dot{\phi} + \ddot{\theta}_1(I_w + Ic^2) - \ddot{\theta}_2(Ic^2) = \tau_1 - \lambda_2 cl \tag{2-24}$$

finally, simplifying the equation 2-24, the third equation of the mobile dynamic model is obtained:

$$m_c cd(\ddot{y}\cos\phi - \ddot{x}\sin\phi) + \ddot{\theta}_1(I_w + Ic^2) - \ddot{\theta}_2(Ic^2) = \tau_1 - \lambda_2 cl \tag{2-25}$$

for i = 4, the differential equation calculated is:

$$\frac{\partial}{\partial t}\left(\frac{\partial K}{\partial \dot{q_4}}\right) - \frac{\partial K}{\partial q_4} = \tau_2 - \lambda_1 a_{14} - \lambda_2 a_{24} \tag{2-26}$$

Replacing the fourth state variable q_4 by θ_2.

$$\frac{\partial}{\partial t}\left(\frac{\partial K}{\partial \dot{\theta_2}}\right) - \frac{\partial K}{\partial \theta_2} = \tau_2 - \lambda_2 cl \tag{2-27}$$

Now, solving the derivatives of equation 2-27, and using equation $\phi = c(\theta_1 - \theta_2)$.

$$\begin{aligned}
\frac{\partial K}{\partial \dot{\theta}_2} &= -m_c cd(\dot{y}\cos\phi - \dot{x}\sin\phi) + I_w(\dot{\theta}_2) - Ic^2(\dot{\theta}_1 - \dot{\theta}_2) \\
\frac{\partial}{\partial t}\left(\frac{\partial K}{\partial \dot{\theta}_2}\right) &= -m_c cd(\ddot{y}\cos\phi - \dot{y}\sin\phi\dot{\phi} - \ddot{x}\sin\phi - \dot{x}\cos\phi\dot{\phi}) + I_w(\ddot{\phi}) - Ic^2(\ddot{\theta}_1 - \ddot{\theta}_2) \\
\frac{\partial K}{\partial \theta_2} &= -m_c cd\dot{\phi}(\sin\phi\dot{y} + \cos\phi\dot{x})
\end{aligned} \tag{2-28}$$

Then, replacing the results in equation 2-27. It is obtained:

$$\begin{aligned}
-m_c cd(\ddot{y}\cos\phi - \ddot{x}\sin\phi) + m_c cd\dot{y}\sin\phi\dot{\phi} + m_c cd\dot{x}\cos\phi\dot{\phi} - m_c cd\dot{y}\sin\phi\dot{\phi} \\
-m_c cd\dot{x}\cos\phi\dot{\phi} - +I_w(\ddot{\theta}_2) - Ic^2(\ddot{\theta}_1 - \ddot{\theta}_2) = \tau_2 - \lambda_2 cl
\end{aligned} \tag{2-29}$$

Simplifying the equation 2-28, the fourth equation of the mobile dynamic model is obtained:

$$-m_c cd(\ddot{y}\cos(\phi) - \ddot{x}\sin(\phi)) - \ddot{\theta}_1(Ic^2) + \ddot{\theta}_2(I_w + Ic^2) = \tau_2 - \lambda_2 cl \tag{2-30}$$

The nonlinear differential system of equations representing the dynamic model of the mobile robot is conformed as:

$$\begin{aligned}
\lambda_1\sin\phi + \lambda_2\cos\phi &= m\ddot{x} - m_c d(\ddot{\phi}\sin\phi + \dot{\phi}^2\cos\phi) \\
-\lambda_1\cos\phi + \lambda_2\sin\phi &= m\ddot{y} + m_c d(\ddot{\phi}\cos\phi - \dot{\phi}^2\sin\phi) \\
\tau_1 - \lambda_2 cl &= m_c cd(\ddot{y}\cos\phi - \ddot{x}\sin\phi) + (Ic^2 + I_w)\ddot{\theta}_1 - Ic^2\ddot{\theta}_2 \\
\tau_2 - \lambda_2 cl &= -m_c cd(\ddot{y}\cos\phi - \ddot{x}\sin\phi) - Ic^2\ddot{\theta}_1 + (Ic^2 + I_w)\ddot{\theta}_2
\end{aligned} \tag{2-31}$$

2.1.4. Dynamic Model of the Motor

In this work, the model described in [19] for energy consumption in a brushed DC motor is used. This detailed model considers the energy dissipated in the resistive winding, the energy required to overcome internal and load friction and the mechanical power delivered to the output shaft. The dynamic model of a DC motor can be expressed by the following system of differential equations [19]:

$$\begin{aligned}
L\dot{i} + Ri + K_w n\dot{\theta} &= V \\
K_t ni - I_s\ddot{\theta} - \nu\dot{\theta} &= \tau + T_m
\end{aligned} \tag{2-32}$$

The first expression in equation 2-32 is the voltage equation for a DC motor, and the second expression reflects the torque of the DC motor. In several studies, such as [41, 42], the torque variable is neglected, which is unrealistic for a real robot. In the proposed model, the load torque value of a dynamic DC motor model is calculated using a mobile robot dynamic model. On the other hand, a calibration procedure is used to estimate the internal friction torque value.
A reduced order model can be achieved for the dynamic behavior of the motor. The electrical response is generally much faster than the mechanical response, in such a way that the inductance of the armature circuit can be ignored. Hence, the first equation yields:

$$i = \frac{V - K_w n \dot{\theta}}{R} \tag{2-33}$$

Equation 2-33 can be used in the second part of equation 2-32 to obtain the torque τ

$$\tau = \frac{K_t n}{R} V - I_s \ddot{\theta} - \left(\frac{K_t K_w n^2}{R} + \nu \right) \dot{\theta} - T_m \tag{2-34}$$

2.1.5. Combination of the Dynamic Models

In order to achieve the energy consumption model, the dynamic models of the robot and the DC motor are combined. The equation for the load torque of the DC motor model, (2-34), can be used in the system of equations for the dynamic robot model, (equation 2-31). Also, $\dot{\phi} = c(\dot{\theta}_1 - \dot{\theta}_2)$, which is calculated from the subtraction of equations 2-2 and 2-3, can be used for re-ordering and writing the resulting combination of the dynamic models in the following matrix equation:

$$M(q)\ddot{q} + F\dot{q} + C(q, \dot{q}) = T\mathbf{V} - A(q)\lambda \tag{2-35}$$

Where:

$$M(q) = \begin{bmatrix} m & 0 & -\alpha_1 & \alpha_1 \\ 0 & m & \alpha_2 & -\alpha_2 \\ -\alpha_1 & \alpha_2 & Ic^2 + I_w + I_s & -Ic^2 \\ \alpha_1 & -\alpha_2 & -Ic^2 & Ic^2 + I_w + I_s \end{bmatrix}$$

$$\alpha_1 = m_c c d \sin\phi$$
$$\alpha_2 = m_c c d \cos\phi$$

$$F = \begin{bmatrix} 0 & 0 & 0 & 0 \\ 0 & 0 & 0 & 0 \\ 0 & 0 & \frac{K_t K_w n^2}{R} + \nu & 0 \\ 0 & 0 & 0 & \frac{K_t K_w n^2}{R} + \nu \end{bmatrix}$$

$$C(q,\dot{q}) = \begin{bmatrix} -m_c d\dot{\phi}^2 \cos\phi \\ -m_c d\dot{\phi}^2 \sin\phi \\ T_m \\ T_m \end{bmatrix} \qquad T = \begin{bmatrix} 0 & 0 \\ 0 & 0 \\ \frac{K_t n}{R} & 0 \\ 0 & \frac{K_t n}{R} \end{bmatrix}$$

$$A(q) = \begin{bmatrix} -\sin\phi & -\cos\phi \\ \cos\phi & -\sin\phi \\ 0 & cl \\ 0 & cl \end{bmatrix} \tag{2-36}$$

2.1.6. Energy Consumption Model

In this section, a state space realization from [92] is used to transform the nonlinear differential equation system representing the combination of the dynamic models into an ordinary differential equation system. In the process, the size of the state space is increased, and the Lagrange multipliers are simplified, using the null space $S(q)$ of the constraint matrix $A(q)$.
Let η represent vector of the new variables, then $A(q)S(q)\eta = 0$, and using equation (2-9), it may also be said that $\dot{q} = S(q)\eta$.
Vector η was chosen as:

$$\eta = \dot{\theta} \text{ where, } \dot{\theta} = [\dot{\theta}_1 \quad \dot{\theta}_2]. \tag{2-37}$$

Being $S(q)$

$$\big[S(q)\big] = \big[s_1(q) \quad s_2(q)\big] = \begin{bmatrix} cl\cos(\phi) & cl\cos(\phi) \\ cl\sin(\phi) & cl\sin(\phi) \\ 1 & 0 \\ 0 & 1 \end{bmatrix}$$

Now, multiplying both sides of equation (2-35) by $S^T(q)$, and using the result $S^T(q)A(q) = 0$, turns into:

$$S^T(q)M(q)\ddot{q} + S^T(q)F\dot{q} + S^T(q)C(q,\dot{q}) = S^T(q)T\mathbf{V} - S^T(q)A(q)\lambda \tag{2-38}$$

Taking the derivative of $\dot{q} = S(q)\eta$ again, the term $\ddot{q}$ is obtained as:

$$\ddot{q} = S(q)\dot{\eta} + \dot{S(q)}\eta \tag{2-39}$$

Replacing $\dot{q}$ and $\ddot{q}$ in equation 2-38.

$$S^T M(S\dot{\eta} + \dot{S}\eta) + S^T F(S\eta) + S^T C = S^T T\mathbf{V} \tag{2-40}$$

Isolating $\dot{\eta}$ from equation 2-40

$$\begin{aligned} S^T MS\dot{\eta} =& S^T T\mathbf{V} - S^T C - S^T FS\eta - S^T M\dot{S}\eta \\ \dot{\eta} =& (S^T MS)^{-1}(S^T TV - S^T C - S^T FS\eta - S^T M\dot{S}\eta) \end{aligned} \tag{2-41}$$

Then, the dynamic model can be represented with a new set of state variables.

$$\mathbf{x} = \begin{bmatrix} x \\ y \\ \theta_1 \\ \theta_2 \\ \dot{\theta}_1 \\ \dot{\theta}_2 \end{bmatrix} = \begin{bmatrix} q \\ \eta \end{bmatrix} \tag{2-42}$$

Equation 2-41 and equation $\dot{q} = S(q)\eta$ may be represented in the state space form as

$$\dot{\mathbf{x}} = f(x) + g(x)V \tag{2-43}$$

where:

$$\begin{aligned} f(x) &= \begin{bmatrix} S(q)\eta \\ -(S^T MS)^{-1}(S^T C + S^T FS\eta + S^T M\dot{S}\eta) \end{bmatrix} \\ g(x) &= \begin{bmatrix} 0 \\ (S^T MS)^{-1} S^T T \end{bmatrix} \end{aligned} \tag{2-44}$$

The voltage variable can be obtained by isolating V from equation (2-40).

$$\mathbf{V} = (S^T T)^{-1}(S^T MS\dot{\eta} + S^T M\dot{S}\eta + S^T FS\eta + S^T C) \tag{2-45}$$

The power estimation model can be calculated with the multiplication of the voltage (equation 2-45) and the current equation (2-33).

$$P(t) = \mathbf{V}^T(t)\, i(t) \tag{2-46}$$

Finally, the energy consumption model can be calculated with the integral of the power estimation model (equation 2-46).

$$E(t) = \int_0^t P(t)\ \ dt \tag{2-47}$$

2.2. Simulation Results

This section is presented the simulation results of the combination of the dynamic models, for several typical robotic tests. Finally, the energy values of the proposed model are compared with the typical motor energy model, using as input a trapezoidal velocity profile.

2.2.1. Simulation of the Dynamic Model Combination

A set of simulations were implemented in Matlab/Simulink, whose results were compared with simulations carried out using Robot Operating System (ROS).
To set up the combination of the dynamic models in Matlab/Simulink, represented by the equation 2-43, the robot and motor parameters of the P3-DX mobile platform presented in Kim's work [41] were used. These parameters are shown in tables (**2-1 2-2**). Also, the P3-DX robot online ROS packages were used to replicate the same experiment in the ROS/Stage simulator.

Table 2-1.: Robot parameters of the P3-DX.

Robot parameters	r	l	d	m_c	m_w
Value	0.095 m	0.165 m	0	6.04 Kg	1.48 Kg

Table 2-2.: Motor parameters of the WMR, P3-DX

Motor parameters	R	ν	I_s	K_w	K_t
Value	0.7 Ω	0.035 Nm /(rad/s)	0.0713 Kg m^2	0.88 (rad/s)/V	0.88 Nm/A

Two different kinds of tests were used for testing the combination of the dynamic models numerically. Failure of any of those tests represents an accumulative error in the mathematical modeling, in the numerical estimation, or the calibration of the dynamic parameters.

Straight path simulation

In the first test, in the Matlab/Simulink simulator, two positive or negative constant voltages were used, with the same amplitude as an input of the motor voltages. It was expected that the center of mass (COM) of the robot would describe a linear movement with the same orientation

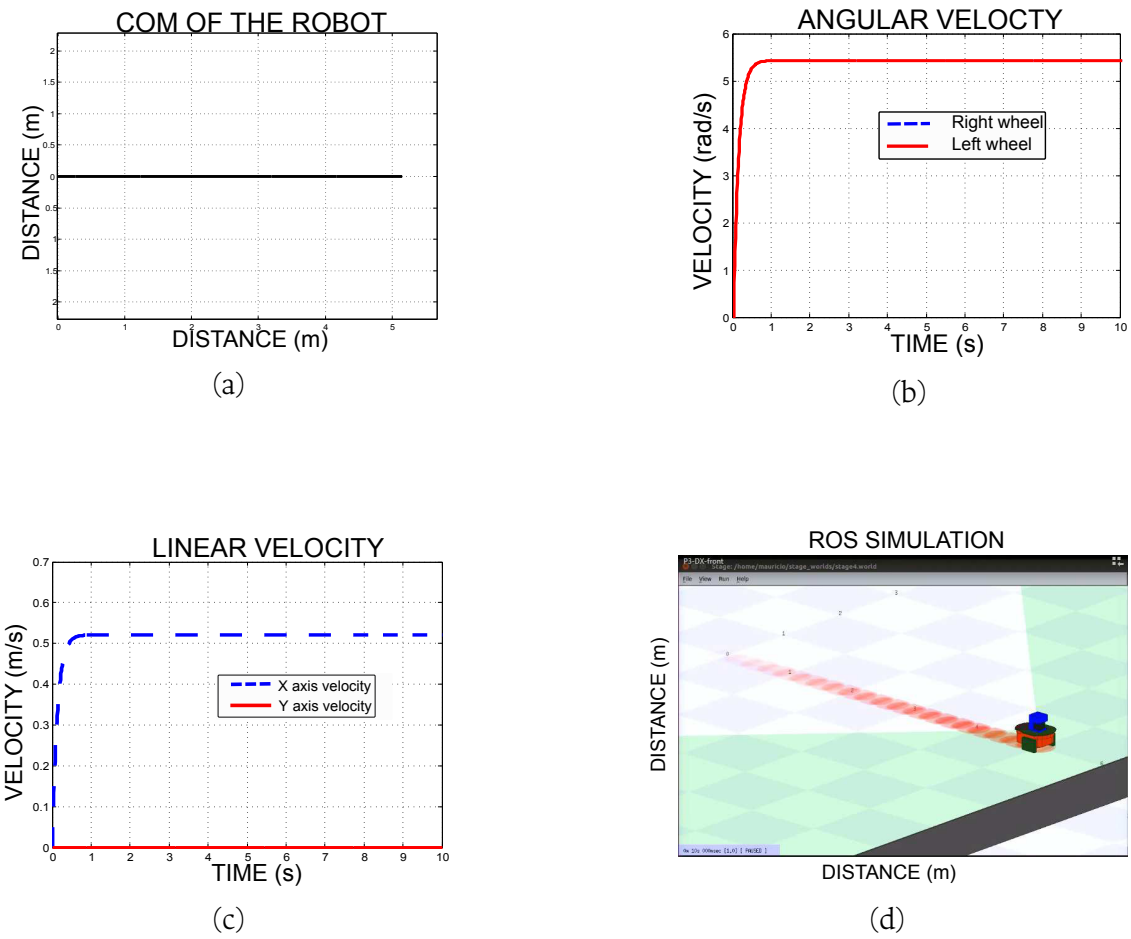

Figure 2-2.: Response of the dynamic model combination to constant 5 V inputs in both motors, with a simulation time of 10 s, with initial conditions equal to zero. The robot describes a linear movement on the x-axis of 5.14 meters. (**a**) Path of the robot COM. (**b**) Angular velocities of the wheels. After bet the internal friction of the motors, the wheels present a constant velocity. (**c**) Linear velocities on the x and y axis. (**d**) Path of the robot COM in ROS/Stage simulator

.

of the initial condition. A deviation of this orientation can represent a failure in the calculation of the angular velocity of the wheels. The failure can be produced by an accumulative error in the numerical approximation of the solution of the differential equations, in the mathematical modeling, or in the initial condition.
Then, the linear velocity of the robot resulting from the Matlab/Simulink simulation was used as input of the ROS/Stage simulation.
In figure **2-2** one simulation result is shown, in this case, the voltage input in both robot motors is 5 V, in a simulation time of 10 s. The final position of the robot in the Matlab/Simulink simulation was 5.14 m, and in ROS/Stage simulation was 4.94 m, giving an error of 0.2 m, and a relative error of 3.8%. In that case, the test presents successful results.

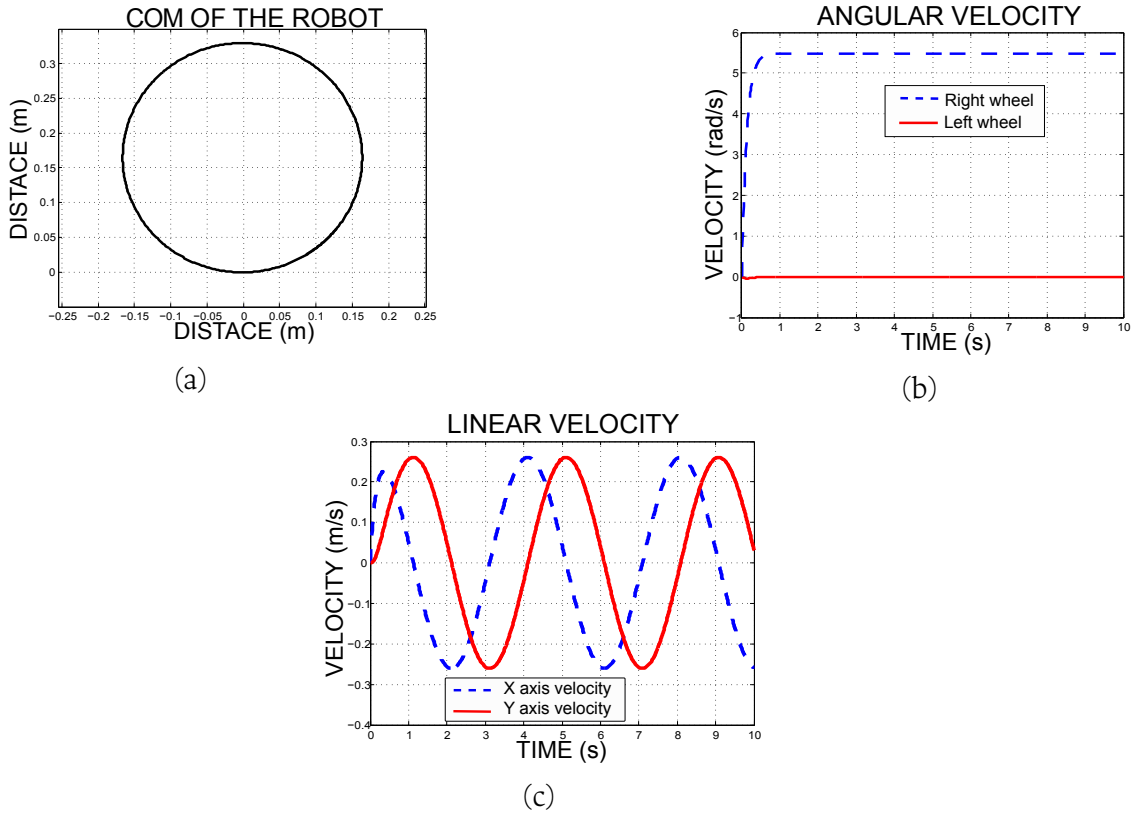

Figure 2-3.: The response of the dynamic model combination to constant 5 V inputs to the left motor, and zero in the other, with a simulation time of 10 s with initial conditions equal to zero. The COM of the robot describes a circumference with a radius of 0.165 m (constant b). (**a**) path of the robot COM and control points. (**b**) Angular velocities of the wheels. After bet the internal friction of the motors, the wheels present a constant velocity. (**c**) Linear velocities along x and y-axis

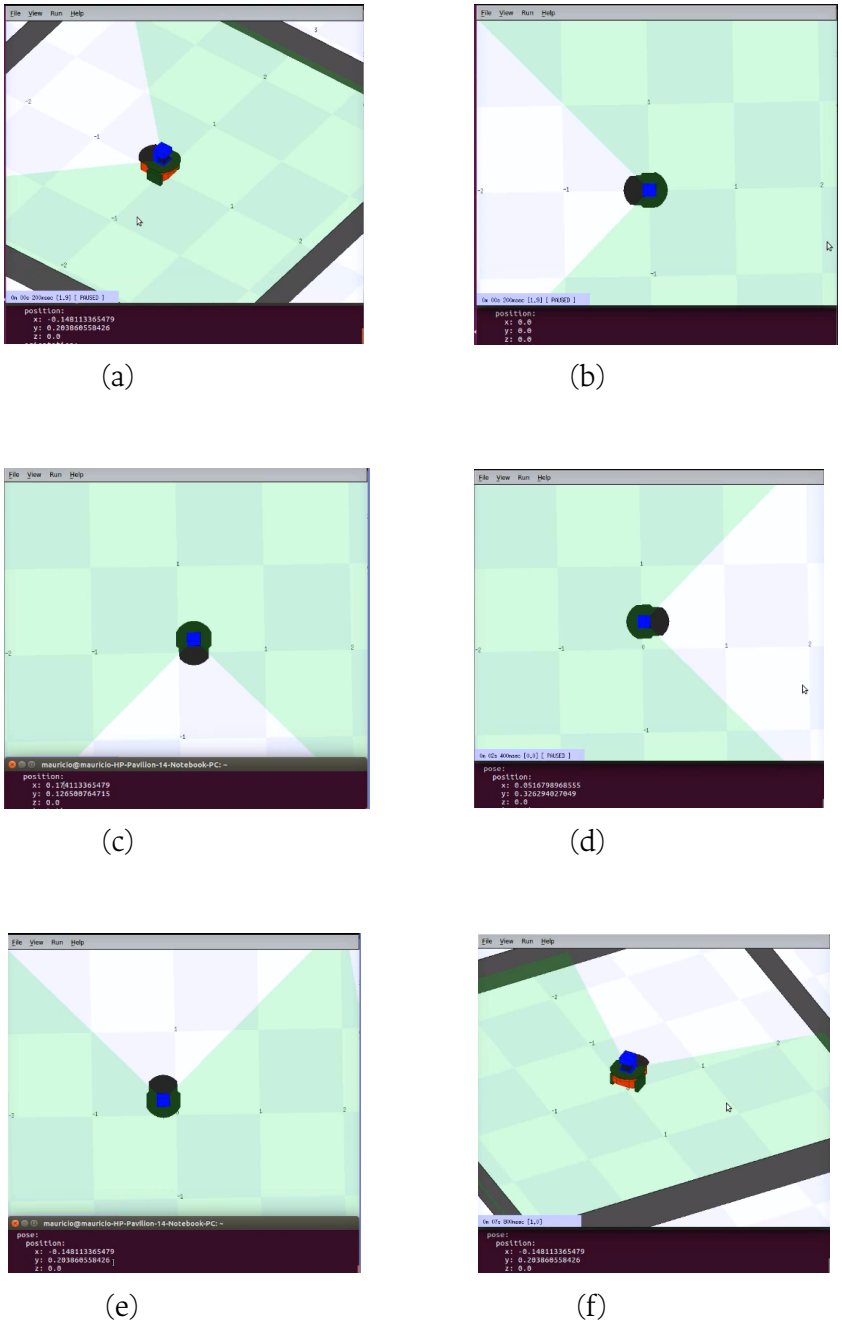

Figure 2-4.: Simulation results in Stage/ROS simulator using as input the linear and angular velocities of the robot, given by the Matlab/Simulink simulator. The radius of the circumference is the distance between the wheels and the axis. (**a**) Start of the simulation with an orientation of the robot equal to 0 rad. (**b**) Robot orientation equal to 0. Top view. (**c**) Robot orientation equal to $\pi/4$. (**d**) Robot orientation equal to $\pi/2$. d) Robot orientation equal to $3\pi/2$. (**e**) The end of the simulation. Robot orientation again to 0 rad. (**f**) Robot orientation equal to 0 rad. Diagonal view.

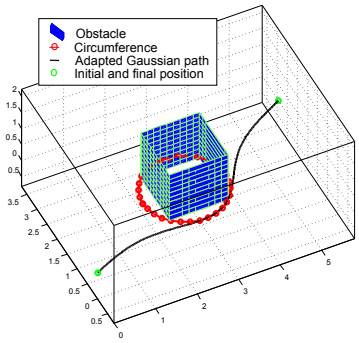

Figure 2-5.: Adapted Gaussian path

Curved path simulations

For the curvature path, a path planning from previous work, based on the Gaussian function, is proposed. In this case, a cube is selected as an obstacle; a circumference delimited the base of the cube. When the mobile robot moves from an initial point to a goal point and has to avoid the obstacle, a Gaussian function is adapted to pass through the circumference, as shown in the Figure **2-5**. The equation that represents the Gaussian function is:

$$y_d = ae^{\frac{-(x_d-f)^2}{2h^2}} \tag{2-48}$$

Where x_d and y_d represents the desired path, f is the position of the center of the peak, and a is the height of the curve's peak. The Gaussian function is adapted to the circumference, if f is the same center of the circumference, and a is the same radius of the circumference. The variable h is the standard deviation that controls the width of the bell. The correct estimation of this variable prevents the desired path from passing through the circumference area.
Once the curvature path is obtained, the angular velocities of the wheels can be calculated using the kinematic inverse of the mobile robot, which is represented by the following matrix:

$$\begin{bmatrix}\dot{\theta}_1\\ \dot{\theta}_2\end{bmatrix} = \begin{bmatrix}\frac{\cos\phi}{r} & \frac{\sin\phi}{r} & \frac{2l}{r}\\ \frac{\cos\phi}{r} & \frac{\sin\phi}{r} & -\frac{2l}{r}\end{bmatrix}\begin{bmatrix}\dot{x_d}\\ \dot{y_d}\\ \dot{\phi}\end{bmatrix} \tag{2-49}$$

2.3. SIMULATION AND FINAL RESULTS

The energy consumption of the mixed energy model represented by Equation (2-47) and the motor energy model [41, 78] is compared, when the mobile robot travels on straight and curvature paths, a path planning usually has these two kinds of paths. In order to set up both energy models, the robot and motor parameters of the P3-DX mobile platform present in Kim's work, were used. These parameters are shown in tables **2-1**, **2-2**.

2.3.1. Simulations of the Energy Estimation Models

Simulations were performed to test the energy estimation model, based on the dynamic model combination using the dynamic parameters contained in tables **2-1**, **2-2**. Energy consumption was compared between the proposed energy model and the motor energy model, with the commonly used trapezoidal velocity profile as the angular velocity of the wheels. First, the angular velocity in both wheels is the same, to the mobile robot following a linear path. Different trapezoidal velocity profiles with a fixed path distance and different load weights are used as input to the models. In figure **2-6**, the input velocities and the COM of the robot are shown.

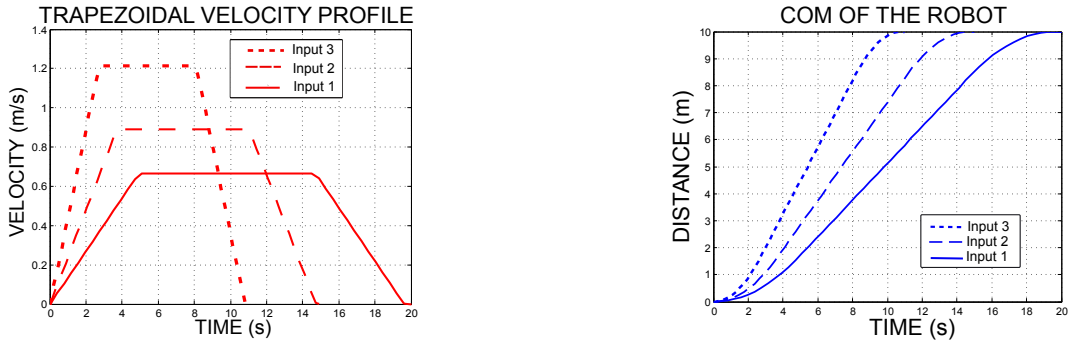

(a) (b)

Figure 2-6.: (**a**) Trapezoidal profile velocities for a linear distance of 10 meters, The velocities increase until the P3-DX robot is at maximum velocity (1.2 m/s). (**b**) Mass center of the robot with the trapezoidal velocity profile as input, with final times of 11, 15 and 20 seconds.

.

Figure **2-7** shows the energy consumption of the proposed energy estimation model, as compared to the motor energy model. In this case, the robot mobile follows a linear path of 10 m, at the maximum trapezoidal velocity (1.2 m/s), with the maximum load weight (7.6 Kg) allowed by the P3-DX mobile robot, and a fixed robot weight of 6.04 Kg. Figure **2-7** also shows that, during the acceleration, the power and energy consumption increase faster in the values given by the combination energy model, but are the same when the velocity profile remains at the maximum value. During the deceleration, a certain amount of energy is regenerated and stored in the batteries. The recovered energy allows the balancing of the higher initial energy consumption values in the proposed energy model. The energy regenerated is equal to 1.05 J for the motor energy model, and 9.07 J for the combination energy model. The total energy consumption in the motor energy model is the 98.84 J, and the proposed energy model is 104.3 J. But, during acceleration, the difference of maximum energy consumed in both models, it is even higher. The energy consumption in the motor energy model is equal to 22.03 J, and in the proposed energy model, 36.74 J.

Table **2-3** shows the energy consumption values given by the energy models when the robot follows a linear path of 10 m, with a payload of 3.76 kg, and with different maximum set velocities

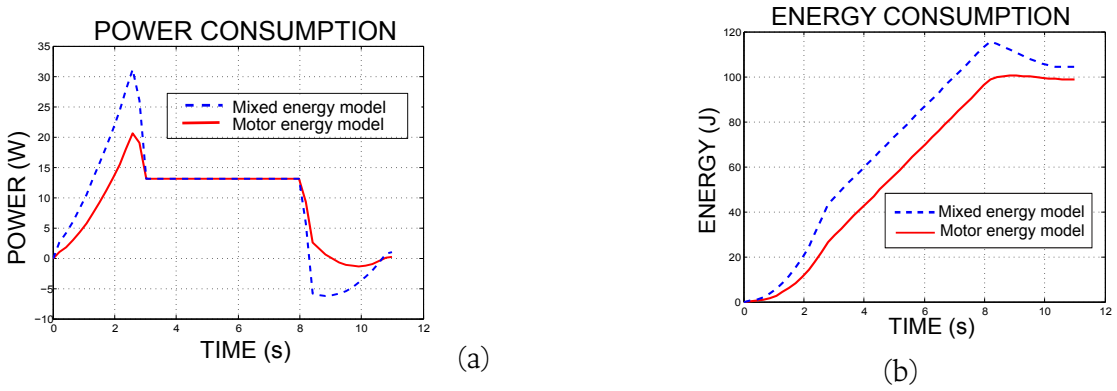

Figure 2-7.: Simulation with a maximum trapezoidal velocity (1.2 m/s), maximum load weight carried by the mobile robot (7.6 Kg), and a robot weight of 6,04 Kg, for a linear distance of 10 meters. **(a)** Power consumption given by the energy models. **(b)** Energy consumption given by the energy models

.

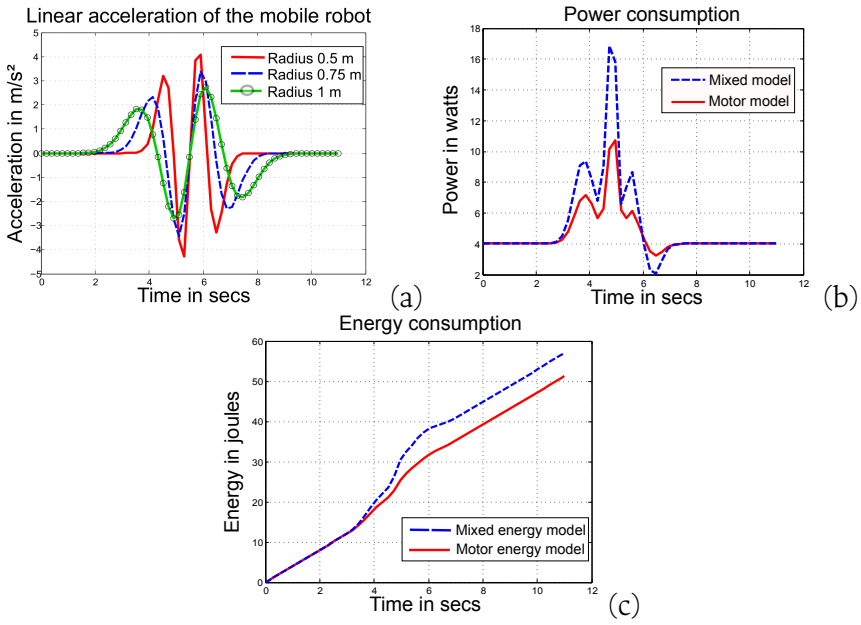

Figure 2-8.: Simulation with a Gaussian function adapted to a circumference that delimited the obstacle, maximum load weight carried by the mobile robot (7.6 kg), and a mobile robot weight of 6,04 kg. (a) Linear acceleration of the wheels for the circumference radius of 0.5 m, 0.75 m, and 1 m. (b) Power consumption is given by the energy models for a radius circumference of 0.5 m. (c) Energy consumption provided by the energy models for a radius circumference of 0.5 m.

of the trapezoidal profile. Energy consumption in both energy models increases as the velocity rise because both models depend on the kinematic robot model and the dynamic motor model. Energy values are higher in the proposed energy model because only this model depends on the dynamic parameters of the robot as a payload and robot weights, as well as moments of inertia. It is for this reason that, in Table **2-4**, when the trapezoidal velocity is 0.88 m/s and the payload increases, only the proposed model is considerably affected. The distance in the testing cases is fixed, because any change of distance with a constant simulation time affects the angular velocity of the wheels. These cases are already studied in the results, with different trapezoidal velocity profiles.

Table 2-3.: Simulation results of the energy models. Different kinds of maximum velocities in the trapezoidal profile, and a fixed load and robot weight were used.

Trapezoidal velocity	Energy consumption	
Maximum velocity	Motor energy model	Proposed energy model
0.66 m/s	53.65 J	54.51 J
0.88 m/s	71.89 J	73.68 J
1.21 m/s	98.85 J	102.9 J

Table 2-4.: Simulation results of the energy models with different load weights, with a fixed robot weight 6.04 Kg, and with a fixed velocity of 0.88 m/s.

Robot parameter	energy consumption	
Load and robot weight	Motor energy model	Proposed energy model
6.04 Kg	71.9 J	73.15 J
9.8 Kg	71.89 J	73.68 J
13.64 Kg	71.88 J	74.25 J

For the study of energy consumption when a mobile robot travels on a curvature path, an initial and goal position for the desired path is (x_d = 6, y_d = 4), the position of the circumference center is (x_c = 3, y_c = 2), the edge length of the obstacle cube is 0.7 meters. The only variable that changes for this study's proposes is the circumference radius that delimited the obstacle. In the Figure **2-8**(a) is shows that the linear acceleration of the mobile robot is inversely related to the circumference radius, because a smaller radius represents a narrow bell of the adapted Gaussian function, forcing the mobile robot to accelerate to reach the peak. Is for that reason that in the table **2-5** with a smaller circumference radius, power and energy consumption is higher, despite the facts that, in the other cases, the travel distance is greater. Finally, in the Figure **2-8** the behavior of the energy models when travels on a curvature path remains the same as on the straight path, the mixed energy model increases its energy values compared to the motor energy model, when the mobile robot accelerate, because the dynamic parameters of the robot, are taken into consideration in the energy model proposed.

Table 2-5.: Energy consumption of the models when the radius circumference of the adapted Gaussian function changing.

Parameters		Energy consumption	
Radius	Distance	Motor	Mixed
0.5 m	7.06 m	51.26 J	56.96 J
0.75 m	7,17 m	50.13 J	52.04 J
1 m	7.28 m	50.74 J	51.66 J

In this chapter, an energy model that takes the robot and motor dynamic parameters into account is proposed. The energy consumption of the combined energy model was compared to a typical motor energy model. The angular velocities of the wheels for traveling on straight and curvature paths are used as input of the models. The simulation results show that the highest percentage of energy consumption came from the motors. However, during mobile robot acceleration, the dynamic parameters of the robot, such as inertia moments, robot weight, or load weight, also influenced total energy consumption. It is for that reason that the energy values in figure **2-7** (b),(c), **2-8** (b), (c), and in tables **2-3**, **2-4**, **2-5** are higher in the mixed energy model than those of the DC motor energy model, because the proposed model consider the DC motor and the mobile robot dynamic models. However, in the deceleration phase, a certain amount of energy was regenerated and stored in the batteries. This behavior allows for the reduction of the total difference in energy consumption between energy models. A good estimation of power and energy consumption, as presented, can be more easily related to the real-time autonomy of mobile robots, which carry their energy source.

3. Hardware Validation of the Proposed Energy Model

The hardware validation of the proposed model was obtained using the Nomad Super Scout differential drive mobile robot test platform, property of Coimbra University of Portugal.
The energy consumption model was implemented in MATLAB/Simulink. In the model, the dynamic parameters of the robot (Table **3-1**), and the dynamic parameters of the DC motors (Table **3-2**), were used.

Table 3-1.: Parameters of the Nomad Super Scout Robot

Parameter	Value	Parameter	Value
r [m]	0.1	m_c [kg]	21.2
l [m]	0.165	m_w [kg]	1.39
d [m]	0		

Table 3-2.: Motor parameters of the Nomad Super Scout Robot. Reference: PITTMAN GM14900

Parameter	Value	Parameter	Value
R [Ω]	2.74	K_w [(rad/s)/v]	0.069
ν [Nm/(rad/s)]	0.0017	K_t [Nm/A]	0.069

The robot is controlled using the built-in Motorola 68332 embedded robot controller and an Orange Pi Pc Plus single-board computer. The robot Operating System (ROS) was used on the Orange Pi to send the desired velocities to the robot and to receive odometry values from the encoders, as well as the power values of the motors from a custom power measurement circuit. Three batteries with weights of 5.7 kg, 2.55 kg and 2.25 kg were used as payloads for the robot. The batteries were fixed on top of the robot in various combinations to achieve payload weights of 2.5 kg, 5.7 kg, 8.25 kg and 10.5 kg (figure **3-1**).

3.1. Calibration Procedure

A calibration procedure was carried out to estimate the internal friction torque of the motors. The internal friction torque is related to opposing forces applied to the robot, e.g. the friction

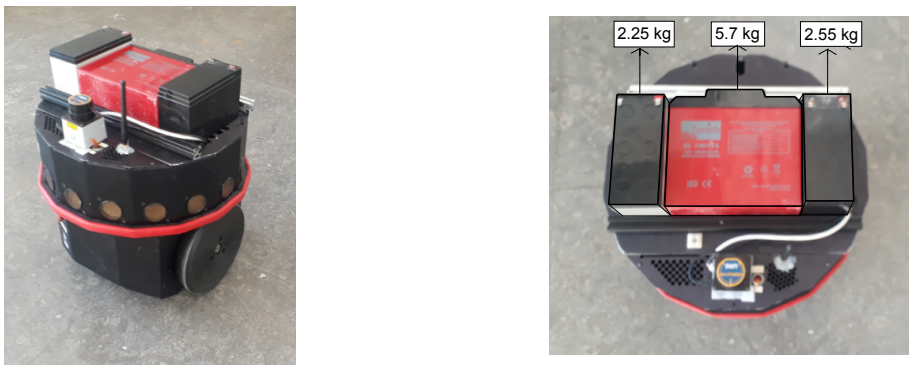

(a) (b)

Figure 3-1.: (**a**) The Nomad Super Scout mobile robot used in this work. (**b**) Top view of the robot, showing all the batteries that were used to vary the payload.

of the wheels with the floor and the friction in the gears. However, the load torque is related to the acceleration, mass of the robot, and the payload, and it is calculated using the dynamic robot model. Therefore, the dynamic motor model can be used for calibration. The friction torque of the motor can be found by assuming no acceleration. In this case, the model can be written as:

$$\begin{aligned} i(t) &= b_1 + b_2\,\dot{\theta} \\ V(t) &= c_1 + c_2\,\dot{\theta} \end{aligned} \tag{3-1}$$

where:

$$b_1 = \frac{T_m}{K_t n} \qquad b_2 = \frac{\nu}{K_t n}$$

$$c_1 = \frac{RT_m}{K_t n} \qquad c_2 = \frac{R\nu}{K_t n} + K_w \text{ n}$$

Then, the averages of the current and voltage were calculated using the power values from the measurement circuit, when the robot reaches and stays in a constant linear velocity. In the experiment, constant velocities ranging between 0.1 m/s and 0.9 m/s were used. In Figure **3-2**, current (**3-2**(a)) and voltage (**3-2**(b)) for a constant velocity of 0.8 m/s are shown. The shaded section represented the acceleration and deceleration of the robot and, is thus excluded from the calibration procedure. Finally, the energy consumed by the robot was calculated using equation (2-47).

The experiment for the calibration procedure was performed without payload, on a marble floor, along a fixed 20 m straight path. The estimate of the friction torque is obtained using least squares fitting. The friction torque values for the motors were found out to be 0.3728 Nm and 0.346 Nm. In figure **3-3**, both the energy consumed by the robot and the energy estimated by the model are shown.

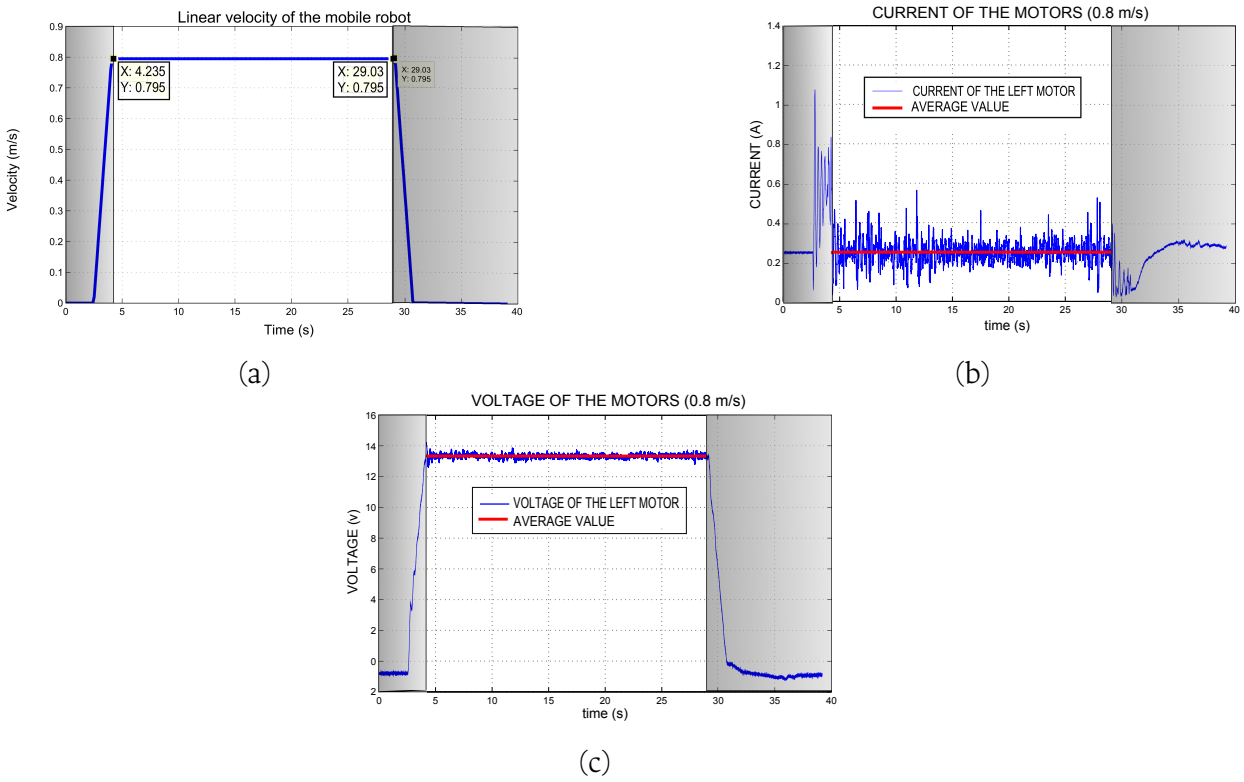

Figure 3-2.: Calibration procedure experiment for a constant velocity of 0.8 m/s. The robot moves in a straight path on marble floor without payload. The acceleration and deceleration of the robot are not taken into account (shaded section): (**a**) odometry values from encoders (maximum velocity 0.8 m/s). (**b**) The current of the left motor and average value. (**c**) The voltage of the left motor and average value.

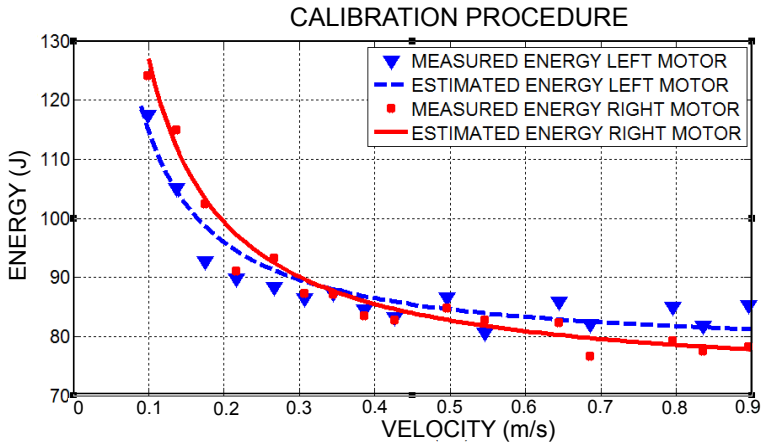

Figure 3-3.: Estimated and measured energy consumption values for different velocities tested in the calibration procedure experiments.

3.2. Experimental Validation of the Proposed Model

For the validation of the proposed power estimation model, the Nomad Super Scout mobile robot was used. A set of experiments were performed to verify the fitness of the power model for a typical mobile robot usage scenario, such as carrying various payloads or moving with different accelerations along straight and curved paths.

3.2.1. Straight Path Validation

In the experiments for the straight path validation, the mobile robot was commanded to cover a distance of 10 m, on a straight path, on a marble floor, with and without payload. A constant acceleration was applied to the robot for 4 s until it reached the desired distance. This test was repeated several times for each acceleration. The weights of the payloads were 2.55 kg, 5.7 kg, 8.25 kg and 10.5 kg, and the various accelerations were 0.125 m/s^2, 0.15 m/s^2, 0.175 m/s^2, 0.2 m/s^2, 0.225, m/s^2 and 0.25 m/s^2. During validation along straight paths, the angular velocity and acceleration of the wheels were the same. This behavior allows us to simplify the mathematical model into a cost function that can be used for the optimization procedure. The simplified power model depends on the angular velocity and acceleration of the wheels, as well as the payloads. The power model equation representing the experimental setup was calculated using equation 2-46 and the robot and motor parameters from Tables **3-1** and **3-2** and it is given by

$$P_1 = 0.0203\ddot{\theta_1}^2 + 0.148\ddot{\theta}_1\dot{\theta}_1 + 0.0014\ddot{\theta_1}^2 m_p + 0.102\ddot{\theta_1} + 0.0017\dot{\theta_1}^2 + 0.005\ddot{\theta}_1\dot{\theta}_1 m_p \\ +0.373\dot{\theta_1} + 0.0034\ddot{\theta}_1 m_p + 0.129; \tag{3-2}$$

$$P_2 = 0.0203\ddot{\theta_2}^2 + 0.148\ddot{\theta}_2\dot{\theta}_2 + 0.0014\ddot{\theta_2}^2 m_p + 0.0949\ddot{\theta_2} + 0.0017\dot{\theta_2}^2 + 0.005\ddot{\theta}_2\dot{\theta}_2 m_p \\ +0.346\dot{\theta_2} + 0.0032\ddot{\theta}_2 m_p + 0.111; \tag{3-3}$$

In Figure **3-4**, the results of a medium acceleration as the robot was carrying 5.7 kg are shown. In the Figure **3-4**(b), it can be seen that the power estimation model predicts the average power consumed by the motor closely.
Measured and estimated energy consumptions for various accelerations is shown in Tables **3-3** and **3-4**. The accelerations were applied to the robot, first without payload, and then with a payload of 8.25 kg. The Tables show a change in the robot's energy consumption when the accelerations of the robot increase. By comparing the results in Tables **3-3** and **3-4**, it is evident that the energy consumption of the robot increases when the robot carries 8.25 kg of payload.

In Figure **3-5**, the experimental results for three different accelerations and the various payloads are summarized. The Figure also shows that no matter the acceleration when the payload

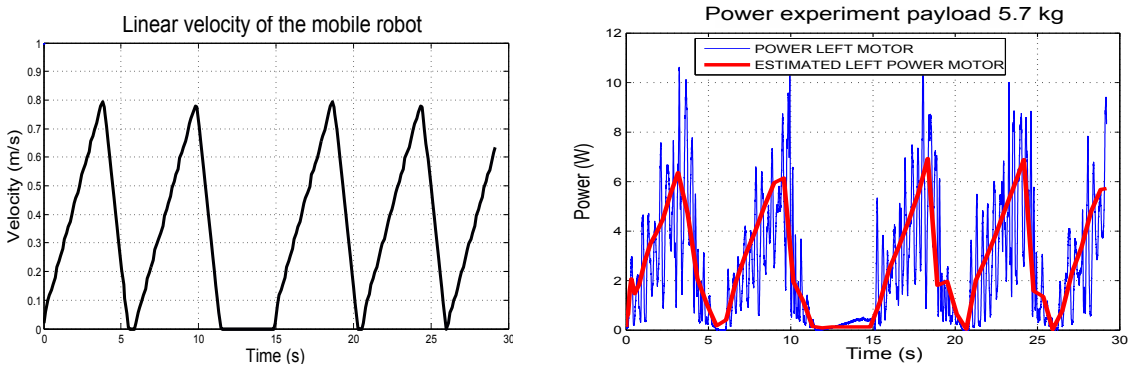

(a) (b)

Figure 3-4.: Validation experiment for accelerations of 0.2 m/s^2: (**a**) The linear velocity of the robot (odometry data). (**b**) Measured and estimated power values.

.

increases, the energy consumption of the robot increases as well. The highest energy consumption of the robot happens at maximum acceleration with maximum payload (162.7 J). Figure **3-5** also shows that maximum acceleration with any payload can generate more robot energy consumption than the lowest accelerations with the same payload.

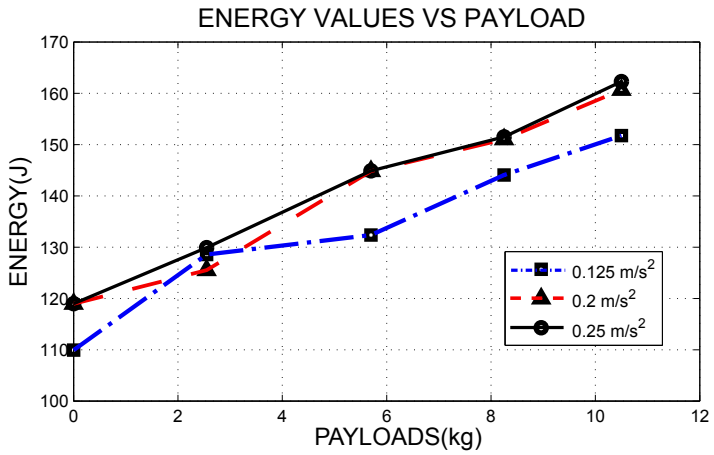

Figure 3-5.: Energy consumption values of the robot with several accelerations and payloads, along a straight path.

Finally, the error percentages between the measured and predicted energy values for different payloads and accelerations are shown in Table **3-5**. The results show the fitness of the power model evaluated along straight paths. It is important to note a successful result of the experiment is attained when the error between the energy estimation and the measured energy values is less than 10% (state-of-the-art good performance [10]). The experiment with 0.225 m/s^2 of acceleration and without payload was the only one with a relative error higher than 10%. However, in almost all other experiments, the error falls below 8%,; in most cases, it falls below 5%. The

Table 3-3.: Energy values of the robot and the estimated model, for the experiment without payload

Energy values - Without payload				
	Robot data (Joules)		Model value (Joules)	
Accelerations	Left motor	Right motor	Left motor	Right motor
0.125 m/s^2	56.25	53.67	60.48	57.6
0.15 m/s^2	58.91	56.92	60.99	58.47
0.175 m/s^2	60.26	56.33	63.57	60.28
0.2 m/s^2	61.26	57.69	64.9	62.77
0.225 m/s^2	60.76	56.78	66.13	64.18
0.255 m/s^2	61.37	57.61	65.14	64.31

Table 3-4.: Measured and estimated energy consumptions with payload along straight paths

Energy values - Payload 8.25 kg				
	Robot data (Joules)		Model value (Joules)	
Accelerations	Left motor	Right motor	Left motor	Right motor
0.125 m/s^2	67.56	64.81	65.11	62.2
0.15 m/s^2	69	67.8	67.16	64.59
0.175 m/s^2	70.4	66.38	70.02	67.7
0.2 m/s^2	74.66	70.17	72.97	70.78
0.225 m/s^2	70.9	66.62	74.34	72.4
0.255 m/s^2	74.7	70.18	78.06	76.26

table shows that the best performance of the power model is at the middle of the validation set of accelerations for medium and high payloads. In this scenario, 29 out of 30 total experiments were successful. The percentage of fitness of the predicted energy consumption compared with the robot energy consumption can be calculated using equation 3-4.

$$fitness(\%) = \frac{Successful\ test}{total\ test} \times 100 \tag{3-4}$$

In that case, the percentage of fitness for the experiment along the straight path equals 96.67%. Overall, test results show that the model is accurate by the standars of the state of the art.

Table 3-5.: Error between the predicted and measured energy. Straight path experiment.

accel/payl	0 kg	2.5 kg	5.7 kg	8.25 kg	10.5 kg
0.125 m/s^2	7.42 %	5.29 %	3.82 %	7.89	9.25%
0.15 m/s^2	3.13%	0.13%	3.69%	5.11 %	8.46%
0.175 m/s^2	5.99%	6.7 %	0.69 %	0.53%	2.85%
0.2 m/s^2	7.33 %	7.2 %	0.75 %	0.2 %	1.92%
0.225 m/s^2	10.86%	8.1 %	6.7 %	5.33 %	0.17%
0.25 m/s^2	8.8%	9.85%	6.52%	7.94 %	5.04 %

3.2.2. Curve path validation

In this experiment, the fitness of the power estimation model along curved paths is evaluated. For this, the mobile robot was moved along third order Bézier curves on the marble surface. The accelerations, payloads, and directions of the robot were varied. The payloads used were 5.7 kg, 8.25 kg, and 10.5 kg. The equation of the third order Bezier curve that was used in this experiment is given by

$$B(t) = (1-t)^3 p_0 + 3(1-t)^2 t p_1 + 3(1-t) t^2 p_2 + t^3 p_3 \tag{3-5}$$

where B is the Bézier curve, t is the parametric variable ($0 < t < 1$), and p_0, p_1, p_2, p_3 are the curvature control points.

The control points were chosen taking into account the dimensions of the hall where the experiment were conducted, leading to $p_0 = 0$, $p_1 = 2.7$, $p_2 = 2.7$ and $p_3 = 2.7$. The robot was commanded to follow the Bézier's curve. The linear and angular velocities of the robot were received from the encoders. In Figure **3-6**, the linear velocity of the robot giving by the odometry along a right bending Bezier's curve with no payload can be seen.

In Figure **3-7**, the pose and linear velocities of the robot at different accelerations are shown (second shaded section) when the robot follows the Bézier curve path. The accelerations are equal to

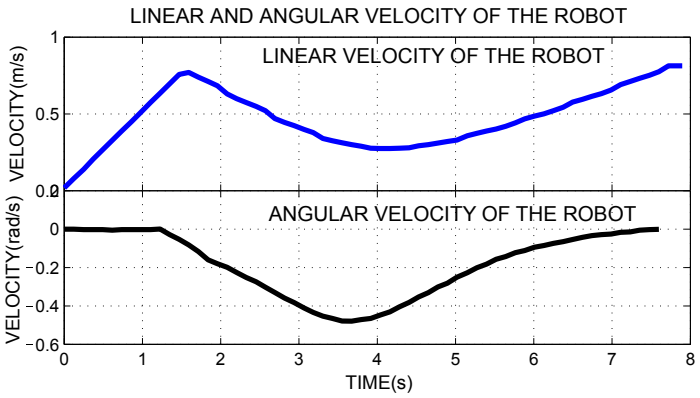

Figure 3-6.: Linear and angular velocities of the robot during a Bézier curve path experiment, with an acceleration of 0.18m/s^2, the right direction, and without payload

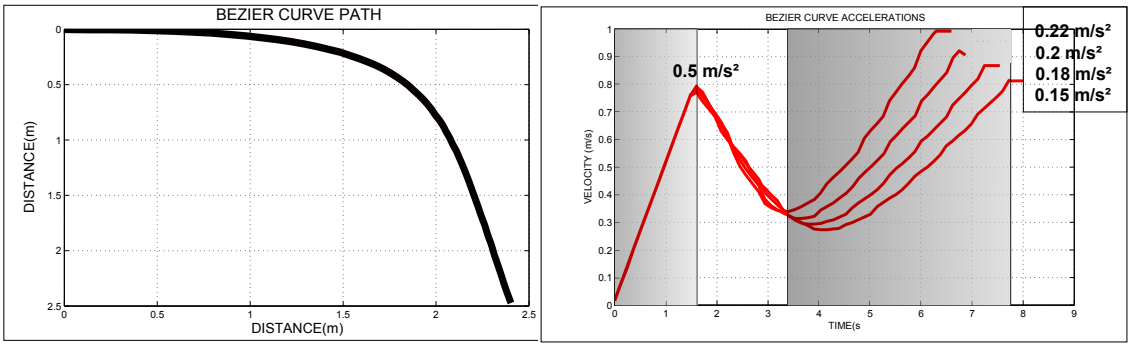

(a) (b)

Figure 3-7.: The pose and linear velocity of the robot with different accelerations. (**a**) Pose of the robot. (**b**) Bézier curve accelerations.

0.15 m/s^2, 0.18 m/s^2, 0.2 m/s^2, and 0.22 m/s^2. The first acceleration in the figure (first shaded section) corresponds to the acceleration applied by the robot controller in order to reach a desired maximum velocity before taking the Bézier curve path. This acceleration is equal to 0.5 m/s^2.
The odometry values given by the encoders are the linear velocity of the robot and the quaternion orientation values. But, the variables needed as an input of the proposed estimation energy model are the angular velocities of the wheels, which can be calculated with the equation 3-6 based on the robot kinematic equations.

$$\begin{aligned} \dot{\theta_1} &= \frac{2v + lw}{2r} \\ \dot{\theta_2} &= \frac{2v - lw}{2r} \end{aligned} \tag{3-6}$$

The only variable remaining is the angular velocity of the robot, which can be calculated using the quaternion orientation provided for the odometry data.
A unit quaternion can be described as:

$$Q = [q_w \; q_x \; q_y \; q_z] \tag{3-7}$$

The quaternion can be transformed into a roll, pitch, and yaw representation, but in this case, only the yaw representation is needed (angular position of the robot ϕ). The equation that transforms the quaternion to yaw representation is shown below:

$$\phi = \text{atan}\left(\frac{2(q_w q_z + q_x q_y)}{q_w^2 + q_x^2 - q_y^2 - q_z^2}\right) \tag{3-8}$$

The angular velocity of the robot is calculated by applying the derivative of the angular position of the robot (Figure **3-6**). Figure **3-8** shows the orientation of the robot and the angular velocities of the wheels calculated using the encoder values for the experiment with an acceleration of 0.15 m/s^2. In this case, the angular velocities of the two-wheels are different around t= 4s, which was necessary to change the direction of the robot.
Finally, the energy consumed by the robot is estimated with the proposed power model, using the angular velocities of the wheels and different payloads as input. These estimated energy values were compared to the energy measured with the power measurement circuit on the robot. In Figure **3-9**, the measured and estimated power values for a no-payload experiment with 0.18 m/s^2 of acceleration, left direction is shown. The measured energy consumption in the left motor was 24.1 J and in the right motor 22.86 J. The estimated energy consumption of the left motor was 26.56 J and of the right motor 24.42 J, giving an error percentage of 9.26% for the left motor, 6.39% for the right motor, and 8.56% for the total.
As evidenced by the data, the proposed power model overestimated the power in the initial acceleration of the robot. This behavior appears because the load torque was calculated with the dynamic robot model, which may be overestimated as well. Nevertheless, this procedure allows the prediction of energy consumption with different accelerations and payloads.

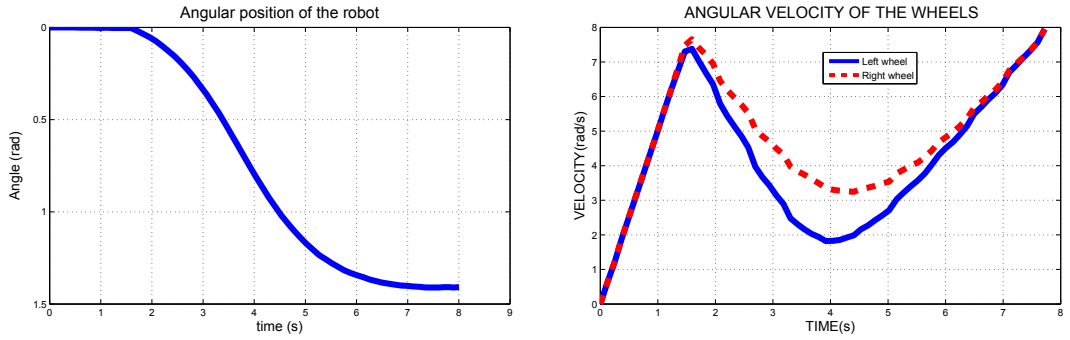

(a) (b)

Figure 3-8.: Measured and estimated power consumptions during a Bézier curve with 0.18 m/s^2 of acceleration, without any payload, along a Bézier curve, left direction. (**a**) Power of the left motor (**b**) Power of the right motor.

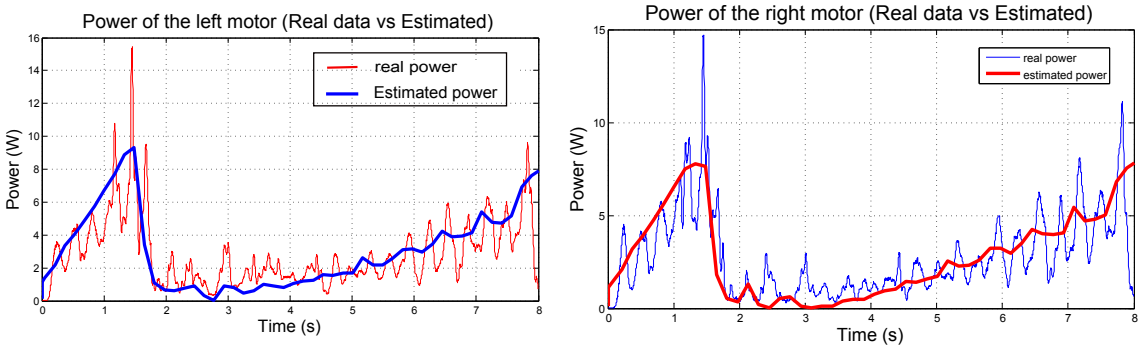

(a) (b)

Figure 3-9.: Measured and estimated power consumptions during a Bézier curve with 0.18 m/s^2 of acceleration, without any payload, along a Bézier curve, left direction. (**a**) Power of the left motor (**b**) Power of the right motor.

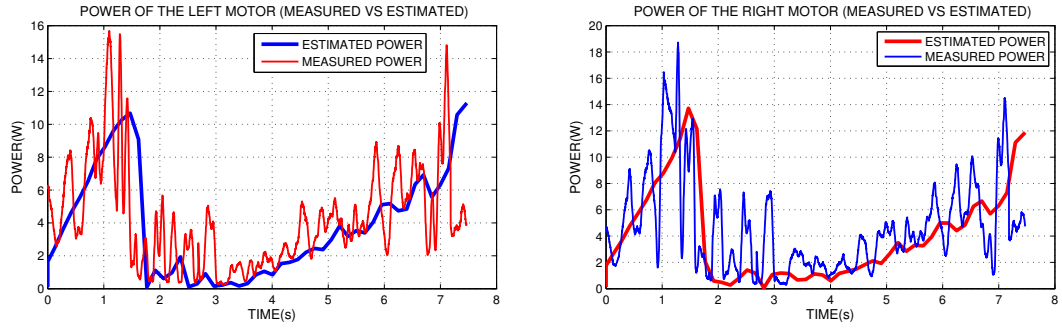

(a) (b)

Figure 3-10.: Measured power robot data compared with the estimation power value. In an experiment with 0.18 m/s^2 of acceleration, with 10.5 kg of payload, along a Bézier curve, left direction. (**a**) Left power motor (**b**) Right power motor.

On the other hand, the overestimated behavior of the proposed model starts to decrease as the payload increases. The experiment result with payload presents a better estimation in the initial acceleration of the robot, as shown in Figure **3-10**. In the Figure, the estimated power shows an underestimated behavior at the start of the second acceleration phase.

In Tables **3-6**, the results of the measurement and predictive energy consumption values of the robot are shown. The behavior of the robot along a Bézier curve is similar to its behavior along a straight path. A small change in the acceleration changes the energy consumption slightly. For example, the Table shows that without payload, the difference in the energy consumed between 0.15 m/s^2 and 0.22 m/s^2 is almost 3 J for the left motor and barely change for the right one. As evidenced in Table **3-7**, substantial changes in payload cause significant changes in consumed energy. For example, a 10.5 kg payload causes the robot to consume almost 12 J more in the left motor and almost 7 J more in the right.
In Figure **3-11**, the behavior of the energy consumed by the robot for three accelerations and various payloads is presented. The Figure also shows the maximum energy consumption of the experiment was 66.97 J, with a medium acceleration at maximum payload. At medium payloads, the energy consumption of the robot increases as the acceleration increases.

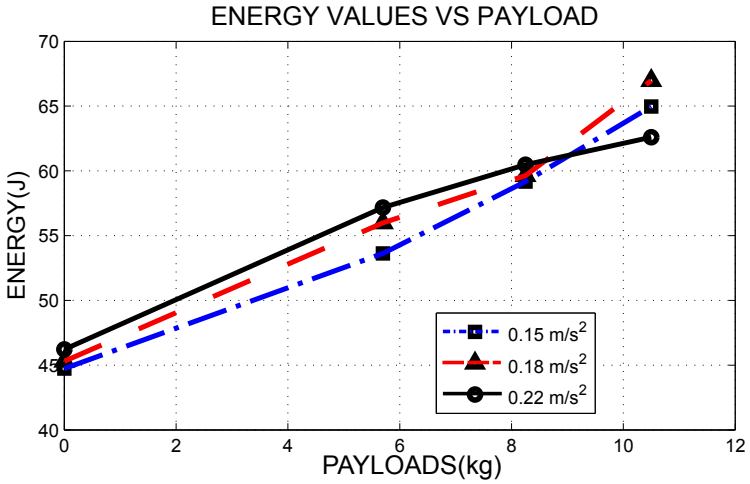

Figure 3-11.: Energy consumption values of the robot with several accelerations and payloads, on Bezier curve path.

Finally, in Table **3-8**, the fitness of the proposed power and energy estimation model along Bézier curve is evaluated for different accelerations and payloads. The error percentages between the measured and predicted energy consumptions in both the right and left directions are shown. Without payload and high velocities, the error percentages are significant. The Table demonstrates that the best performance of the power model is located throughout the set of validation accelerations for medium payloads. The error percentages between the predictive and measured values fall below 5%.
The results show that the fitness of the energy estimation model compared with the measured

Table 3-6.: Measured and estimated energy consumption, for a Bézier's curve experiment without payload, right direction

Energy values - Without payload				
	Robot data (Joules)		Model value (Joules)	
Accelerations	Left motor	Right motor	Left motor	Right motor
0.15 m/s^2	21.96	22.77	26.65	22.57
0.18 m/s^2	22.84	22.47	23	22.69
0.2 m/s^2	22.02	22.02	25.6	24.72
0.22 m/s^2	22.53	22.53	26.19	24.68

Table 3-7.: Measured and estimated energy consumption, for a Bézier's curve experiment with payload, right direction

Energy values - Payload 8.25 kg				
	Robot data (Joules)		Model value (Joules)	
Accelerations	Left motor	Right motor	Left motor	Right motor
0.15 m/s^2	34.24	30.73	28.47	27.51
0.18 m/s^2	35.33	31.64	31.67	30.89
0.2 m/s^2	36.28	36.62	32.3	30.45
0.22 m/s^2	33.02	29.58	31.39	29.58

values given by the robot is equal to 81.25 % (using equation 3-4) for a Bézier curve path in both directions. The results also present that 26 out of 32 experiments accurately estimated the energy consumption of the robot.

Table 3-8.: The error between the predicted and measured energy, in the Bézier curve path experiment, right direction.

accel\payl	0 kg kg	5.7 kg	8.25 kg	10.5 kg
0.15 m/s^2	1.1 %	4.57 %	6.19 %	13.84 %
0.18 m/s^2	0.84%	8.31%	5.06%	5.31%
0.2 m/s^2	10.79%	1.07 %	2.64 %	9.45%
0.22 m/s^2	10.45%	1.14 %	0.41 %	2.6 %

Table 3-9.: The error between the predicted and measured energy, in the Bézier curve path experiment, left direction.

accel\payl	0 kg kg	5.7 kg	8.25 kg	10.5 kg
0.15 m/s^2	6.28 %	1.32 %	8.17 %	14.01 %
0.18 m/s^2	8.56%	1.02%	4.79%	8.98 %
0.2 m/s^2	13.43%	0.85 %	3.74 %	8.85%
0.22 m/s^2	13.36%	2.64 %	0.26 %	5.61 %

Finally, the MAPE (Mean Absolute Percentage Error) of the power estimation model can be calculated with the mathematical formula:

$$MAPE = \frac{1}{n}\sum_{i=1}^{n}\left(\frac{P_{measured_i} - P_{estimated_i}}{P_{measured_i}}\right)$$

Where:
$P_{estimated_i}$ is the power estimation values.
$P_{measured_i}$ is the power measured values.
n is the number of experiments.

The MAPE of the straight path experiments was 5.25%, for the curved path was 5.08%, and for all the experiments was 5.53%.
To validate the proposed model is necessary to compare the MAPE result with others in the state of art.
It was difficult to find any important research focus on the differential guide mobile robot configuration, or at least that presents the MAPE value of his experiments. On the other hand, in the literature can be found very important works focus on the skid steering robot configuration.

For example, Chuy in his experiments show a MAPE result of 7.55%, and Gupta a MAPE of 19.87%. In that case, our MAPE of 5.53% validates the proposed power estimation model.

3.3. Summary

In this chapter, a power and energy estimation model that takes into account the robot and motor dynamic parameters was proposed. The internal friction torque of the motors was estimated using a calibration procedure. In the dynamic motor model, the load torque is directly proportional to the input current, the mass (including the payload), and the acceleration. This behavior allows the proposed power model to predict the power and energy consumption for different payloads and accelerations, evaluated for straight and Bézier curve paths.
The proposed model was experimentally validated using a two-wheel drive mobile robot, namely the Nomad Super Scout. The results show that, when the accelerations of the robot increases the consumed energy increases. Similarly, increasing the payload increases the consumed energy as well. The fitness of the predictive power and energy estimation model compared with the energy consumed by the robot was equal to 81.25% for the Bézier curve path experiments and 96.67% for the straight path experiments. Also, the MAPE value was 5.53%, validating the proposed power estimation model. The straight path results suggest that the simplification carried out in the model is still valid, and the resulting expressions represent the dynamic behavior of the actual system.

4. Trajectory Planning for a Differential drive Mobile Robot

For mobile robots that carry their energy source, such as batteries, it is crucial that they optimize their energy consumprion in order to fulfill long-term tasks.
In this chapter, a closed-form trajectory planning solution for differential drive mobile robots, which provides the angular velocities of the wheels that optimize the energy consumption, on a given straight path, is calculated. In this case, the Hamiltonian function is employed, based on the proposed power estimation model and the Lagrange constraints.
Energy optimization can be beneficial in long-term robotic applications, including covered paths or SLAM outdoor solutions.

4.1. Function cost of the trajectory planning for a straight path

In this section, the cost function used in trajectory planning is depicted. When the mobile robot moves along a straight path, the angular velocities of the wheels are the same, which permits the simplification of the proposed power estimation model. The function that represents robot and motor power (adding equations 3-2 and 3-3) is as follow:

$$P = 0.0406\ddot{\theta}^2 + 0.296\ddot{\theta}\dot{\theta} + 0.0028\ddot{\theta}^2 m_p + 0.197\ddot{\theta} + 0.0034\dot{\theta}^2 + 0.01\ddot{\theta}\dot{\theta}m_p + 0.719\dot{\theta} \\ +0.0066\ddot{\theta}m_p + 0.24; \tag{4-1}$$

where:

$\dot{\theta}$ is the angular velocity of the wheels.
$\ddot{\theta}$ is the angular accelerations of the wheels.
m_p is the payload mass.

Subsequently, the Lagrange multipliers are added to the power estimation model, in order to obtain the Hamiltonian function of the motors. Variable change is also proposed.

$$H(a_\theta, v_\theta, \lambda_1, \lambda_2) = 0.0406a_\theta^2 + 0.296a_\theta v_\theta + 0.0028a_\theta^2 m_p + 0.197a_\theta + 0.0034v_\theta^2 \\ +0.01a_\theta v_\theta m_p + 0.719v_\theta + 0.0066a_\theta m_p + 0.24 + \lambda_1 v_\theta + \lambda_2 a_\theta; \tag{4-2}$$

Where:
a_θ is $\ddot{\theta}$,
v_θ is $\dot{\theta}$
λ_1,λ_2 are the Lagrange multipliers.

In this case, the Hamiltonian is the cost function for optimization. Under certain conditions, it is possible to obtain a closed-form solution may be obtained for the angular velocities of the wheels that minimize robot energy consumption. The optimization conditions are presented in the next section.

4.2. Hamiltonian function optimization

The conditions necessary to optimize the Hamiltonian function at all times $t \in [0, t_f]$, are those show below:

$$\dot{\theta_1} = \frac{\partial H_1}{\partial \lambda_1} \qquad \dot{\lambda_1} = -\frac{\partial H_1}{\partial \theta_1}$$
$$\dot{v_{\theta_1}} = \frac{\partial H_1}{\partial \lambda_2} \qquad \dot{\lambda_2} = -\frac{\partial H_1}{\partial v_{\theta_1}}$$
$$0 = \frac{\partial H_1}{\partial a_{\theta_1}}$$

Partial derivative development yields:

$$v_{\theta_1} = \dot{\theta_1} \qquad a_{\theta_1} = \dot{v_{\theta_1}} \qquad \dot{\lambda_1} = 0$$

$$\dot{\lambda_2} = -0.296a_\theta - 2(0.0034)v_\theta - 0.01a_\theta m_p - 0.719 - \lambda_1 \tag{4-3}$$

$$0 = 2(0.0406)a_\theta + 0.296v_\theta + 2(0.0028)a_\theta m_p + 0.197 + 0.01v_\theta m_p + 0.0066m_p + \lambda_2 \tag{4-4}$$

Then, by differentiating equation 4-4, and isolating $\dot{\lambda_2}$:

$$\dot{\lambda_2} = -2(0.0406)\dot{a_\theta} - 0.296\dot{v_\theta} - 2(0.0028)\dot{a_\theta} m_p - 0.01a_{\theta_1} m_p \tag{4-5}$$

The corresponding formulation for $\dot{\lambda_2}$, from equation 4-5, is then replaced in equation 4-3:

$$-2(0.0406)\dot{a_\theta} - 0.296a_\theta - 2(0.0028)\dot{a_\theta}m_p - 0.01a_\theta m_p = -0.296a_\theta - 2(0.0034)v_{\theta_1} \\ -0.01a_{\theta_1}m_p - 0.719 - \lambda_1 \tag{4-6}$$

The simplification of similar terms and equation re-ordering produces the below equation:

$$2\dot{a_\theta}(-0.0406 - 0.0028m_p) + 2v_\theta 0.0034 + 0.719 + \lambda_1 = 0 \tag{4-7}$$

The differential equation that results from changing $\dot{a_\theta}$ = variables is:

$$c_1\ddot{v_\theta} - c_2 v_\theta - \frac{c_3 + \lambda_1}{2} = 0 \tag{4-8}$$

Where:
$\dot{a_{\theta_1}} = \ddot{v_{\theta_1}}$
$c_1 = 0.0406 + 0.0028m_p$
$c_2 = 0.0034$
$c_3 = 0.719$
Finally, the solution of the differential equation is found to be:

$$v^*_{\theta_1} = s_1 e^{tk} + s_2 e^{-tk} - \frac{c_3 + \lambda_1}{2c_2} \tag{4-9}$$

Where:
$k = \sqrt{\frac{c_2}{c_1}}$
Equation 4-9 represents the optimal angular velocity profile that minimizes the energy consumption, for a given straight path. In order to calculate the optimal angular acceleration profile, the equation 4-9 is integrated. In the same way, to calculate the optimal angular wheel pose, equation 4-9 is derived.

$$\theta^*_1(t) = \frac{s_1}{k}e^{kt} - \frac{s_2}{k}e^{-kt} - \frac{\lambda_1 + c_3}{2c_2}t + s_3 \tag{4-10}$$

$$a^*_{\theta_1}(t) = s_1 k e^{kt} - s_2 k e^{-kt} \tag{4-11}$$

4.2.1. Optimization Constraint Equations

The s_1, s_2, s_3 and λ_1 variables are unknown, but may be determinated through the use of the initial and final conditions of velocity and acceleration condition as optimization problem constraints. To determine these terms, the constraints equations are given by:

$$\theta_1(0) = 0 \quad v_{\theta_1}(0) = v_o \quad \theta_1(t_f) = \theta_f \quad v_{\theta_1}(t_f) = v_f$$

Where
v_o and v_f are the initial and final angular velocities of the wheels.

θ_f is the total angular position, when the robot moves forward.

A non-linear equation system is obtained by replacement of the initial and final conditions in equations (2-41) and (4-10).

$$\begin{gathered}
\frac{s_1}{k} - \frac{s_2}{k} + s_3 = 0 \\
s_1 + s_2 - \frac{\lambda_1 + c_3}{2\, c_2} = v_o \\
\frac{s_1}{k} e^{k\, t_f} - \frac{s_2}{k} e^{-k\, t_f} - \frac{\lambda_1 + c_3}{2\, c_2} t_f + s_3 = \theta_f \\
s_1\, e^{k\, t_f} + s_2\, e^{-k\, t_f} - \frac{\lambda_1 + c_3}{2\, c_2} = v_f
\end{gathered} \tag{4-12}$$

The system solution gives a mathematical expression for the unknown variables, in terms of the final time t_f .

$$s_1 = \frac{v_f - v_o + \theta_f k - \delta_1 + \delta_2 - v_f k t_f - \delta_3 + \delta_4}{\delta_{13}}$$

$$s_2 = \frac{v_f - v_o - \theta_f k - \delta_5 + \delta_6 + v_f k t_f + \delta_7 - \delta_8}{\delta_{13}}$$

$$\lambda_1 = -a - b$$

where:

$$a = \frac{2c_3 e^{kt_f} - 4v_f c_2 - 4v_o c_2 - 4c_3 + 2c_3 e^{-kt_f} + 2v_f c_2 e^{kt_f}}{\delta_{13}}$$

$$b = \frac{2v_f c_2 e^{-kt_f} + \delta_9 + \delta_{10} - \delta_{11} + \delta_{12} - c_3 k t_f e^{kt_f} + c_3 k t_f e^{-kt_f}}{\delta_{13}}$$

$$\delta_1 = v_f e^{-kt_f} \qquad \delta_2 = v_o e^{-kt_f}$$
$$\delta_3 = \theta_f k e^{-kt_f} \qquad \delta_4 = v_o k t_f e^{-kt_f}$$
$$\delta_5 = v_f e^{kt_f} \qquad \delta_6 = v_o e^{kt_f}$$
$$\delta_7 = \theta_f k e^{kt_f} \qquad \delta_8 = v_o k t_f e^{kt_f}$$
$$\delta_9 = 2v_o c_2 e^{kt_f} \qquad \delta_{10} = 2v_o c_2 e^{-kt_f}$$
$$\delta_{11} = 2c_2 \theta_f k e^{kt_f} \qquad \delta_{12} = 2c_2 \theta_f k e^{-kt_f}$$
$$\delta_{14} = 2e^{kt_f} \qquad \delta_{15} = 2e^{-kt_f}$$
$$\delta_{16} = kt_f e^{kt_f} \qquad \delta_{17} = kt_f e^{-kt_f}$$
$$\delta_{13} = \delta_{14} + \delta_{15} - \delta_{16} + \delta_{17} - 4$$

The t_f values is calculated using the additional boundary condition known as the transversality condition. A detection event program is used to solve the equation.

$$H_1(a_\theta(t_f), v_\theta(t_f), \lambda_1(t_f), \lambda_2(t_f)) = 0; \tag{4-13}$$

where:

$$\begin{aligned} &0.0406a_\theta^2(t_f) + 0.296a_\theta(t_f)v_f + 0.0028a_\theta^2(t_f)m_p + 0.197a_\theta(t_f) + 0.0034v_f^2 \\ &+0.01a_\theta(t_f)v_f m_p + 0.719v_f + 0.0066a_\theta(t_f)m_p + 0.24 + \lambda_1(t_f)v_f + \lambda_2(t_f)a_\theta(t_f) = 0; \end{aligned} \tag{4-14}$$

4.3. Simulation and numerical validation

In this section, simulations which test the optimal velocity profile that minimizes robot energy consumption, for different parameters are presented. The mobile robot Nomad Super Scout was commanded to follow various straight path distances, with payloads of 5.7 kg and 10.5 kg, and with different initial and final velocities. The robot energy consumption with the optimal velocity profile was compared to a typical triangular and trapezoidal velocity profile.

4.3.1. Simulation set-up

Maximum trapezoidal velocities 0.35 m/s, 0.5 m/s and 0.65 m/s were used. The experiment time for each signal phase (acceleration, constant velocity, and deceleration) was 5 s. In triangular velocity profile case, the maximum linear velocities totaled 0.6 m/s, 0.8 m/s and 1.0 m/s, with an experimental time for the acceleration phase of 4 s.
The mobile robot was commanded to move, following a triangular velocity profile, with different initial and final velocities, as well. The payloads chosen for the tests were 5.7 kg and 10.5 kg.

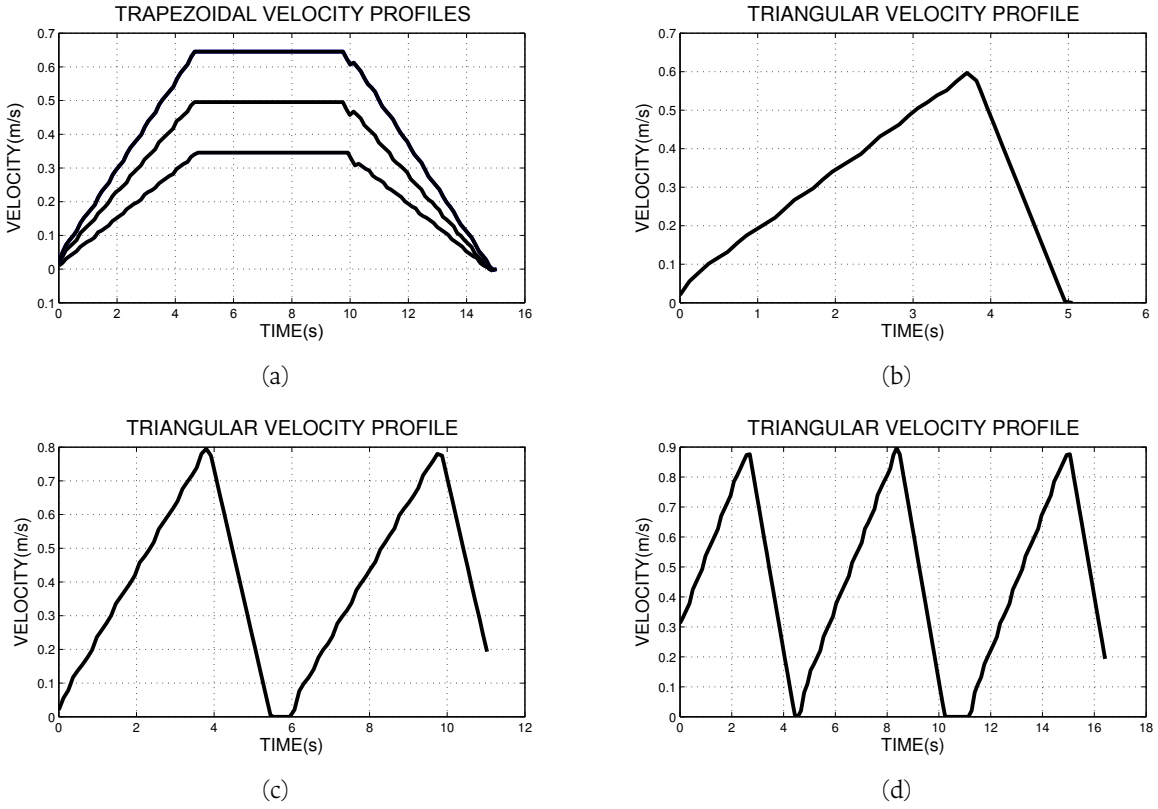

Figure 4-1.: Odometry values received from the encoders of the trapezoidal and triangular velocity profiles. (**a**) Trapezoidal velocity profiles with different maximum velocities. (**b**) Triangular velocity profile with a maximum velocity of 0.6 m/s (**c.**) Triangular velocity profiles with two accelerations, with a maximum velocity of 0.8 m/s, and initial velocity of 0.2 m/s. (**d**) Triangular velocity profile, with three accelerations. with a maximum velocity of 1.0 m/s, with an initial velocity of 0.3 m/s, and a final velocity of 0.2 m/s.

In Figure **4-1**, the trapezoidal and triangular velocity profiles received from the encoders are shown.

On the other hand, Figure **4-2** shows the optimal velocity profiles that minimize the energy consumption for a mobile robots that travels along a straight path. Figure **4-2**(a) and **4-2**(b) present the optimal velocity profiles with varying distances and payloads. Changes in these variables influence the optimal times and maximum velocities.

In Figure **4-2**(c) and **4-2**(d), the optimal velocity profiles with different initial and final velocities, are depicted. In these cases, the optimal time avries, but the maximum velocity changes minimally.

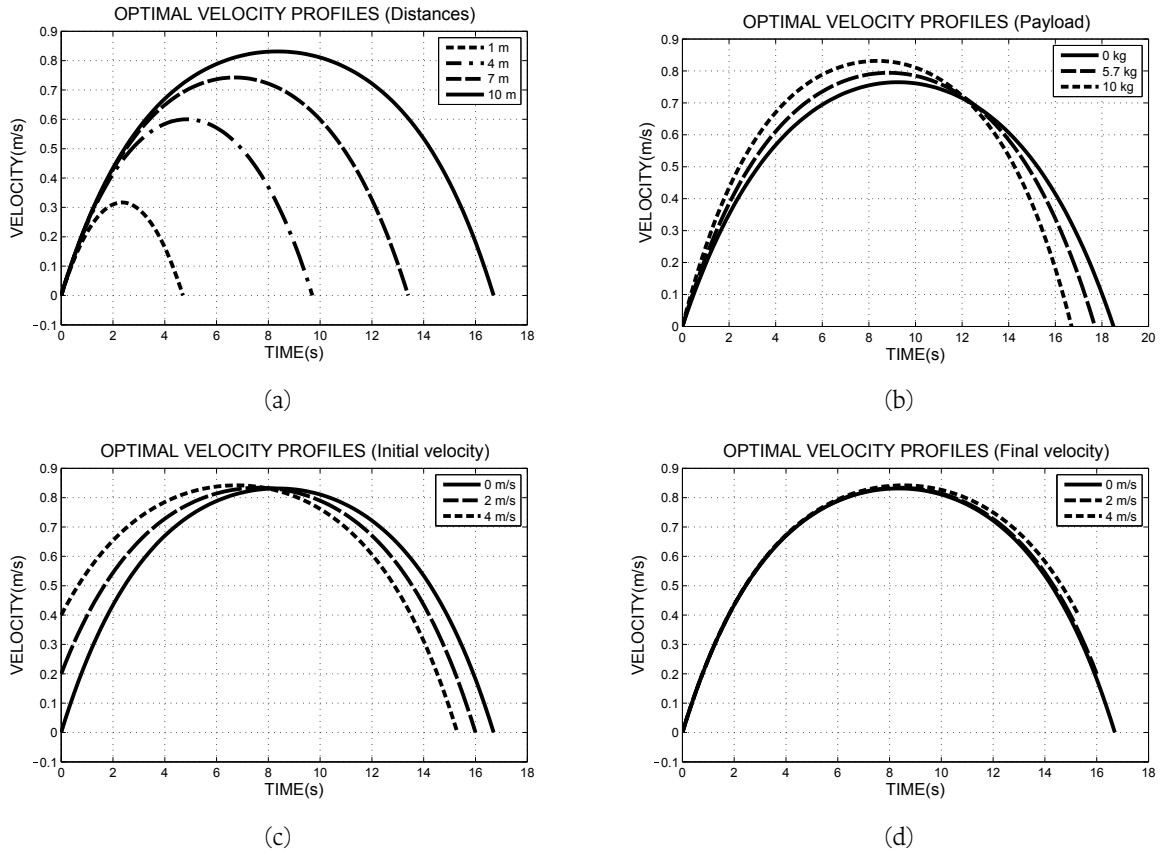

Figure 4-2.: Optimal velocity profiles. (**a**) Optimal velocity profiles with various distance (1.0 m, 4.0 m, 7.0 m and 10.0 m). (**b**) Optimal velocity profiles with payload changes (0.0 kg, 5.7 kg and 10.5 kg). (**c.**) Optimal velocity profiles with different initial velocities (0.0 m/s, 2.0 m/s and 4.0 m/s). (**d**) Optimal velocity profiles with various final velocities (0.0 m/s, 2.0 m/s, and 4.0 m/s).

4.3.2. Energy optimization for a trapezoidal velocity profile

In this test, the mobile robot was commanded to follow a straight path with a trapezoidal velocity profile that demanded high energy consumption. Then, the mobile robot moved along the same path as the optimal velocity profile. The distances traveled in the experiment totaled 1.92 m, 5 m, and 8.1 m. The energy consumption for both velocity profiles was compared, showing the significance of robot energy saving. For the length of 1.92 m, without payload, robot energy consumption was measured at 28.19 J, and the optimal energy consumption was 16.03 J. At a maximum distance and payload, the measured energy value was 93.95 J, and the optimal energy value was 64.53 J. In Figure **4-3**, the measured and optimal power values are compared. Figure also shows that, with an increase in distance and payload, the energy consumption increases as well. It is evident that, use of optimal velocity profile to move the robot with the same distance that as that of trapezoidal velocity, decreases the energy consumption considerably. This energy-saving behavior for different velocities and payloads is shown in Table **4-1**. Finally, the optimal velocity-time approached trapezoidal velocity-time as the distance and payload increased.

Table 4-1.: Measured and optimal energy, with different trapezoidal profiles and payloads.

Payloads	0 kg		5.7 kg		10.5 kg	
Max Vel	Measured	Optimal	Measured	Optimal	Measured	Optimal
0.2 m/s	28.19 J	16.03 J	27.63 J	16.28 J	33.96 J	16.44 J
0.5 m/s	49.89 J	40.08 J	56.1 J	40.33 J	63.32 J	40.53 J
0.8 m/s	64.3 J	52.06 J	85.94 J	64.31 J	93.95 J	64.53 J

4.3.3. Energy Optimization of a Triangular Velocity Profile

The Nomad Super Scout robot was commanded to follow a straight path with a different triangular velocity profile that generated high robot energy consumption. Also, a payload change s and different initial and final velocities were presented in the test. The robot moved along the same path as the optimal velocity profile. Robot energy consumption, with both velocity profiles, was then compared, which showed significant robot energy savings .

In Figure **4-4**, a triangular velocity and an optimal velocity profiles, for a distance of 1.57 m, are shown. Figure **4-4** also indicates measured power consumption, as compared to the optimal power estimation. In this test, the energy measured was 17.55 J, and the optimal energy totaled 13.34 J. Table **4-2** shows the measured and optimal energy consumption for a triangular and optimal velocity profiles, without payload, and at a distance of 1.57 m, 4.2 m, and 7.5 m.

Table **4-3**, indicates the energy measured from the triangular velocity profile, with two accelerations, with a final velocity of 0.2 m/s (Figure **4-1**(c)) and a payload of 5.7 kg are shown. The different triangular accelerations represent the case in which the robot reaches several checkpoints, and consumes a significant amount of energy. It also shows robot energy optimization.

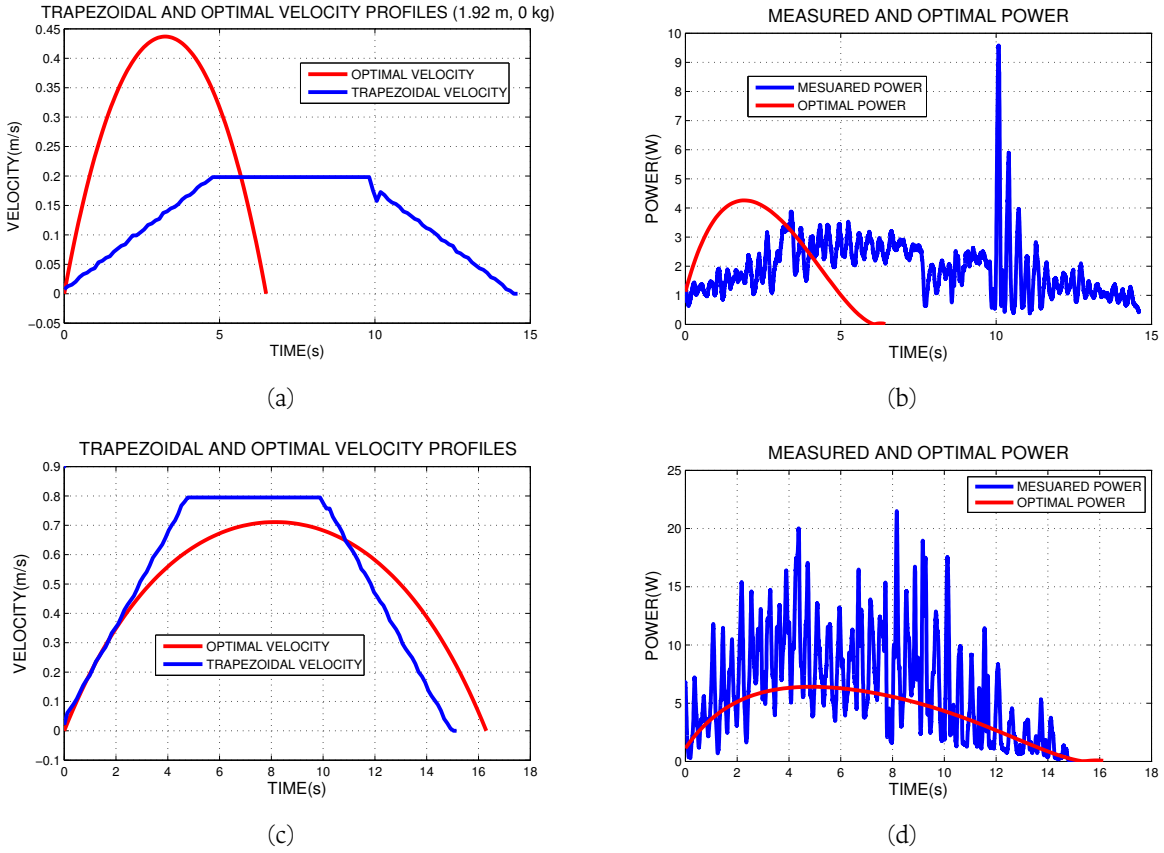

Figure 4-3.: Trapezoidal and optimal velocities. Measured and optimal power. (**a**) Trapezoidal and optimal velocities, without payload and a distance of 1.91 m. (**b**) Measured and optimal power, without payload and a distance of 1.91 m. (**c.**) Trapezoidal and optimal velocities, with 10.5 kg of payload and a distance of 8.1 m. (**d**) Measured and optimal power, with 10.5 kg of payload and a distance of 8.1 m.

Table 4-2.: Triangular and optimal power consumption without payload.

Max vel	0.6 m/s	0.8 m/s	1 m/s
Measured	17.55 J	50.61 J	83.44 J
Optimal	13.34 J	35.58 J	59.79 J

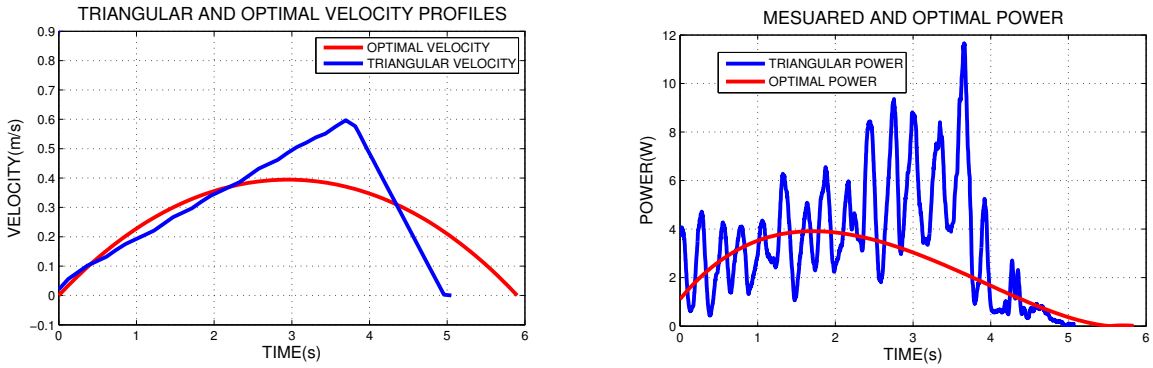

(a) (b)

Figure 4-4.: Triangular and optimal velocities. Measured and optimal power. (**a**) Triangular and optimal velocities, without payload, and at a distance of 1.57 m. (**b**) Measured and optimal power, without payload, and at a distance of 1.51 m.

.

Table 4-3.: Triangular and optimal power consumption with a payload of 5.7 kg. Triangular velocity profile with two accelerations, and final velocity of 0.2 m/s.

Max vel	0.6 m/s	0.8 m/s	1 m/s
Measured	42.17 J	62.07 J	80.89 J
Optimal	27.12 J	38.03 J	48.85 J

In this final test, the optimal velocity profile, a triangular velocity with three accelerations, an initial and final velocity, and a payload of 10.5 kg was utilized. In Figure **4-5**, the triangular velocity profile employed, and the optimal velocity profile is shown. In Figure **4-5**, the power of the triangular and optimal velocity is shown as well. Measured energy totaled 68.26 J, and the optimal energy was 36.18 J.

In figure **4-6**,the robot energy consumption calculated with the triangular experimental time and with the optimal time are compared. The measured energy was 68.26 J, estimated energy with the experimental time was 41.81 J, and the optimal energy with the optimal time was 36.18 J. Notice that, with the optimal velocity profile calculated with the optimal time, the robot consumes less energy.

The table presentes the same experiments with different maximum triangular velocity profiles, and the same energy-saving behavior.

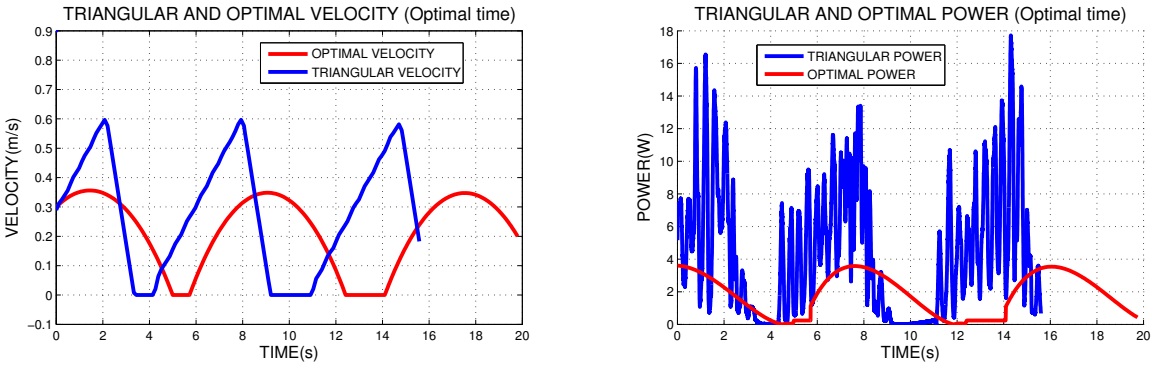

(a) (b)

Figure 4-5.: (**a**) Triangular and optimal velocities calculated with optimal time. (**b**) Measured and optimal power m.

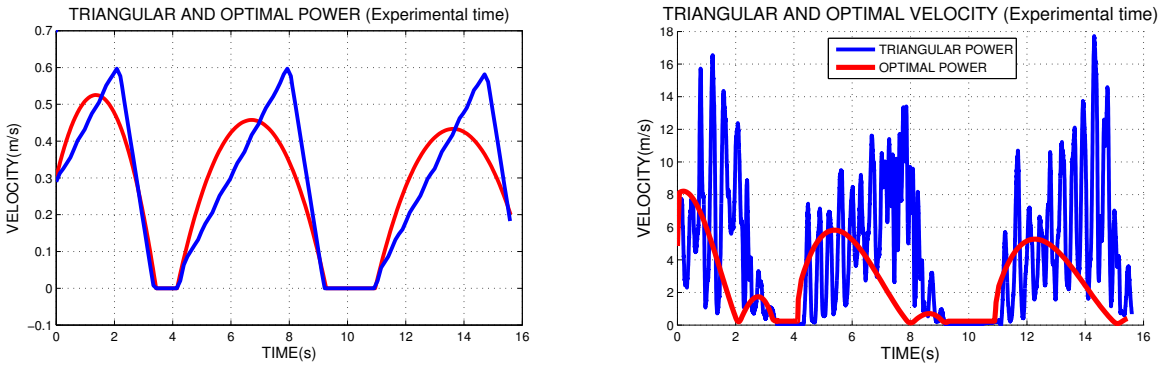

(a) (b)

Figure 4-6.: (**a**) Triangular and optimal velocities calculated with experimental time. (**b**) Measured and optimal power.

Table 4-4.: Energy consumption for a triangular velocity, experimetal and optimal velocity

Max vel	0.6 m/s	0.8 m/s	1 m/s
Measured	68.26 J	97.36 J	135.53 J
Triangular time	41.81 J	65.19 J	96.78 J
Optimal time	36.18 J	51.53 J	71.7 J

The proposed energy optimization model allows to calculated velocity profiles that minimize the amount of energy a mobile robot must carry to complete a predefined task before deployment and deviations in the predefined estimate due to unexpected changes in the payload in real-time. This allows charge optimization and scheduling not only for a single load-carrying robot but also for multiple load-carrying robots operating in warehouses with a limited number of charge stations.
In the next chapter, the energy optimization model is applied in a typical robotic problem such as in SLAM examples.

5. Simultaneous Localization and Mapping (SLAM) Simulation

In this chapter, the proposed optimal velocity profile, which minimizes robot energy consumption, is tested in a typical mobile robot problem, such as the SLAM. As resolution of the the SLAM problem is not the main goal of this study, the focus of the present chapter is to offer a path and optimal velocity solution to the SLAM problem. In this case, the accumulative error that the sensors are permitted is not considered, avoiding an estimation of the robot pose, using typical state of the art solution such as Kalman filters.

The methodology employed is as follows: first, the environment is classified into seen, unseen, and occupied nodes. Then, a Next Best View (NBV) point is calculated, so as to guarantee the maximum visual range of the unseen nodes. Finally the path planning Dist Bug is used to command the mobile robot to reach the NBV, until the environment is fully explored.

5.1. SLAM simulation set up

The simulation was performed in Matlab. The environment was limited 20 m in the x-axis and y-axis. This distance is similar to Nomad Super Scout mobile robot hardware validation scenario. Two square obstacles were placed in the environment, and occupied an area of 16 m^2 each one. The mobile robot is represented by a circle with a radius of 1 m, this dimension is large than the radius of the Nomad Super Scout robot, which is 0.165 m. The offset guarantees robot safety. In the circle, there is a point that represents the mobile robot orientation. In the simulation, there is a sensor with a visual range of 90 degrees, with which the robot can explore360 degrees from its current position, in four rotations.

5.1.1. Study cases

Five study cases were chosen for the simulation test. These cases are representative scenarios, which may reveal several visual occlusions between the obstacles and different robot position. In Table **5-1**, the centroid of the obstacle (px_1, py_1, px_2, py_2), the initial robot position (R_x, R_y), and the initial robot orientation (ϕ) is shown.

Table 5-1.: Different SLAM cases of study

PARAMETERS	CASE 1	CASE 2	CASE 3	CASE 4	CASE 5
R_x (m)	10	10	10	10	5
R_y (m)	3	3	10	10	16
P_{x1} (m)	15	5	5	5	12
P_{y1} (m)	5	15	10	5	11
P_{x2} (m)	7	7	15	15	15
P_{y2} (m)	10	10	12	6	6
ϕ (rad)	$\pi/4$	$\pi/4$	$\pi/2$	$\pi/2$	π

5.2. Clasification of the environment

In this section, the classification of the environment is presented. Nodes are located to discretized the space. They are classified as either seen or unseen nodes. The nodes in the same area from those obstacles labeled occupied nodes. Those nodes that are seen depend upon the the robot sensors visual range, and the unseen nodes are related to the visual occlusions that depend on both the robot and obstacle poses. Figure **5-1**, shows the space classification for each of the five cases.
It also shows, the seen nodes (green), unseen nodes (gray), occupied zone (brown), the obstacles (blue), the obstacle offset (red), the robot (red circle) and its orientation (black point).
Figure **5-2** display the first robot exploration 360 degrees, after four rotations in the same position.

5.3. Next Best View (NBV)

The NBV allows the robot to move to the point of maximum exploration, assuring the check of more quantity of unseen nodes. In the state of the art, many approaches are presented. The algorithm chosen is based on the algorithm used in Connolly (Visual sphere)[12]. A visual circumference is drawn around the unseen nodes. Then, NVB candidates are chosen from the visual circle every 45 degrees.
In Figure **5-3**, the NBV calculations for different robot exploration are shown. Therein, when one candidate is located outside of the workspace, it is relocated to a point perpendicular to an environment axis limit. Should the NBV candidates pose be the same as the unseen nodes or occupied zone, they are eliminated.
The NBV candidate with the most observed unsen nodes is the winner. In Tables **5-2** and **5-2** the number of unseen nodes reached by all the NBV candidates in two SLAM examples is revealed. In Figure **5-3**, in the first example of the SLAM problem, the NBV winner is Candidate 6, with 76 unseen nodes observed. In the second example, the NBV winner is Candidate 1, with 73 unseen

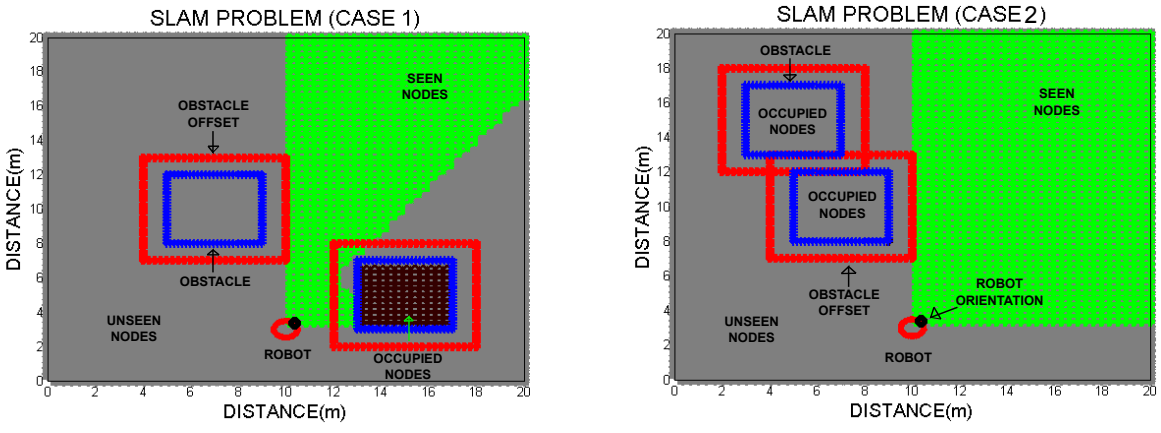

(a)

(b)

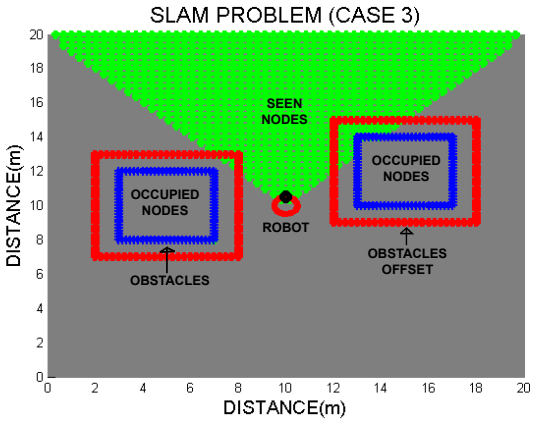

(c)

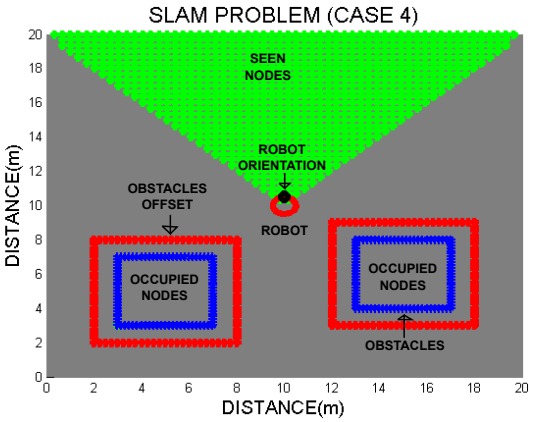

(d)

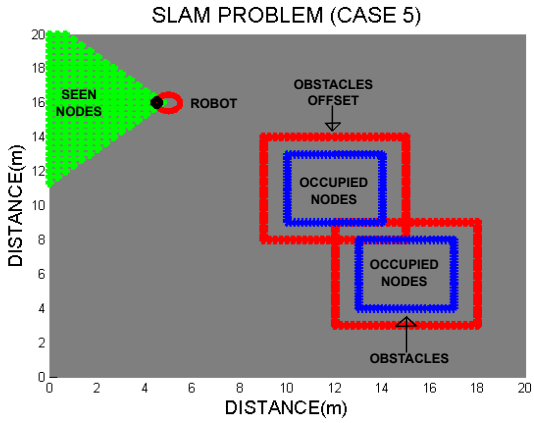

(e)

Figure 5-1.: Studied SLAM cases. Classification of the space. (**a**) Case 1. (**b**) Case 2. (**c**) Case 3. (**d**) Case 4. (**e**) Case 5.

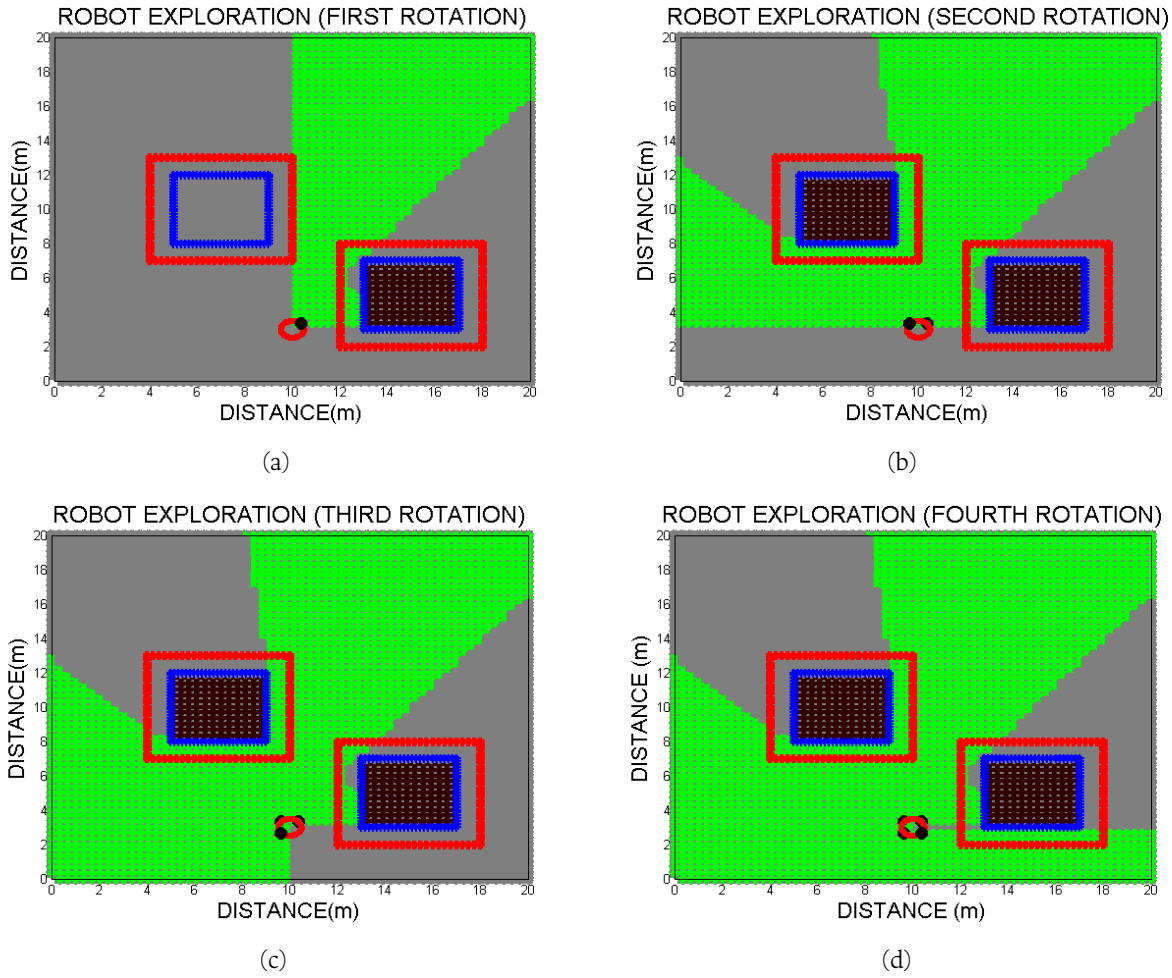

Figure 5-2.: Robot exploration (360 degrees) in the same pose. (**a**) First rotation. (**b**) Second rotation. (**c**) Third rotation. (**d**) Fourth rotation.

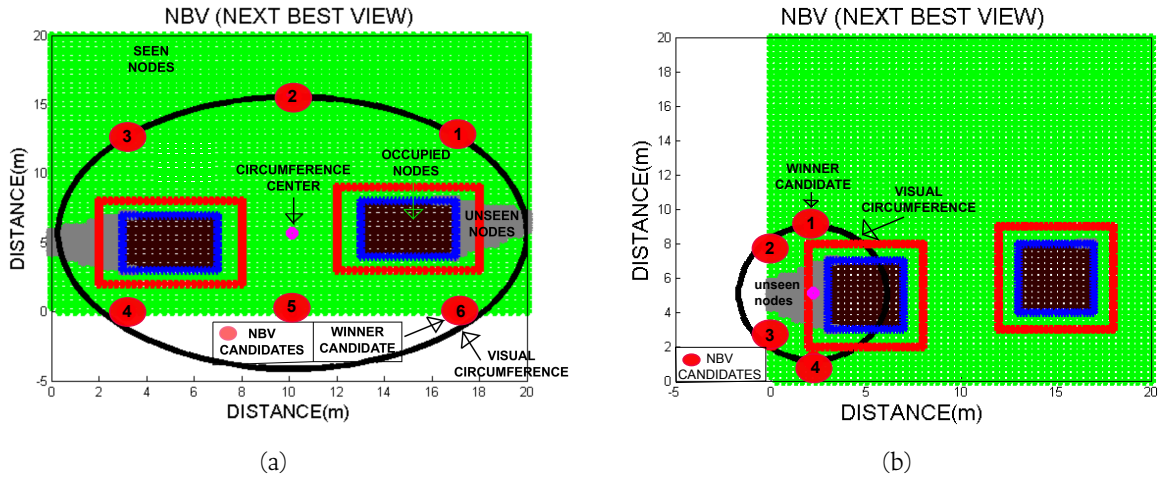

Figure 5-3.: Next Best View (NBV) calculation. (**a**) NBV example 1. (**b**) NBV example 2.

Table 5-2.: Unseen nodes observed for all the NBV candidates for the SLAM example 1.

NBV candidates	NBV1	NBV2	NBV3	NBV4	NBV5	NBV6
Unseen nodes observed	59	59	75	71	1	76

Table 5-3.: Unseen nodes observed for all the NBV candidates for the SLAM example 2.

NBV candidates	NBV1	NBV2	NBV3	NBV4
Unseen nodes observed	73	73	54	61

nodes observed.

5.4. Path planning methodology

Path planning allows the mobile robot to reach the NBV from its current position. The path planning calculates a secure route, in order to avoid collisions with the obstacles, and unseen nodes.

In the state of the art, many approaches are presented. In this study, however, Bug path planning was chosen, more specifically the DistBug. This path plan better suits the numerical environment in Matlab (squares obstacles). The DistBug reaches the NBV, and surrounds the obstacles, if necessary.

In Figure **5-4**, path planning based on DistBug is shown. First, the mobile robot is commanded to reach the NBV (red node 1), but the path is blocked, owing to collision risk. Then, the corners of the obstacle offsets (red), are listed in ascending order, based on their closeness to NBV. In Figure **5-4** shows that, for the robot, from its current position, it is impossible to reach the corners 2,3,4 and 5, because of the collision risk. For that reason, that the robot moves to the Corner 6. This behavior is repeated until it reaches the NBV. In the example contained in Figure **5-4**, the robot follows the corner sequences of 6,5,3 and 1. In this case, the mobile robot orientation is always aligned with the DistBug path node winner.

In Figure **5-5**, the algorithm diagram for the SLAM solution is shown. The stop limit for exploration finalization was fixed in 15 nodes, representing an error of less than of 0.2% In Figure **5-6**, the solution of the SLAM problem, case 1, is shown. Overall all the cases present successful results. The total number of unobserved unseen nodes without observation in the first case was 9 nodes, in the second was 2 nodes, in the third was 7 nodes, in the fourth was 5 nodes and in the fifth was 4 nodes. In this case, the exploration error was close to 0.2%.

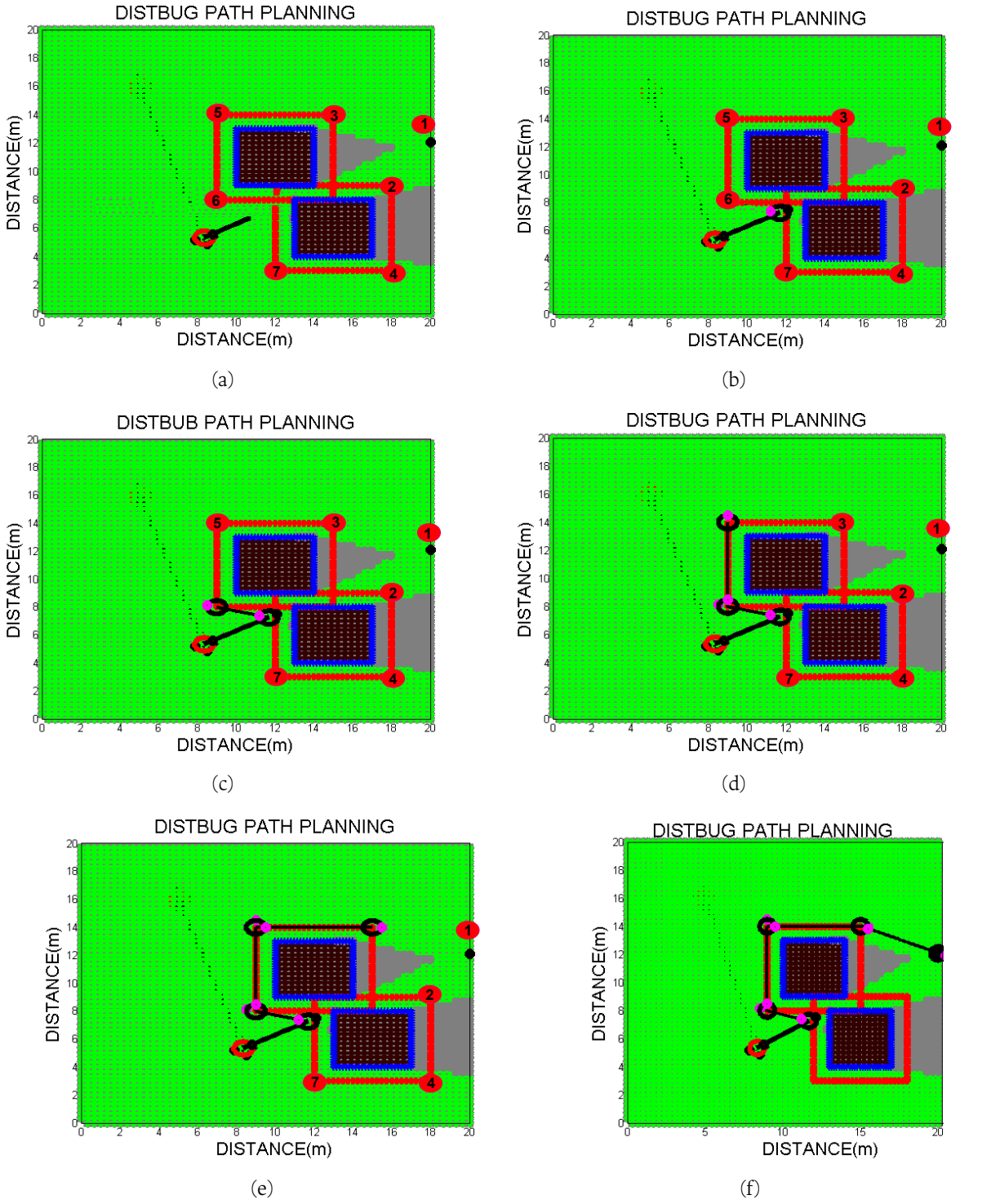

Figure 5-4.: DistBug path planning. (**a**) Distbug first phase. (**b**) Distbug second phase. (**c**) Distbug third phase. (**d**) Distbug fourth phase. (**e**) Distbug fifth phase. (**f**) Distbug sixth phase.

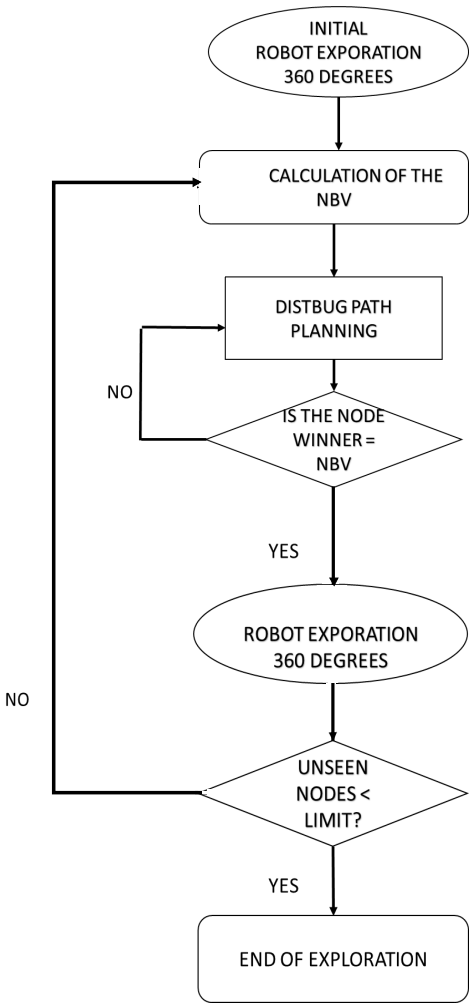

(a)

Figure 5-5.: SLAM solution algorithm scheme

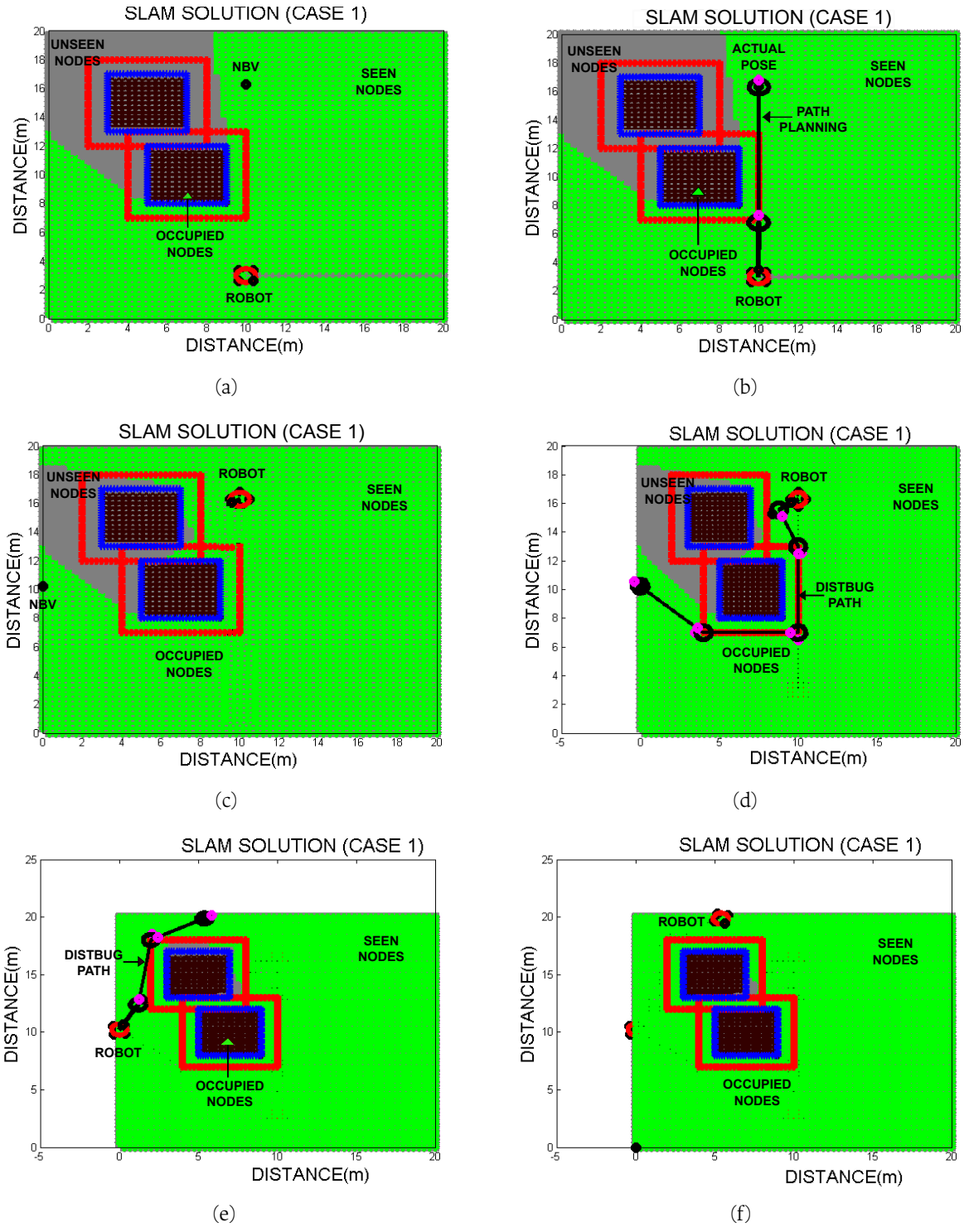

Figure 5-6.: SLAM solution case 1. (**a**) First robot exploration. (**b**) Reaching the first NBV. (**c**) DistBug path planning. (**d**) Second robot exploration. (**e**) Second DistBug path planning. (**f**) End of exploration

5.5. Trajectory path planning for the SLAM solution

In this section, a set of optimal velocities, which minimizes the energy consumption of the robot, based on the path that solves the SLAM problem is presented. The robot is commanded to follow a set of straight paths and turns in the same position. This behavior is repeated until to accomplishing the exploration of the unknown environment. For the straight path, a triangular velocity profile with a maximum velocity of 1 m/s was used. For the rotations, a constant velocity positive and negative with the same amplitude was calculated. As shown in Figure **5-7**, at the time of robot rotation, the linear velocity thereof was zero, and when the robot moved forward, the angular velocity was zero.

In Figure **5-8**, the optimal linear velocity and the angular robot velocities, which satisfy the SLAM solution in the first case, are shown. The angular velocity for both figures is the same because the optimization was calculated for the straight path. Optimal velocity presents a reduction of the simulation time and the maximum velocities, compared to the triangular velocity. In Figure **5-9**, robot power consumption, with a triangular velocity profile, is indicated. Also, in Figure **5-10**, robot power consumption, with the optimal velocity profile, is presented as well. Energy consumption with the triangular velocity totaled 505.88 J, and the energy consumption with the optimal velocity was 165.44 J. These results show a significant robot energy consumption savings in the first SLAM example.

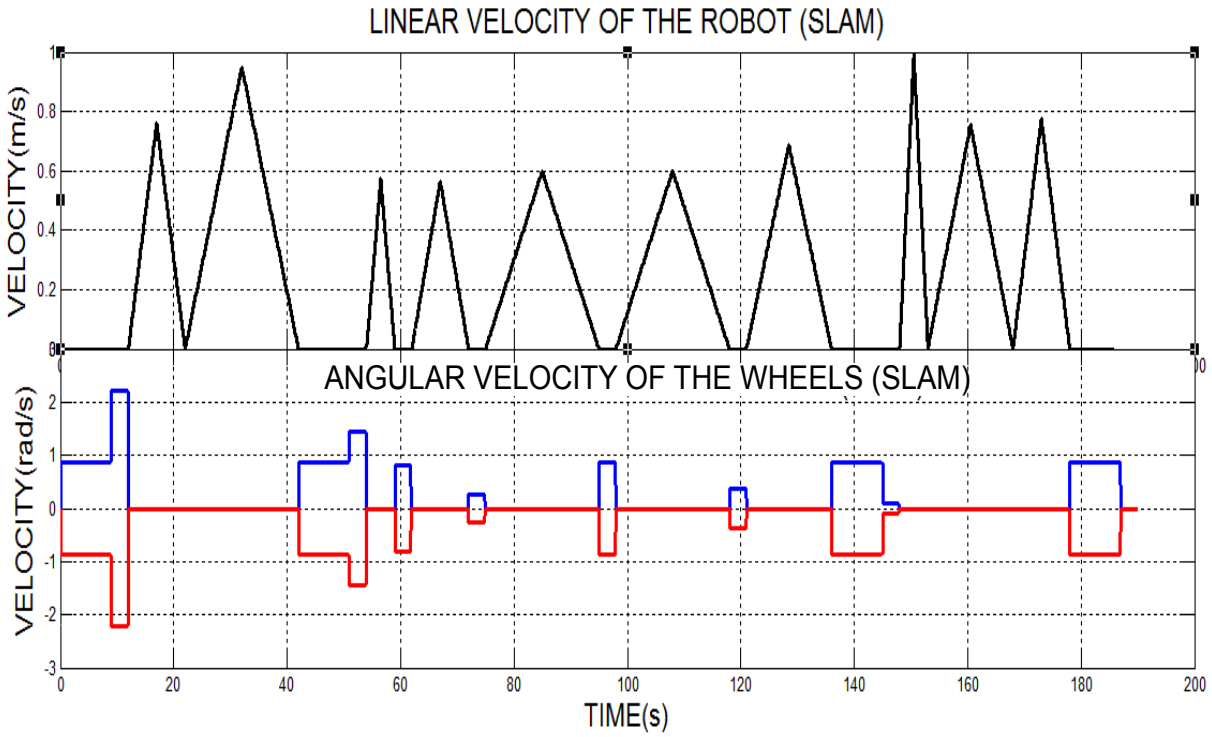

Figure 5-7.: Linear and angular velocities that satisfy the SLAM solution in the first case.

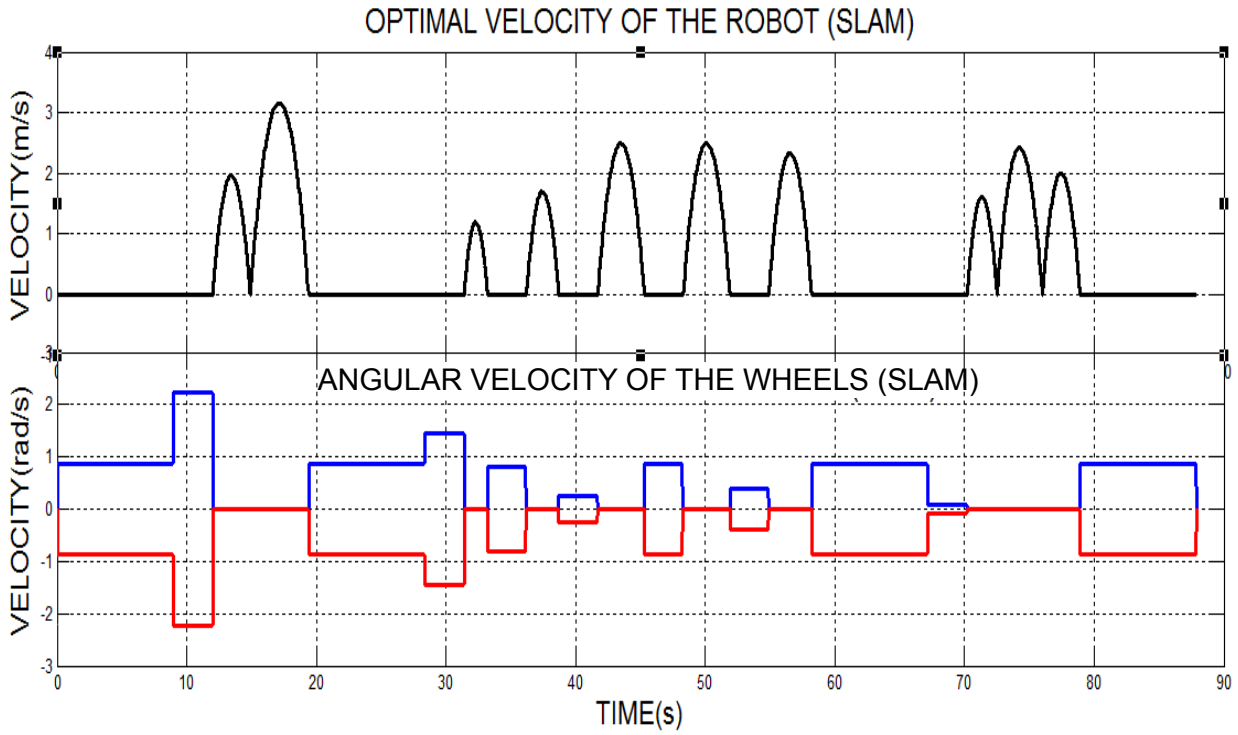

Figure 5-8.: Optimal linear velocity and angular velocities that satisfy the SLAM solution of the first case.

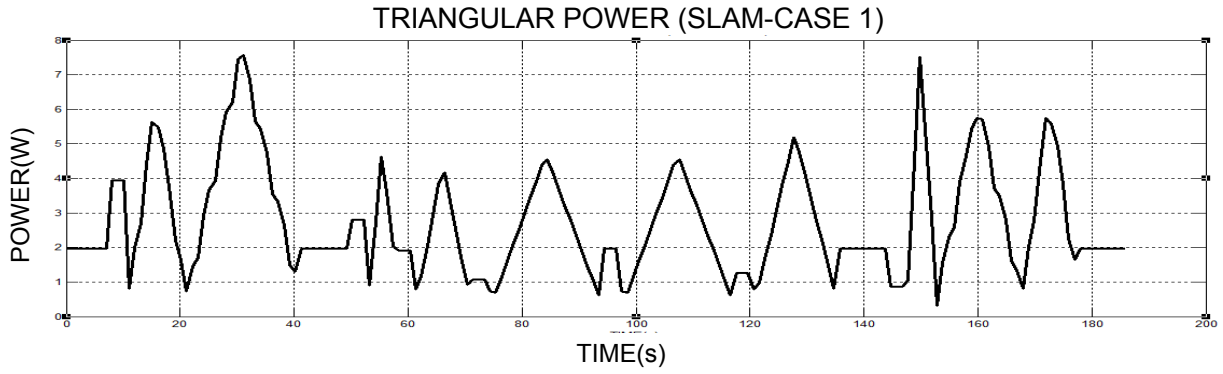

Figure 5-9.: Power consumption of the robot with the triangular and constant velocity profiles that satisfy the SLAM solution in the first case.

Robot energy consumption depends on the total distance of the path, as well as, the number of rotations. It is for that reason that the SLAM cases in which the robot used the Dist-Bug to avoid an obstacle and reach the NBV are those cases with high energy consumption.
For example, the energy consumption with the triangular velocity was 378.65 J and with the

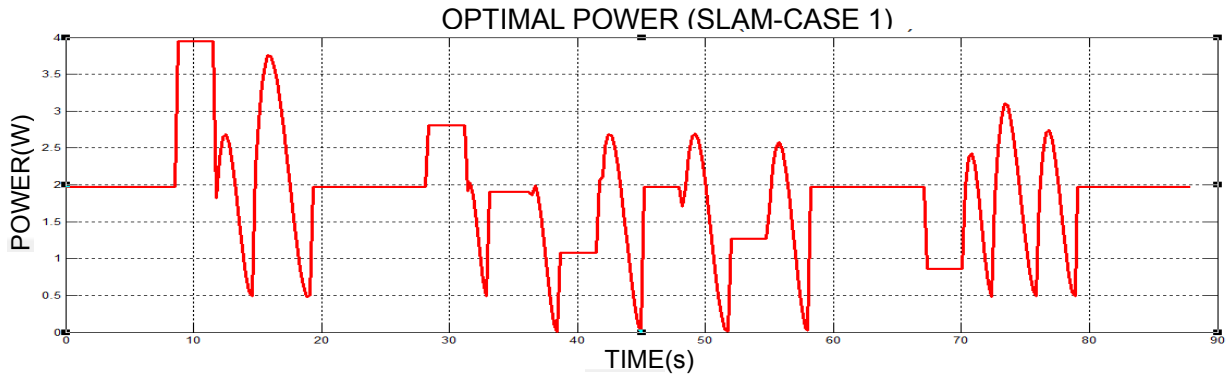

Figure 5-10.: Power consumption of the robot with the optimal velocity profiles that satisfy the SLAM solution of the first case.

optimal velocity, it totaled 112.87 J, in the second SLAM case. Comparison of robot energy consumption between the first and second cases demonstrates higher energy consumption in the first case. In Figure **5-11** the triangular velocity of the robot, which satisfies the SLAM solution in the second case, is shown. Also, in Figure **5-12**, robot optimal velocity that satisfies the SLAM solution in the second case is presented as well. In Figures **5-13** and **5-14**, robot power consumption, with triangular and optimal velocities, is depicted.

Table 5-4.: Energy consumption results of all the simulation cases, for different payloads

		Robot energy consumption	
	Payload	Triangular	Optimal
Case 1	0 kg	505.88 J	165.44 J
	5.7 kg	505.75 J	166.98 J
	10.5 kg	505.65 J	168.61 J
Case 2	0 kg	378.65 J	112.87 J
	5.7 kg	378.51 J	113.73 J
	10.5 kg	378.48 J	114.67 J
Case 3	0 kg	360.94 J	114.87 J
	5.7 kg	360.46 J	115.93 J
	10.5 kg	360.08 J	117.69 J
Case 4	0 kg	543.98 J	159.18 J
	5.7 kg	543.83 J	160.57 J
	10.5 kg	543.69 J	162.15 J
Case 5	0 kg	290.99	103.81
	5.7 kg	290.9	105.59
	10.5 kg	290.82	105.46

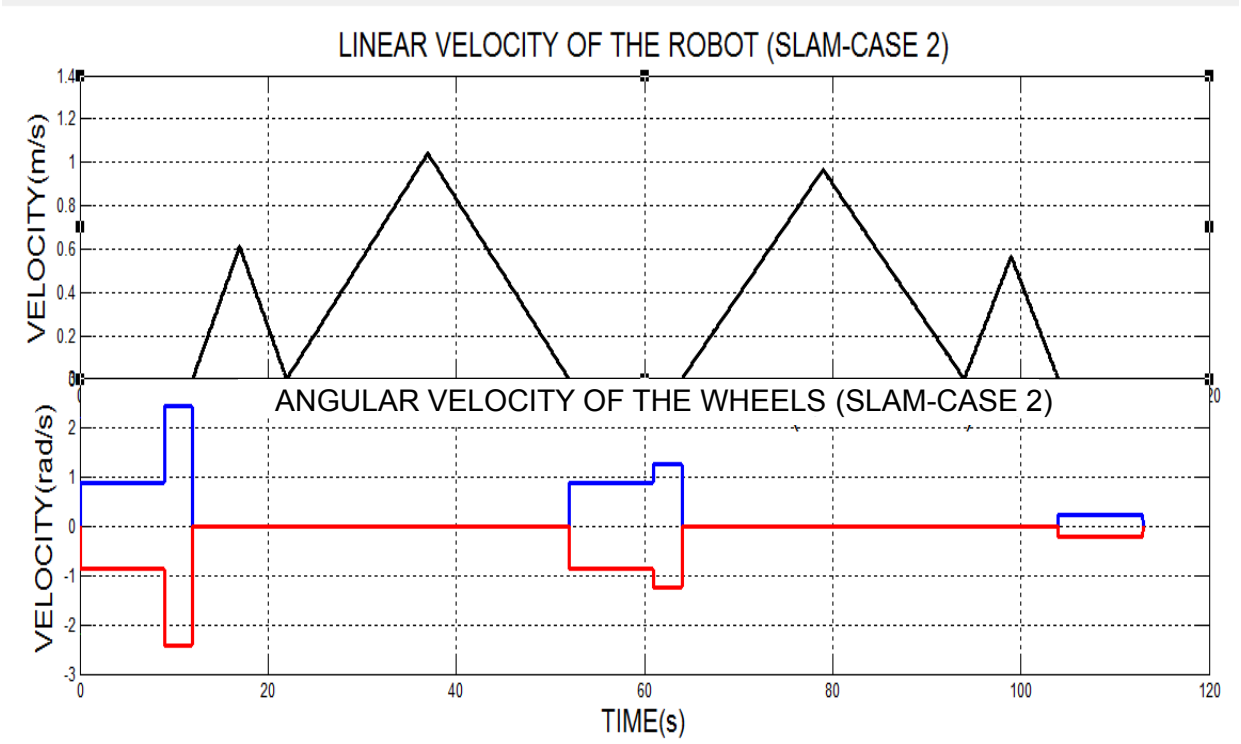

Figure 5-11.: Linear and angular velocities that satisfy the SLAM solution in the second case.

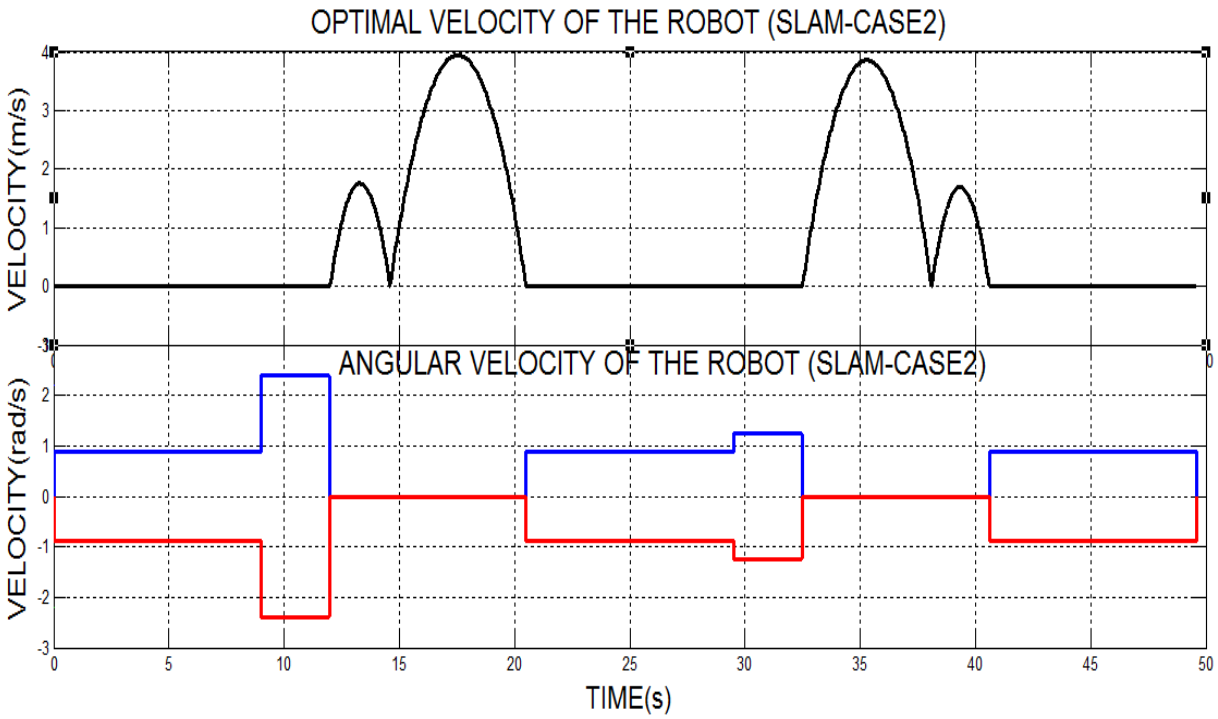

Figure 5-12.: Optimal linear velocity and angular velocities that satisfy the SLAM solution in the second case.

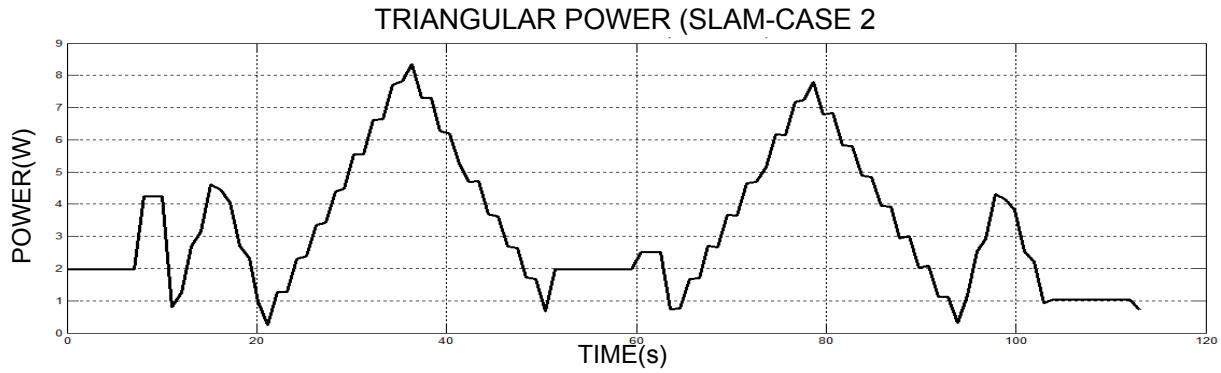

Figure 5-13.: Robot power consumption with the triangular and constant velocity profiles that satisfy the SLAM solution in the second case.

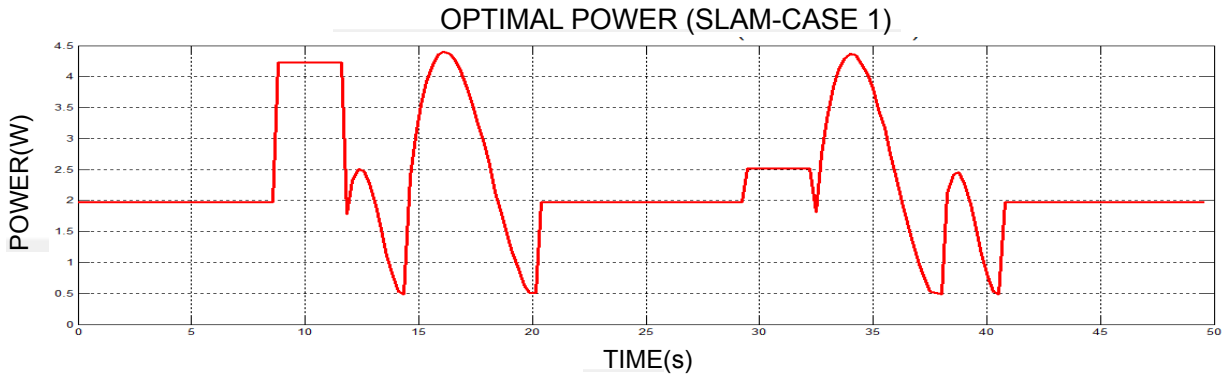

Figure 5-14.: Robot power consumption with the optimal velocity profiles that satisfy the SLAM solution in the second case.

In Table **5-4**, the robot energy consumption for al the SLAM cases is shown. It can be seen that the payload doesn't affect the energy consumption with triangular velocity, and barely change for energy consumption with optimal velocity. Cases 3 and 5 present the lowest energy consumption. It can be noticed that those cases don't have to avoid obstacles to reach the NBV. Finally, in all the study cases, the robot energy consumption with the optimal velocity profile, save a significant amount of energy, compared with the energy with a triangular velocity profile. This saving-energy behavior can be necessary for long-term robot applications, when the robot carries their energy source, such as batteries.

6. Conclusions and Future Work

- A power and energy estimation model that takes into account the robot and motor dynamic parameters was proposed. The internal friction torque of the motors was estimated using a calibration procedure. In the dynamic motor model, the load torque is directly proportional to the input current, the mass (including the payload), and the acceleration. A contribution of this study based on the power model proposed is to predict the power and energy consumption for different payloads and accelerations, evaluated for straight and Bezier curve paths.

  The proposed model was experimentally validated using a two-wheel drive mobile robot, namely the Nomad Super Scout. The results show that when the accelerations of the robot increases, the consumed energy increases. Similarly, increasing the payload increases the consumed energy as well. The fitness of the predictive power and energy estimation model compared with the energy consumed by the robot was equal to 81.25% for the Bézier curve path experiments and 96.67% for the straight path experiments. The straight path results suggest that the simplification carried out in the model is still valid, and the resulting expressions represent the dynamic behavior of the actual system.

- Another contribution of this work is to present a closed-form solution for an optimal velocity profile that minimizes the robot energy consumption, for a given straight path, that takes into account the payload. A hamiltonian function is used as a cost function to optimize based on the power estimation model. This function allows calculating an optimal velocity profile that minimizes the robot energy consumption. The main contribution to this topic is to introduce the payload as a parameter of the optimization function. In the validation, the robot energy consumption evaluated with the optimal velocity, and with different triangular and trapezoidal velocity is compared. The results present a significant energy-saving of robot energy consumption. This behavior may be necessary for long-term applications, when it carries their energy source, such as batteries. Finally, the optimal velocity profile is compared with a triangular velocity profile when the robot follows a path that solves various SLAM cases solutions. In the results, the energy-saving behavior of the optimal velocity profile remains.

- For future works, to improve the results of the Bezier's curve validation of the proposed power estimation model, the calculation of the internal motor friction and the friction of the wheels against the floor remains. Also, a closed-form solution of the optimal veloc-

ity that minimizes the robot energy consumption evaluated for a curved path for future research is proposed.

A. Anexo: Publications

The following papers were published in an international robotic journal and conferences using the results presented in this thesis:

- **International Conference on Information in Control Automation and Robotics (ICINCO 2018).**
  Paper: Mixed Energy Model for a Differential Guide Mobile Robot Evaluated with Straight and Curvature Paths.
  Authors: Mauricio F. Jaramillo Morales (Corresponding author) y Juan Bernardo Gómez Mendoza.
  Location: Porto (Portugal).
  Date: 29-31 July 2018.
  Modality : Oral presentation.
  DOI:10.5220/0006912004730479
  Corpus ID: 116304525
  SciTePress 2018, ISBN 978-989-758-321-6
  Volume 2.

- ·**International Conference on Methods and Models in Automation and Robotics (MMAR 2018).**
  paper: Mixed Energy Model for a Differential Guide Mobile Robot.
  authors: Mauricio F. Jaramillo Morales (Corresponding author) y Juan Bernardo Gómez Mendoza.
  Location: Miedzyzdroje (Poland).
  Date: 27-30 August 2018.
  Modality: Oral presentation.
  Pages: 114-119
  Electronic ISBN: 978-1-5386-4325-9
  USB ISBN: 978-1-5386-4324-2
  Print on Demand(PoD) ISBN: 978-1-5386-4326-6.
  **Nominated as best paper by PhD students.*

- **IEEE International Conference on Robotic Computing (ICR 2019).**
  Paper: Predictive Power Estimation for a Differential Drive Mobile Robot Based on Motor and Robot Dynamic Models.
  Autores: Mauricio F. Jaramillo Morales (Autor principal), Sedat Dogru, Juan Bernardo Gómez Mendoza y Lino Marques.
  Location: Nápoles(Italia).
  date: 25-27 January 2019.
  Modality: Oral presentation.
  Pages: 301-307.
  Electronic ISBN: 978-1-5386-9245-5.
  Print on Demand(PoD) **ISBN:** 978-1-5386-9246-2.
  INSPEC Accession Number: 18548205.
  Acceptance rate 27.77% .

- **International Journal of Advanced Robotic Systems**.
  Paper: Energy estimation for differential drive mobile robots on straight and rotational trajectories.
  Authors: Mauricio F. Jaramillo Morales (Autor principal), Sedat Dogru, Juan Bernardo Gómez Mendoza y Lino Marques.
  Publication date: 1 April 2020.
  Category: American journal Q2.
  https://doi.org/10.1177/1729881420909654

B. Bibliography

[1] Abazari, M-R. ; Danesh, M.: Optimize path planning of a planar parallel robot to avoid obstacle collision using genetic algorithm. In: *Iranian Conference on Intelligent Systems (ICIS).*, 2014

[2] AL-Taharwa, I. ; Sheta, A. ; Al-Weshah, M.: A mobile robot path planning using genetic algorithm static environment. In: *Journal of Computer Science 4*, 2014

[3] Barraquand, J. ; Langlois, B. ; Latombe, J-C.: Numerical potential field techniques for robot path planning. In: *EEE transactions on systems, man, and cybernetics, 22(2).*, 1992

[4] Belta, C. ; Isler, V ; Pappas, G-J: Discrete abstractions for robot motion planning and control in polygonal environments. In: *IEEE transactions on robotics, 21(5).*, 2005, S. 864–874

[5] Bensekrane, I ; Kumar, P. ; Amara, Y. ; Merzouk, R.: Towards adaptive power consumption estimation for over-actuated unmanned vehicles. In: *IEEE International Conference on Robotics and Biomimetics, Macau SAR, China* Bd. 18, 2017, S. 92–97

[6] Buniyamin, N. ; Wan, N. ; Sariff, N.: A simple local path planning algorithm for autonomous mobile robots. In: *International journal of systems applications, engineering development, 5.*, 2011

[7] Calisi, D. ; Farinelli, A. ; Iocchi, L. ; Nardi, D.: Autonomous navigation and exploration in a rescue environment. In: *IEEE International Conf. in Safety, Security and Rescue, Kobe,Japan*, 2005

[8] Camarena, J-F.: Análisis cinemático, dinámico y control en tiempo real de un vehículo guiado automáticamente. In: *Tesis de maestría en ciencias, Centro Nacional de Investigación y Desarrollo Tecnológico Departamento de Mecatrónica, Cuernavaca, Morelos, México.,*, 2009

[9] Choi, Y-H. ; Oha, S-Y. ; Lee, T-K. ; Baeka, S-H.: Smooth coverage path planning and control of mobile robots based on high-resolution grid map representation. In: *Robotics and Autonomous Systems,*, 2011, S. 801–812

[10] Chuy, O. ; Collins, E. ; Yu, W. ; Ordonez, C.: Power modeling of a skid steered wheeled robotic Ground Vehicle. In: *IEEE International Conference on Robotics and Automation, Kobe, Japan*, 2009, S. 4118–4123

[11] Conceićão, A. ; Moreira, A. ; Costa, P: Practical approach of modeling and parameters estimation for omnidirectional mobile robots. In: *IEEE/ASME Transactions on Mechatronics* Bd. 14, 2009, S. 377–381

[12] Connolly, C.: The determination of next best views. In: *IEEE International Conference on Robotics and Automation, St. Louis, MO, USA*, 25-28 March 1985

[13] Connolly, C-I. ; Burns, J-B. ; Weiss, R.: planning using laplace's equations. In: *IEEE transactions on robotics.*, 1990

[14] Costello, B. ; Davies, E. ; Strickland, L. ; Rogers, J.D.: A modular mobile robotic system for cooperative payload manipulation. In: *IEEE International Conference on Automation Science and Engineering (CASE), Fort Worth, TX, USA*, 2012

[15] Delingette, H. ; Hebert, M. ; Ikeuchi, K.: Trajectory generation with curvature constraint based on energy minimization. In: *IEEE/RSJ Int. Conf. Intelligent Robots and Systems*, 1991, S. 206–211

[16] Denker, A. ; Iseri, M.: Design and implementation of a semi-autonomous mobile eearch and rescue robot: SALVOR. In: *International Artificial Intelligence and Data Processing Symposium (IDAP), Malatya, Turkey.*, Sept 16-17, 2017

[17] Dogru, S. ; Marques, L: A physics-based power model for skid-steered wheeled mobile robots. In: *IEEE Transactions on Robotics* Bd. 34, 2018, S. 421–433

[18] Dudek, G. ; Jenkin, M. ; Milios, E. ; Wilkes, D.: Robotic exploration as graph construction. In: *IEEE transactions on robotics and automation*, 1991

[19] Electro-Craft, Corporation: DC motors, speed controls, Servo systems: an engineering handbook. In: *Pergamon Press* Bd. 3, 1977

[20] Escalera, A. ; Armingol, J-M. ; Moreno, L. ; Salichs, M-A.: Landmark perception planning for mobile robot localization. In: *International Conference on Robotics Automation.*, 1998

[21] Esteves, C. ; Murrieta-Cid, R. ; Hayet, J-B. ; Carlos, H.: Motion planning for maintaining landmarks visibility with a dierential drive robot. In: *Robotics and Autonomous Systems.*, 2014

[22] Feixiang, G. ; Xiaopeng, Y.: Dynamic Path Planning for Underwater Vehicles Based on Modified Artificial Potential Field. In: *Fourth International Conference on Digital Manufacturing Automation*, 2013

[23] Gallagher, B. ; Sica, W. ; Dellaert, F. ; Ok, K. ; Ansari, S. ; Stilman, M.: Path planning with uncertainty: Voronoi uncertainty fields. In: *IEEE International Conference on Robotics and Automation (ICRA)*, 2013

[24] Gay, S-E. ; Emadi, A. ; Ehsani, M. ; GAo, Y.: Análisis cinemático, dinámico y control en tiempo real de un vehículo guiado automáticamente. In: *Fundamentals, Theory and Design, Ed. CRC Press.*, 1980

[25] Ge, S. ; Cui, Y.: New potential functions for mobile robot path planning. In: *IEEE transactions on robotics and automation*, 2000

[26] Gholipour, A. ; Yazdanpanah, M.: Dynamic tracking control of nonholonomic mobile robot with model reference adaptation for uncertain parameters. In: *European Control Conference (ECC), Cambridge, UK* Bd. 39, Sep 1-4, 2003

[27] Goodrich, M-A. ; Beard, R-W. ; McLain, T-W. ; Anderson, E-P.: Coordinated target assignment and intercept for unmanned air vehicles. In: *IEEE Transactions on Robotics and Automation, 18(6)*, 2002

[28] Grisales, E.: Control de un robot móvil en entornos domésticos. In: *Tesis de Maestría en Automatización industrial. Universidad Nacional sede Manizales,*, 2013

[29] Guo, R. ; Han, L. ; Sun, Y. ; Wang, M.: A Mobile robot for inspection of substation equipments. In: *International Conference on Applied Robotics for the Power Industry,Montréal, Canada*, October 5-7, 2010

[30] Guowei, Z. ; Bin, L. ; Zhiqiang, L. ; Cong, W. ; Handuo, Z. ; Hong, S. ; Weijian, H. ; Tao, Z: Development of robotic spreader for earthquake rescue. In: *12th IEEE International Symposium on Safety, Security, and Rescue Robotics, oyako-cho, Hokkaido, Japan*, October, 2014

[31] Gupta, N. ; Ordonez, C. ; Emmanuel, G. ; Collins, Jr.: Dynamically feasible, energy eficient motion planning for skid-steered vehicles. In: *Autonomous Robots* Bd. 41, 2017, S. 453–471

[32] Hachour, O.: Path planning of autonomous mobile robot. In: *International journal of systems applications, engineering development*, 2008

[33] Ho, D. ; Chehida, k. ; Miramond, B. ; Michel Auguin, M: Towards a multi-mission QoS and energy manager for autonomous mobile robots. In: *Second IEEE International Conference on Robotic Computing, Laguna Hills, CA, USA*, February 2, 2018

[34] Hongo, T. ; akahashi, A. ; Ninomiya, Y.: local path planning and control for agv in positioning. In: *Proc. IEEE/RSJ Int. Conf. Intelligent Robots and Systems*, 1989

[35] Hou, L. ; Zhang, L. ; Kim, J.: Energy modeling and power measurement for mobile robots. In: *Energies, MDPI, Open Access Journal* Bd. 12(27), 2019

[36] Hwang, N. Y-K.and A. Y-K.and Ahuja: A potential field approach to path planning. In: *IEEE transactions on robotics and automation 8(1).*, 2005

[37] J-C, Latombe.: Robot Motion Planning. In: *Kluwer Academic Publishers Norwell, MA, USA*, 1991

[38] Jaramillo, Mauricio-F. ; Gomez, Juan-B.: Diseño de un planificador de trayectorias orientado a la reconstrucción en 3d de entornos desconocidos. In: *Tesis de Maestría en Automatización Industrial. Universidad Nacional sede Manizales*, 2010

[39] Kanayama, y. ; Hartman, B-I.: Local path planning for autonomous vehicles. In: *Proc. IEEE Int. Conf. Robotics and Automation.*, 1989, S. 1265–1270

[40] Khatib, O.: Commande dynamique dans i'espace opkrational des robots manipulateurs en prcsence d'obstacles. In: *Ph.D. dissertation, Ecole nationale Supkieure de I'AeCronatique et de I'Espace (ENSAE), France,*, 1980

[41] Kim, B. ; Kim, H.: Minimum-energy motion planning for differential-driven wheeled mobile robots, motion planning. In: *Xing-Jian Jing (Ed.), ISBN: 978-953-7619-01-5, InTech, Croatia*, 2008

[42] Kim, H. ; Kim, B.: Minimum-energy rotational trajectory planning for differential-driven wheeled mobile robots. In: *The 13th International Conference on Advance Robotics, Jeju, Korea*, August 21-24, 2007

[43] Kim, Y-J. ; Lee, J-Y.: Vision-based corridor path search of a mobile robot. In: *International Conference on Control, Automation and System.*, 2011

[44] Knowles, K. ; Lauber, J. ; Georgios, T-M. ; Kladis, P. ; Economou, J: Energy conservation based fuzzy tracking for runmanned aerial vehicle. Engineering Applications of Artificial Intelligence. In: *Engineering Appli- cations of Artificial Intelligence*, 2011, S. 278–294

[45] Koenig, S. ; Likhachev, M.: Fast replanning for navigation in unknown terrain. In: *IEEE transactions on robotics*, 2005

[46] Kozlowski, K. ; Pazderski, D: Modeling and control of a 4-wheel skid-steering mobile robot. In: *Math. Comput. Sci*, 2016, S. 477–496

[47] Krishnamurti, R. ; Wang, P. ; Gupta, K.: Metric view planning problem with traveling cost and visibility range. In: *IEEE International Conference on Robotics and Automation.*, 2007

[48] Lee, G. ; Mei, Y. ; Lu, Y-H. ; Hu, Y-C.: Energy-eficient mobile robot exploration. In: *Proceedings of the 2006 IEEE International Conference on Robotics and Automation.*, 2006

[49] Liscano, R. ; Green, D.: Implementation of a trajectory generator for an indoor mobile robot. In: *Proc. IEEE/RSJ Int. Conf. Intelligent Robots and Systems, Tsukuba, Japan.*, 1989, S. 380–385

[50] Liu, A. ; Sun, D.: Optimal motion planning of a mobile robot with minimum energy consumption. In: *IEEE/ASME International Conference on Advanced Intelligent Mechatronics (AIM). Budapest, Hungary.*, 2014

[51] Liu, S. ; Sun, D.: Optimal motion planning of a mobile robot with minimum energy consumption. In: *2011 IEEE/ASME International Conference on Advanced Intelligent Mechatronics (AIM),Budapest, Hungary.*, 2011

[52] Lumelsky, V. ; Skewis, T.: Incorporating range sensing in the robot navigation function. In: *IEEE transactions on systems, man, and cybernetics, 20(5)*, 1990

[53] Machado, T. ; Malheiro, T. ; Monteiro, S. ; Erlhagen, W. ; Bicho, E.: Multi-constrained joint transportation tasks by teams of autonomous mobile robots using a dynamical systems approach. In: *IEEE International Conference on Robotics and Automation (ICRA), Stockholm, Sweden*, May 16, 2016

[54] Masuta, H. ; Watanabe, H. ; Sato, K. ; Lim, H.: Recognition of branch pipe for pipe inspection robot using fiber grating Vision Sensor. In: *10th International Conference on Ubiquitous Robots and Ambient Intelligence (URAI),Jeju, Korea*, October 31 November 2, 2013

[55] Mei, L-Y. ; George, C-S. ; Lu, Y-H ; Y. ; Hu, C.: Energy-eficient mobile robot exploration. In: *Proceedings of the 2006 IEEE International Conference on Robotics and Automation.*, 2006

[56] Mei, Y. ; Lu, Y. ; Hu, Y.: A case study of mobile robot's energy consumption and conservation techniques. In: *ICAR '05. Proceedings., 12th International Conference on Advanced Robotics, Seattle, WA, USA*, 2005, S. 4344–4349

[57] Meyer, J-A. ; Filliat, D.: Map-based navigation in mobile robots: Ii. a review of map-learning and path-planning strategies. In: *Cognitive Systems Research*, 2003, S. 283–317

[58] Min, H. ; Xiong, H.: Global path planning for omnidirectional vehicles based on bezier curve and dynamic constraints. In: *10th International Conference on Fuzzy Systems and Knowledge Discovery (FSKD).*, 2013, S. 605–610

[59] Mohammed, M. ; Nadarajah, V. ; Lazim, N. ; Zamani, N. ; Al-Sanjary, M. O.and A. O.and Ali ; Al-Youif, S.: A mobile robot for inspection of substation equipments. In: *IEEE Conference on Systems, Process and Control (ICSPC),Melaka, Malaysia*, December 14-15, 2018

[60] Morales, J. ; Martinez, J. ; Mandow, A: Power consumption modeling of skid-steer tracked mobile robots on rigid terrain. In: *IEEE Transactions on Robotics*, 2009, S. 1098–1107

[61] Nelson, W-L: continuous curvature paths for autonomous vehicles. In: *Proc. IEEE Int. Conf. Robotics and Automation,*, 1989, S. 1260–12643

[62] O, Parlaktuna. ; A, Yazici. ; G, Kirlik. ; A, Sipahioglu.: planning approach for multirobot sensor-based coverage considering energy constraints. In: *IEEE traansaction on cybernetics*, 2014

[63] O'Hara, K. ; Nathuji, R. ; Raj, H. ; Schwan, K. ; Balch, T.: AutoPower: toward energy-aware software systems for distributed mobile robots. In: *IEEE International Conference on Robotics and Automation, Orlando, Florida*, May, 2006

[64] Ohashi, F. ; Kaminishi, K. ; Figueroa, J. ; Kato, H. ; Ogata, H. ; Hara, T. ; Ota, J.: Realization of heavy object transportation by mobile robots using handcarts and outrigger. In: *Robomech journal*, 2016

[65] Patro, S-N. ; Pradipta, P. ; Das, K.: D* lite algorithm based path planning of mobile robot in static environment. In: *International Journal of Computer Communication Technology (IJCCT)*, 2011

[66] Piazzi, A. ; Bianco, L-G.: g -splines for trajectory planning of autonomous vehicle. In: *Proc. IEEE Intelligent Vehicles Symp., Dearborn*, 2000, S. 198–203

[67] Qian, L. ; Liu, H.: Path following control of A quadrotor UAV with a cable suspended payload under wind Disturbances. In: *IEEE Transaction on Industrial Electronics*, 2019

[68] Ramviyas, K. ; Prithvi, M.: Model based on-line energy prediction system for semi-autonomous mobile robots. In: *The Fifth International Conference on Intelligent Systems, Modelling and Simulation, Malasya*, 2014

[69] Rimon, E. ; Koditschek, D-E.: Exact robot navigation using artificial potential functions. In: *IEEE transactions on robotics and automation, 8(5)*, 1992

[70] Rosenblatt, J-K. ; Payton, D-W. ; Keirsey, D-M.: Plan guided reaction. In: *IEEE Trans. Syst. Man Cyber, 20(6)*, 1990

[71] Ruiz, D. ; Caicedo, C. ; Bacca, B.: Strategy based on swarms algorithms to cooperative payload transport using a non-holonomic mobile robots group. In: *IEEE Latin America Transactions*, 2016, S. 445–456

[72] Sadrpour, A. ; Jin, J. ; Ulsoy, A.G.: Mission energy prediction for unmanned ground vehicles. In: *IEEE International Conference on Robotics and Automation, Saint Paul, MN, USA*, 2012

[73] Santos, P. Gonzalez-de ; Ribeiro, A. ; Fernandez-Quintanilla, C.: Fleets of robots for environmentally-safe pest control. In: *Precision Agriculture*, 2017, S. 574–614

[74] Seo, B. ; Kim, S. ; Choi, H.: Fleets of robots for environmentally-safe pest control in agriculture. In: *10th International Conference on Ubiquitous Robots and Ambient Intelligence (URAI), Jeju, Korea,*, August 21-24, 2013

[75] Sheta, M. ; Agarwal, V. ; Paluri, N: A new energy optimal control scheme for a separately excited DC motor based incremental motion drive. In: *International Journal of Automation and Computing*, 2009, S. 267–276

[76] Shi, H. ; Chen, L. ; Liu, C. ; Gao, B.: Robot planning algorithm based on improved arti cial potential field. In: *Third International Conference on Instrumentation, Measurement, Computer, Communication and Control.*, 2014, S. 228–232

[77] Stentz, A.: Optimal and eficient path planning for partially-known environments. In: *IEEE transactions on automatic control*, 1994

[78] Tokekar, P. ; Karnad, N. ; Isler, V.: Energy-optimal trajectory planning for car-like robots. In: *Autonomus Robots Journal*, 2014, S. 279–300

[79] Tsitsiklis, J-N.: Eficient algorithms for globally optimal trajectories. In: *IEEE transactions on automatic control, 40(9)*, 1995

[80] Wahab, M. ; Gutierrez, F. ; Shahat, A.: Energy modeling of differential drive robots. In: *IEEE SoutheastCon, Fort Lauderdale, Florida,*, April 9, 2015

[81] Wang, H. ; Huang, Y. ; Xu, C.: ADRC Methodology for a quadrotor UAV transporting hanged payload. In: *IEEE International Conference on Information and Automation, Ningbo, China*, August, 2016

[82] Wang, Y. ; Xiong, W. ; Yang, J. ; Jiang, Y. ; Wang, S: Tracking control algorithm for an indoor carrier robot considering energy optimization. In: *Energies, MDPI, Open Access Journal* Bd. 12(10), 2019

[83] Xiao, J. ; Michalewicz, Z. ; Trojanowski, K.: Adaptive evolutionary planner/navigator for mobile robots. In: *IEEE Trans. Evolutionary Computation*, 1997

[84] Xie, Li. ; Henkel, C. ; Stol, K. ; Xu, W.: Power-minimization and energy-reduction autonomous navigation of an omnidirectional mecanum robot via the dynamic window approach local trajectory planning. In: *International Journal of Advanced Robotic Systems* Bd. 12, 2018

[85] Xie, R. and Wang h-Y. Jun. W. Jun. Wen: Path planning of mobile robot based on voronoi diagram by approximation structuring and zonal ant colony algorithm. In: *International Conference on Computational Intelligence and Software Engineering*, 2009, S. 1–4

[86] Y., Mei ; Lu, Y. ; Hu, Y. ; Lee, C.: Energy-efficient motion planning for mobile robots. In: *IEEE International Conference on Robotics and Automation, New Orleans, USA,*, 2004, S. 4344–4349

[87] Yacoub, M. ; Necsulescu, D. ; Sasiadek, J.: Energy consumption optimization for mobile robots in three-dimension motion using predictive control. In: *9th Asian Control Conference (ASCC), Istanbul, Turkey*, June 23-26, 2013

[88] Yamamoto, Y. ; Yun, Y: Coordinating locomotion and manipulation of a mobile manipulator. In: *IEEE Transactions on Automatic Control* Bd. 39, 1994, S. 1326–1332

[89] Yang, S. ; Xian, B.: Adaptive control design for the quadrotor UAV system with a Suspended Payload. In: *IEEE Transaction on Industrial Electronics*, 2019

[90] Yazdanpanah, M-J. ; Gholipour, A.: Dynamic tracking control of nonholonomic mobile robot with model reference adaptation for uncertain parameters. In: *Control and Intelligent Processing Center of Excellence, Electrical and Computer Engineering Department, University of Tehran, IRAN*, 2002

[91] Yen, J. ; uger, N-P.: Plan guided reaction. In: *IEEE Trans. Syst. Man Cyber, 25(6).*, 1995

[92] Yun, X. ; Yamamoto, Y.: Internal dynamic of a whelled mobile robot. In: *IEEE/RSJ International Conference on Intelligent Robots and Systems, Yokohama, Japan,*, 1993, S. 1288–1294

[93] Zelinsky, A.: A mobile robot exploration algorithm. In: *IEEE transactions on robotics and automation*, 1992

[94] Zhu, D. ; Latombe, J-C.: New heuristic algorithms for ecient hierarchical path planning. In: *IEEE transactions on robotics and automation, 7(1)*, 1991

[95] Zhuang, Y. ; Wang, W. ; Chen, H. ; Zheng, K.: 3d scene reconstruction and motion planning for an autonomous mobile robot in complex outdoor scenes. In: *International Conference on Modelling, Identification and Control (ICMIC).*, 2010, S. 692–697